JUSTUS-LIEBIG-
UNIVERSITÄT
GIESSEN

Bis(bis(8-quinoloyl)amide)metal(II) complexes for organic electronics

Dissertation zur Erlangung des akademischen Grades
Doktor der Naturwissenschaften (Dr. rer. nat.)
am Fachbereich Chemie der Justus-Liebig-Universität Gießen

vorgelegt von

Harald Locke

geboren in Fürth

Gutachter:

1. Prof. Dr. Peter. R. Schreiner
2. Prof. Dr. Derck Schlettwein

Gießen, November 2020

Acknowledgment

I would like to thank the following people, without whom this work would have not been possible and who have been supporting me during this phase of my life.

First, I want to state my sincere gratitude to my supervisor Prof. Dr. Peter R. Schreiner for inviting me to his group and giving me the opportunity to work in the field of organic electronics. I am glad, that he has always been approachable when I had a question.

Furthermore, I am grateful to Prof. Dr. Derck Schlettwein for being my co-supervisor and supporting the project with a lot of suggestions regarding experiments.

I also want to thank Dr. Martin Güngerich for organizing the "DFG-Graduiertenkolleg 2204".

I give thanks to Dr. Georg Albrecht for the strong collaboration in planning and executing this project.

I thank Pascal Schweitzer for the motivating cooperation in solving the remaining problems of this project as the successor of Dr. Georg Albrecht.

I thank Dr. Jonathan Becker for measuring and analyzing the countless crystals of all the materials regarding this project.

I also want to thank Dr. Clemens Geis, Thi Hai Quyen Nguyen, and her Bachelor student Sophie Göbel from the Schlettwein group for sharing their knowledge about several measurement techniques and providing data.

I thank Paul Debes and Anna McCurry, who supported me in the laboratory when I was supervising them.

I would like to thank the whole Schreiner group for a nice and profitable working atmosphere.

Declaration

I declare that I have completed this dissertation single-handedly without the unauthorized help of a second party and only with the assistance acknowledged therein. I have appropriately acknowledged and cited all text passages that are derived verbatim from or are based on the content of published work of others, and all information relating to verbal communications. I consent to the use of an anti-plagiarism software to check my thesis. I have abided by the principles of good scientific conduct laid down in the charter of the Justus-Liebig-Universität Gießen„Satzung der Justus-Liebig-Universität Gießenzur Sicherung guter wissenschaftlicher Praxis“ in carrying out the investigations described in the dissertation.

Gießen, 25$^{\text{th}}$ November 2020 Harald Locke

Contents

1 Introduction

1.1 Motivation

Organic electronics promise great advances in semiconductor technology. So far silicon is the main component in electronic devices and although it is very abundant its processing requires huge amounts of energy[1] and therefore its ecological footprint is a major downside. Also silicon technology is reaching its limitations as further miniaturization of electrical components are limited by thermal noise.[2] The thermal energy of the charge carriers allows the tunneling between component structures as the decrease in size is accompanied by a decrease of the barrier height separating them. There are inorganic alternatives for silicon, like Germanium[3] and gallium arsenide[4] but besides sharing the high processing cost they are way less abundant and quite a lot of them fall under the definition of critical materials and have a damaging impact on the environment.[5, 6] Devices consisting of organic materials are supposed to be able to overcome the downsides of inorganic materials, they can be processed at low temperatures and even allow advanced processing methods like ink jet printing[7, 8] and spin coating[9] and they offer the possibility of further miniaturization without the appearance of tunneling currents. The feed stock for organic materials can be extracted from crude oil and in future renewable feed stocks might make them available for all time.[10] Additionally, the materials allow flexible low weight devices.[11, 12] But there is, of course, no light without shadow, the organic materials have lower charge carrier density and charge carrier mobility resulting in low electrical conductivities. Doping of these materials is still challenging and the mechanisms lying behind it are not well understood.[13, 14] Consequently, a major goal is to find organic materials that are getting closer to the performance of inorganic materials and optimize processing including the addition of suitable dopants. The developement of organic light emitting diodes pioneered the field as they already have reached market maturity and are now competing with other technology on an even ground. But in the field of organic field effect transistors suitable materials are still lacking, especially electron conducting semiconductors are scarce.[15] Other challenges are the reduction of contact resistances and an improvement in pattern techniques.[16] This work revolves around the creation and characterization of transition metal organic complexes suitable for electronic devices. The underlying concept aims to direct the arrangement of the materials within the bulk by selected molecular features. In the next chapters the underlying processes for conduction in organic materials will be presented. Developments in the field of organic materials with a focus on metal organic complexes will be expounded. Next the design concept of the aforementioned complexes will be explained, their synthesis and characterization will be described followed by studies about testing preliminary devices using these materials. The work closes with discussion about the utility of these materials and the outlook for future experiments and possible applications.

1.2 Advances in organic field-effect transistors

1.2.1 General concept of organic field-effect transistors

An organic field-effect transistor consists of an organic semiconducting layer that connects the source and drain electrode. Parallel to this organic layer is an insulating layer that separates the semiconductor from the gate electrode. There are several possibilities to arrange the layers and electrodes for an OFET setup. Depending on the arrangement the gate, source and drain electrodes can either be on the bottom or the top of the device (figure 1.1). Usually in organic electronics top gate devices show better performances as the most sensitive semiconducting layer is sandwiched and protected by the substrate and the gate. On the downside the semiconducting layer can be strained thermally and chemically when deposing the gate electrode in such a setup.

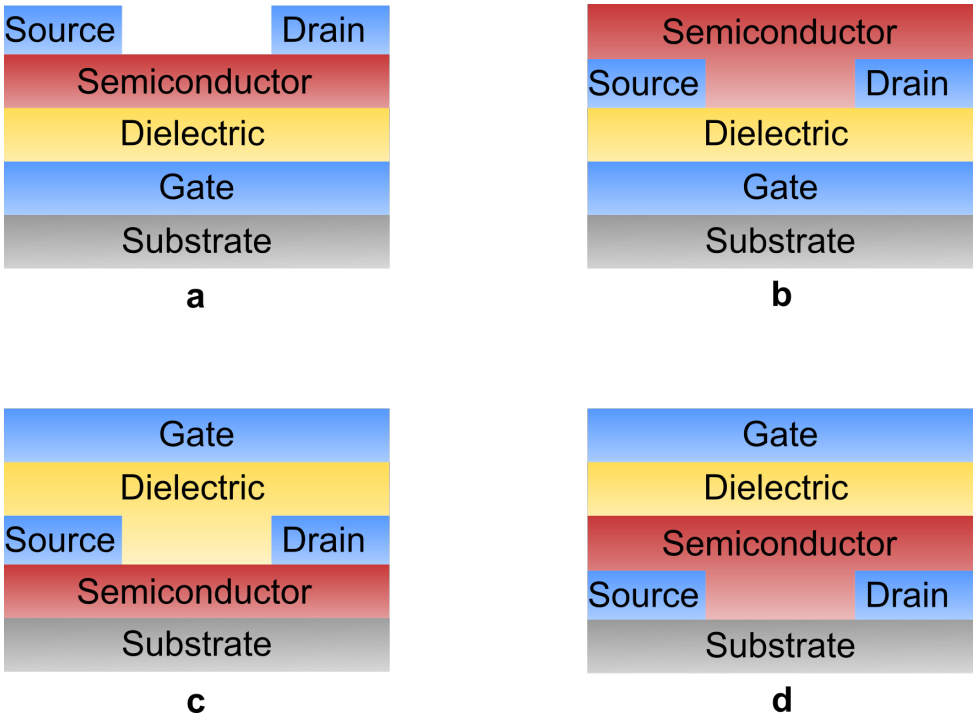

Figure 1.1: Different setups for an OFET: bottom gate top contacts (a), bottom gate bottom contacts (b), top gate top contacts (c) and top gate bottom contacts (d)

When no voltage is applied to the gate electrode no source-drain current can be measured for semiconductors with a low concentration of charge carriers. When a voltage is applied between the source and gate electrodes, charge carriers are gathered at the interface layer between the insulator and the semiconductor and form a layer with an increased charge carrier concentration[17] so that a source-drain current will be observed, if a voltage between the two electrodes is applied. This current reaches a certain maximum called the saturation current, which is space-charge limited by the extraction of charge carriers from the pinched-off conductive channel to the drain electrode. There are several design

concepts for an OFET. The most prominent in science is to use a bottom gate configuration with top or bottom contacts, as it is the easiest to prepare as substrate and gate can be the same material. The performance of an OFET is determined by several important parameters. The first one is the charge carrier mobility μ [$\mathrm{cm^2\,V^{-1}\,s^{-1}}$] that gives the drift velocity [$\mathrm{cm\,s^{-1}}$] of an electron or hole in the presence of an applied field [$\mathrm{V\,cm^{-1}}$]. The higher it is the less voltage is necessary to operate the device and the more energy efficient it becomes. The charge carrier mobility is primarily determined by the material in use and its processing as the later one determines its grain sizes and its morphology. But other properties of an OFET also have an influence like the surface roughness of the insulating layer and the exposure towards doping agents. All of this will be covered by examples in later sections. The second important parameter is the threshold voltage, its magnitude is the minimum gate voltage that is necessary to create a layer of charge carriers at interface between the dielectric layer and the semiconductor. In a theoretically optimal case the threshold voltage is zero, but in reality trap states are present. These trap states capture charge carriers and are localized such that the carrier cannot escape. Therefore, these states have to be filled before a conductive layer forms. When trap states are present the threshold voltage is negative for hole conducting (p-type) and positive for electron conducting (n-type) materials. In some cases, without an applied gate voltage, already enough charge carriers are present, mostly due to excessive doping, and the threshold voltage then determines the voltage to fully compensate the semiconductor and to switch the device off. In this context the on/off-ratio is the ratio between the maximum obtainable current and the smallest obtainable current in respective on- and off-states of the device.

1.2.2 Electronic processes in organic materials

In contrast to the ionic and covalent bonds in inorganic materials, organic material are bound by dispersion interactions.[18–20] These forces are weaker and also harder to describe as molecular structures are quite complex compared to spherical atoms and ions in inorganic materials. The most important dispersion interactions for organic semiconductors are π–π interactions as they couple the aromatic systems in organic materials. The aromatic systems absorb low-energy photons and host charges. So strong intermolecular forces between them result in lower barriers for the transfer of charges. For π–π interactions to occur, different alignments of the aromatic systems are possible (figure 1.2). For small systems like benzene an edge-to-face or also called T-shaped alignment is the most stable configuration. As π-systems increase in size a parallel displaced alignment is energetically preferable. From a theoretical point of view a completely co-facial alignment of the π-systems would result in the highest charge carrier mobility, but this would also be the case with the highest electrostatic repulsion.[21] Therefore such a case will not occur in reality. Even small changes in the molecular structure, which themselves have a small influence on packing, can have quite a large effect on transfer integrals and therefore charge transport. Examples for this consist in the introduction of steric hindrance[22] and exchanging hydrogen with fluorine atoms.[23] Unfortunately, it is still not possible to predict the crystal packing from a given molecular structure.[24] Thus, in order to find new promising materials for organic electronics, it is necessary to synthesize materials

based on an educated guess and test them with a large amount of experiments rather than relying on calculation to select promising candidates.

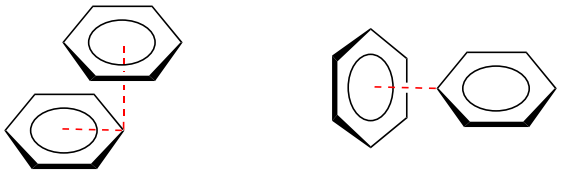

Figure 1.2: parallel displaced (left) and edge-to-face (right) π–π stacking

To describe charge transport the conductivity σ is an important measure that depends on the amount of charge carriers n, their charge carrier mobility μ and their charge e.

$$\sigma = |e| \sum_i n_i \mu_i \tag{1.1}$$

The charge carrier mobility itself in general is defined by the drift velocity $\vec{v}$ of the charge carrier divided by the electric field $|\vec{E}|$.[21]

$$\mu = \frac{\vec{v}}{|\vec{E}|} \tag{1.2}$$

For organic field-effect transistors the charge carrier mobility[21] can be extracted incorporating the geometric factors, channel width W, and channel length L, as well as the device dependant threshold voltage V_T and the capacitance across the gate dielectric C. I_d and V_d denote the drain current and voltage. V_g denotes the gate voltage. Additionally the formula depends, whether the linear regime or the saturation regime of the I–V curve is considered. For the linear regime the expression is the following:

$$\mu = \frac{L}{WCV_d} \frac{\partial I_d}{\partial (V_g - V_T)} \tag{1.3}$$

And for the saturation regime the formula becomes independent of the drain voltage.

$$\mu = \frac{2L}{WC} \left(\frac{\partial \sqrt{I_d}}{\partial (V_g - V_T)} \right)^2 \tag{1.4}$$

It is important to again emphasize that although the charge carrier mobility is calculated based on technical parameters like the size of the device it is strongly influenced by the material applied and its processing. As it is one of the parameters that has most influence on device performance a lot of effort in research resolves around improving the processing.

The intrinsic charge carrier concentration n in organic semiconductors is negligibly low. It can be increased by intended and unintended doping and will be discussed later. Charges can also be generated by the dissociation of electron-hole pairs, which are created themselves by the absorbance of photons. This effect is important for solar cells but obviously plays no role for organic transistors. But suitable charge carrier concentrations are yielded by

the extrinsic injection of charge carriers by the electrodes. This has additional implications on organic devices. The current in a device can be injection limited, which means the current is solely determined by the injection rate of the electrodes. In this case, there is no possibility to identify charge carrier mobility as all correlations of the current with the electric field or the temperature are attributed to their influence on the injection process. The other possibility is that of space charge limited current. The electrode creates more charge carriers than the interface layer is able to transport. A space charge region emerges at the electrode which prevents further charge injection. For this case the current density j can be described by the *Mott-Gurney equation.*[25]

$$j = \frac{9}{8}\epsilon_r\epsilon_0\mu\frac{V^2}{d^3} \tag{1.5}$$

The theory behind this equation assigns a drift velocity to every charge carrier. This drift velocity and therefore the current is neither linearly dependant on the applied voltage V nor on the inverse of the distance d between the two electrodes. As this theory relies on the concept of drift velocity the current is linearly dependent on the charge carrier mobility μ. ϵ_0 denotes the dielectric constant of vacuum and ϵ_r the dielectric constant of the semiconductor.

1.2.3 Important materials and advancements

Studies of organic electronics have been conducted for decades and the first organic field effect transistor was already created in 1986.[26] The semiconducting material used was polythiophene, the parent of one of the most prominent structural motifs,[27–29] that has been in use until today. One derivative poly(3-hexylthiophene)[30] belongs to the best investigated materials overall, concerning its molecular weight[31, 32], its morphology,[33, 34] and its processing conditions.[35–37] Another very prominent semiconductor is pentancene, which was first tested for OFET applications in 1991.[38] In the following years the performance of pentacene-based devices increased steadily and reached a charge carrier mobility of 1.5 $cm^2\,V^{-1}\,s^{-1}$[39] in 1997, which is comparable to the charge carrier mobility of amorphous silicon, a benchmark value for organic semiconductors. Pentacene can be processed with a variety of methods. The standard is to use vapor deposition and the temperature and pressure dependence was investigated.[40] The effect of grain size was also investigated by the comparison between experiment and simulations.[41] Also crystals were grown by sublimation and then mechanically incorporated into the device.[42] Pentacene is hardly soluble in most organic solvents at room temperature. Obviously heated solutions can be used to process the material.[43] More common is the use of suitable soluble precursors that allow solution processing. These precursors are coated on the surface and then heated to give pentacene by the means of a retro-Diels-Alder reaction.[44, 45] Both of the aforementioned materials, P3HT and pentacene are hole-conducting. The most prominent class for n-type materials are rylene diimides.[46] Among them naphthalene and perylene diimides are encountered most often. *N,N'*-bis(cyclohexyl) naphthalene-1,4,5,8-bis(dicarboximide)[47] is one of the record holders as it showed improved packing behavior and the charge carrier mobility came close to 6 $cm^2\,V^{-1}\,s^{-1}$. One of the major

issues of electron conducting organic materials is their sensitivity towards oxygen, which is also true for rylene diimides. But tuning of the rylene core as well as the side chains can improve air stability.[48]

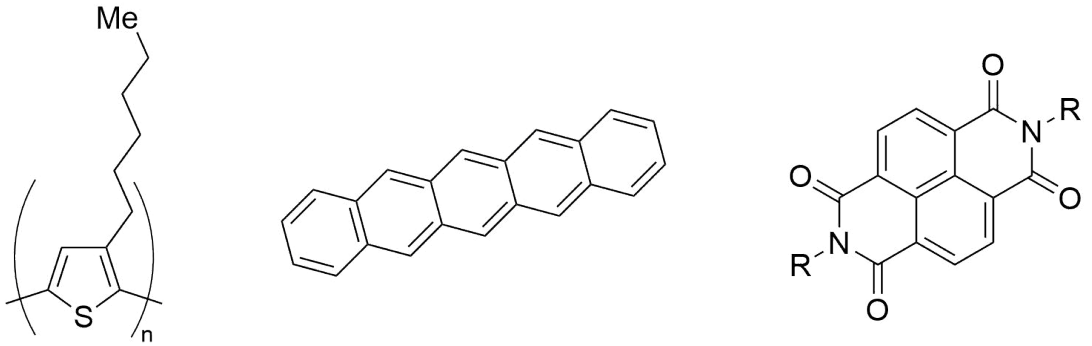

Scheme 1.1: Molecular structure of P3HT (left), pentacene (middle) and naphthalene diimide (right)

But not only the number and properties of materials has improved in the past years. Fabrication of integrated circuits using pentacene and P3HT was already achieved in the year 2000[49] and some applications were proposed.[50] Over the years more and more applications have been realized, for example printed[51] and also flexible[52, 53] displays, vapor sensors[54] and radio-frequency identification circuitry.[55] The achievements in the field of printable devices were already reviewed.[56]

Of course, a lot more different materials and applications have been created, but the sheer amount of research cannot be covered in and also does not fit into the scope of this work. Plenty of reviews about the whole topic can be found elsewhere, with limited examples given here.[15, 57–60]

1.2.4 Organometallic complexes

Phthalocyanine complexes have been the major class of compounds in the field or organometallic molecules for application in organic electronics. They are easily synthezied from cheap phthalic acid derivatives, are available with a variety of metals, including square planar, pyramidal, and octahedral metal centers,[61] and thermally and chemically stable.[62] Their applicability strongly depends on the metal center with huge differences in charge carrier mobility.[63] Phthalocyanine complexes are usually hole conducting but when ligands with enough electron withdrawing groups, for example hexadecafluorinated phthalocyanine, are used, the resulting complex is electron conducting.[64] In one study sulphonated phthalocyanine derivatives were used. $NiPc(SO_3Na)_x$ (with x giving the average number of sodium sulphonate groups at a complex molecule) was spin coated on an interdigital structure.[65] The OFETs obtained this way were outclassing OFETs produced by evaporation of NiPc and a maximum charge carrier mobility of 1.8 $cm^2\,V^{-1}\,s^{-1}$ was measured for x = 1.5. The effect of increased charge carrier mobility through sulphonation was also discovered for other metal centers.[66] When the substrate temperature

was increased to 150 °C while vacuum depositing, TiOPc films OFETs with outstanding charge carrier mobilities of up to 10 $cm^2\,V^{-1}\,s^{-1}$ were obtained.[67] This is attributed to highly ordered crystalline films in the α-phase of the materials. The α-phase of this materials shows very short distances between π-systems, to which the high performance is attributed. Processing at lower temperature results in amorphous films or films with mixed phase (α-TiOPc and β-TiOPc). Phthalocyanines were also investigated as ligands in sandwich-like or triple-decker rare earth complexes.[62] The Lutetium pthalocyanine sandwich[68] is one of the better semiconducting materials with an effective mobility of 1.3 $cm^2\,V^{-1}\,s^{-1}$. A series of Langmuir-Blodgett films of Europium, Holmium, and Lutetium triple-decker complexes[69] were investigated and their comparable high carrier mobilities were attributed to their ability to form stable monolayers on the water surface with their crown ether heads.

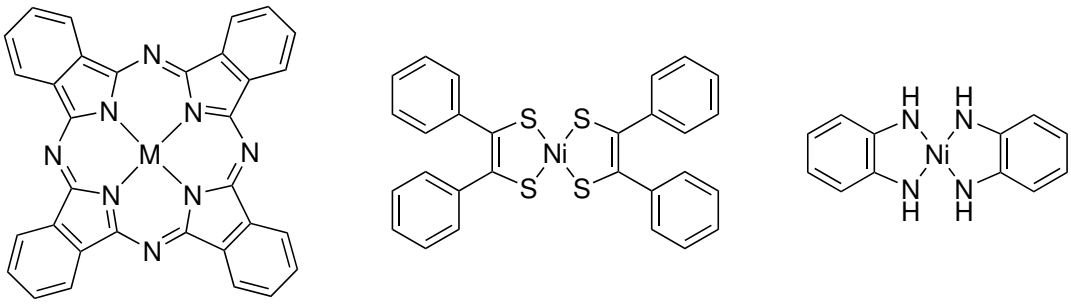

Scheme 1.2: Molecular structure of a phthalocyanine complex (left), bis(dithiobenzil)nickel(II) (middle) and bis(o-diiminobenzosemiquinonate) nickel(II) (right)

Nickel(II) complexes are often applied in organic electronics. Their square planar center with its empty d_{z^2}-orbital can easily fit into conjugated system incorporating the π-system of the ligands. Nickel-dithiolenes[70, 71] are a subclass that have been investigated well. The first OFET was reported in 1994[72] and the Langmuir-Blodgett films had an charge carrier mobility of $2.4 \cdot 10^{-5}$ $cm^2\,V^{-1}\,s^{-1}$ after deposition, but the mobility could be drastically improved by doping with iodine, which gave an value of $1.8 \cdot 10^{-1}$ $cm^2\,V^{-1}\,s^{-1}$. Vacuum deposited bis(dithiobenzil)nickel(II) films[73] showed n-type characteristics and a mobility of $2.0 \cdot 10^{-1}$ $cm^2\,V^{-1}\,s^{-1}$. After short air exposure the carrier mobility is decreased and the threshold voltage increased. Air exposure for several hours completely suppresses any conductivity. A study eventually investigated the air stability of bis(dithiobenzil)nickel(II) derivatives with different aromatic substitution patterns[74] and air stability was achieved for fluorinated species which showed only minor differences between experiments conducted under air or vacuum. A high electron mobility of 2.8 $cm^2\,V^{-1}\,s^{-1}$ was obtained when silver was used as the cathode material for a bis(dithiobenzil)nickel(II) derivative.[75] Pretreatment of the silicon oxide insulator with octadecyl-trichlorosilane or polystyrene followed by the vacuum depositon of the nickel complexes resulting in carrier mobilities up to 0.18 $cm^2\,V^{-1}\,s^{-1}$.[76] Other metallodithiolenes with different metal centers have not been used in electronics despite their synthetic availability. Another series of Ni(II)-complexes are based on bis(o-diiminobenzosemiquinonate) nickel(II)[77] which was vacuum deposited on a doped n-type silicium wafer which resulted in an OFET with $\mu = 3.8 \cdot 10^{-2}$ $cm^2\,V^{-1}\,s^{-1}$. The methylated derivative also showed a hole mobility of $7.1 \cdot 10^{-5}$ $cm^2\,V^{-1}\,s^{-1}$[73] which

is doubled upon air exposure accompanied by an increase of the off-current. Based on bis(o-diiminobenzosemiquinonate) nickel(II) a metal-organic framework was created[78] which showed conductivity of up to 40 $S\,cm^{-1}$ and can be seen as an graphene analogue. Besides nickel(II) its higher homologues and copper(II) offer a square planar geometry. A bi-nuclear copper(II) complex with an ligand based on the salen moiety was grafted on a carbon nanotube[79] to obtain an ambipolar FET.

1.2.5 Practical aspects of doping

Doping in organic materials is comparable to that of inorganic materials. An impurity is added to the host material which provides additional holes or electrons to the valence or conduction band respectively. Although, it is questionable, whether this terminology holds true for organic materials. The electronic states are rather tightly bound than it is the case in inorganic bulk materials. It can be rather seen as an addition or removal of an electron to or from a molecule. The charge carrier mobility follows a different trend in organic materials than in inorganic ones. One possibility for doping is achieved by exposure of the already prepared thin film of the organic material towards oxidizing gases like oxygen in air[80, 81] or halogen vapors.[82] Air exposure was also reported to switch films of TiOPc from n-type to p-type conduction.[83] But doping with these strong oxidants can also result in degradation of the semiconductor.[84] Also the incorporation of oxygen can lead to the generation of trap states,[85, 86] which reduce device performance. The presence of trap states counteracts the effect of additional charge carriers and it depends on the specific material, whether the overall net effect is beneficial for the device performance. Another possibility for the post-processing of films is the evaporation of alkaline metals onto already generated films, which was performed for fullerens the first time.[87] As can be expected this kind of doping is very air-sensitive.

Besides this harsh doping with elemental species, doping can be achieved with a variety of substances. Metal oxides[88] can be incorporated as p-dopants. Molybdenum trioxide[89] is one of the most prominent dopants in this class, as it requires rather low temperatures to co-evaporate it. But also rhenium trioxide,[90] tungsten trioxide,[91] and iron(II,III) oxide[92] can be used for this purpose. Metal oxides form nanoclusters[93] within the prepared devices and the size and distribution of these clusters strongly effect the charge generation efficiency and therefore their processing is crucial for the overall performance. N-type seminconductors in turn can be doped with several alkaline salts such as carbonates[94–97] ceasium phosphate, caesium azide,[98] and lithium nitride[99]. These salts are usually co-evaporated and due to the elevated temperatures needed the used materials decompose partially and form different oxides.

Doping is also possible by Brønsted and Lewis acids. Polythiophene films which were exposed to tridecafluoro-1,1,2,2-tetrahydrooctyl trichlorosilane[100] showed an increase in conductivity of up to six orders of magnitude. The conductive polymer poly(3,4-ethylene-dioxythiophene):poly(4-styrenesulfonate) (PEDOT:PSS) and related substances can also be seen as highly acid doped organic semiconductors. Iron(III) chloride and antimony pentachloride[101] are simple Lewis acids which are used for doping.

But the most advanced doping is performed with small molecules including transition metal complexes. The first benefit of these, compared to doping with elemental species, is that they cannot at all or only barely diffuse into the host material which results in a higher device stability. The probably most prominent class of molecular p-dopant is 2,3,5,6-Tetrafluoro-7,7,8,8-tetracyanoquinodimethane (F_4-TCNQ). This small molecule can either be co-evaporated when doping a molecular semiconductor like ZnPc[102] or a blend of the semiconducting polymer and the dopant can be spin-coated onto the substrate.[103–105] Several derivatives of this dopant were synthesized and tested. An (adamantan-1-yl)propyl substituted analogue showed improved processibility.[106] Other studies consider the substitution pattern of the molecule in order to improve its performance.[107] Also the beneficial electric properties of inorganic materials such as the aforementioned p-dopant molybdenum trioxide can be combined with an organic frame[108] to obtain a well performing and processible dopant. For n-doping electron-rich molecules are used such as highly sulfur containing aromatic compounds like bis(ethylenedithio)-tetrathiafulvalene[109] and tetrathianaphthacene[110], amino-functionalized stable radicals like the tris[4-(dime- thylamino)phenyl]methyl radical[111] and transition metal complexes like cobaltocene.[112, 113] Despite for the increased air-sensitivity of n-doped organic material, a certain passivation effect was discovered for fullerene doped with a binuclear tungsten complex.[114, 115] One problem of incorporating dopant molecules is their influence on the crystallinity of the material. Attempts were made to circumvent this by having dopants with a very similar structure as the host material. In one case a radical anion of a perylene diimide was used which nearly completely resembled the host material.[116] In the case of metal organic compounds such doping can be achieved by using blends of complexes with identical ligands but different metal centers. A 9:1-mixture of CuPc and NiPc was used to generate an OFET which showed better performance than ones consisting of only one of the aforementioned materials.[117]

1.2.6 Surface preparation and interface engineering

Interfaces play a crucial role in organic electronics. The interface between the electrodes and the semiconductor influences charge carrier injection and the interface between insulator and semiconductor influences the charge carrier transport. Also in the construction of bottom gate OFETs prefuctionalization and choice of the insulator might result in a preferable morphology of the semiconductor. Pentacene thin film morphology relies on the interactions with the surface.[118] In general when pentacene is deposited on flat, inert materials like oxides its main molecular axis is aligned perpendicular to the surface, but for reactive surfaces like pure metals its main axis is arranged parallel to the surface. Surface roughness plays a crucial role in device performance, too. Increasing roughness of the insulator surface corresponds with a decrease in hole mobility for pentacene OFETs.[119] Also despite obeserving similar crystal sizes, OFETs grown on rough silicon nitride surfaces performed inferior to their smooth counterparts.[120] The same tendency was observed for silicon oxide surfaces.[121] In case of silicon nitride surfaces[120] a polystyrene layer was spin-coated onto the rough surface to smooth it and corresponding device had an increase in charge carrier mobility by nearly two orders of magnitude. Pentacene thin films grown on

silicion oxide pre-treated with different alkyl- and arylchlorosilanes showed large differences in their hole mobilities.[122] Another investigation also probed different insulator materials with and without pre-treatment and found the best mobility for silicon oxide pre-treated with n-octyltrichlorosilane despite the relatively small crystal size observed in this case.[123] Additionally, interface SAMs were further functionalized with amine or methyl groups and thin films of poly(3-hexylthiophene) were spin coated onto the formed layers.[124] The planes of the thiophene moieties were aligned perpendicular towards the underlying surface in case of the amine functionalisation and parallel to it in case of methyl groups present. After annealing at 240°C the charge carrier mobility for P3HT on the amine functionalized layer had a higher mobility of 0.28 $cm^2\,V^{-1}\,s^{-1}$ compared to 0.08 $cm^2\,V^{-1}\,s^{-1}$ for the other case. Pentacene and C_{60}-fullerene thin films were deposited onto silicon oxide surfaces with differently functionalized monolayers.[125] Perfluoroalykl, alkyl, and amino groups were attached to the monolayers and it was found, that perfluoroalkyl groups increased the hole density at the interface layer and therefore the charge carrier mobility for pentacene devices, while amino groups gave the best results for fullerene devices respectively. Nine different silanes were used for prefunctionalizing the silicon oxide surface in a study to test the influence of SAMs on charge carrier mobilities and threshold voltages of pentacene films.[126] Both, charge carrier mobility, and threshold voltage varied depending on the material applied during prefunctionalization without observing a clear trend based on molecule functionality. Despite the aforementioned study the perfluorinated species rather resulted in low device performance in this case. SAMs of different chain length also performed well as an insulating layer[127] with tunneling barriers outperforming metal oxides and reaching the theoretical limit. Phenol ethers were utilized as end groups for a SAM dielectric for a pentacene-based OFET.[128] This prevented penetration of semiconductor molecules into the insulating layer which is hypothesized to be the cause of gate leakage. The device performed well with operating voltages of 2 V or less and a charge carrier mobility of 1 $cm^2\,V^{-1}\,s^{-1}$. Attempts to create a similar performing device while having linear end groups failed. In a comparable study docosyltrichlorosilane was applied to alter the silicon substrate surface and the semiconductor P3HT was spin-coated onto it.[129] The large polymer molecules behaved well on the purely alkyl functionalized SAM and the device operated with voltages below 2 V. Polymer dielectrics can also have beneficial effects on the charge carrier mobility. Vinylphenol-based polymers were spin-coated onto the silicon gate and heated to 200 °C for cross-linking.[130] Pentacene was deposited onto the dielectric in vacuum and mobilities up to 3.0 $cm^2\,V^{-1}\,s^{-1}$ were measured. An overall very well-performing petacene thin-film OFET was obtained when polyvinyl alcohol was utilized as the insulator resulting in a threshold voltage of -0.98 V and a charge carrier mobility of 1.1 $cm^2\,V^{-1}\,s^{-1}$.

In summary the insulator surface drastically modifies device performance, especially in the case that the semiconductor layer is also deposited onto it. A majority of the studies resolved around pentacene or P3HT as their properties and handling are well-known and it raises the question which surface modifications work best for other materials. As a consequence in the long run a variety of surface preparation methods need to be tested for the molecules presented in this work to approach the maximum effectiveness of them. But to establish their suitability as semiconductors in general it is not necessary. So in order

to save time and keep simplicity these methods will not be applied to the experimental devices here.

1.3 Preparation and measurement methods

1.3.1 Synthetic concepts

Skraup reaction

The Skraup sythesis to produce quinolines has been known since the late 19th century[131] and is named after its inventor Zdenko Hans Skraup, a Czech chemist. Its usefulness was reviewed even long after Skraup's life.[132, 133] For the original synthesis aniline, sulfuric acid, glycerol, and nitrobenzene as an oxidant were mixed. The sulfuric acid dehydrated glycerol to produce acroleine, which reacts with the aniline to give dihydroquinoline. This is subsequently oxidized to quinoline by nitrobenzene (scheme 1.3). Different variations of the reaction are known exchanging the sulfuric acid for example with methanesulfonic acid and the oxidant with arsenic pentoxide or ferric oxide. As the reaction tolarates quite some functional groups present on the aniline ring, it was chosen for the synthesis of the quinoline compounds in this work.

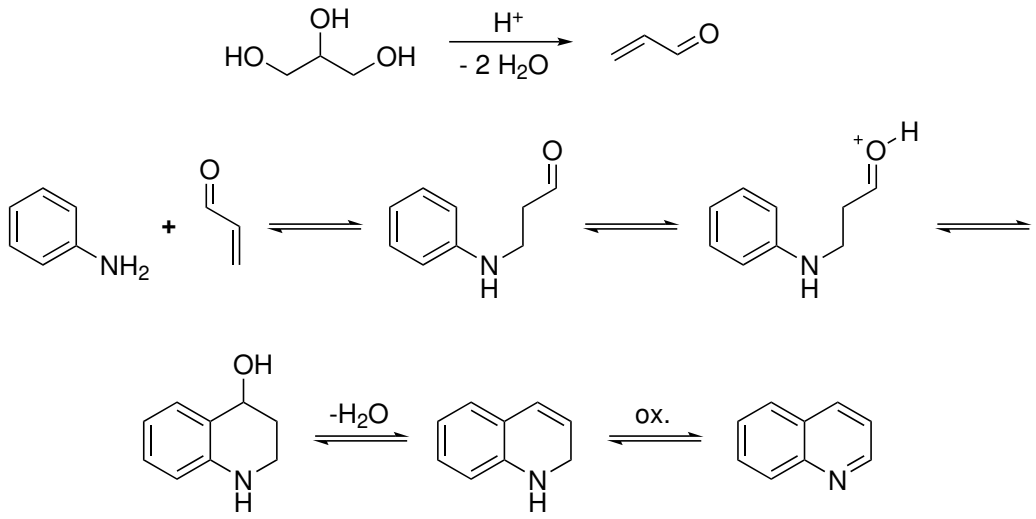

Scheme 1.3: Skraup synthesis mechanism

Reduction of nitro-groups with palladium on charcoal

The hydrogenation using palladium on carbon is one of the most common reactions in organic chemistry. It works under ambient conditions and with a variety of substrates and solvents. It was also already shown that the reduction of nitroquinolines to aminoquinolines work without reducing the aromatic system.[134]

Buchwald-Hartwig coupling

The Buchwald-Hartwig reaction was investigated independently by the groups of John. F Hartwig[135] and Stephen L. Buchwald[136] and published individually in 1994. The reaction is the palladium catalyzed coupling of an aryl halide with an amine under the presence of a base. The reaction has been extensively applied in synthetic chemistry using a variety of substrates and catalysts and has also been reviewed in detail.[137] The mechanism was also studied in detail[138] and is depicted here for the case of SPhos as the applied ligand and phenyl halide together with propylamine as the substrates (scheme 1.4). The catalytic cycle starts with the oxidative addition of the phenyl halide towards the palladium(0) complex. This is followed by the addition of the amine to the complex. The acidity of the amine is increased through binding to the metal center and it is depronated by the added base accompanied by the elimination of the halide. The next step is the reductive elimination which results in the formation of the product and the regeneration of the original catalytically active species.

The ligand precursor *N*-8-Quinolinyl-8-quinolinamine was already synthesized using this method[139] and as the Buchwald-Hartwig coupling is quite tolerant towards functional groups, it was also employed to generate derivatives of *N*-8-Quinolinyl-8-quinolinamine.

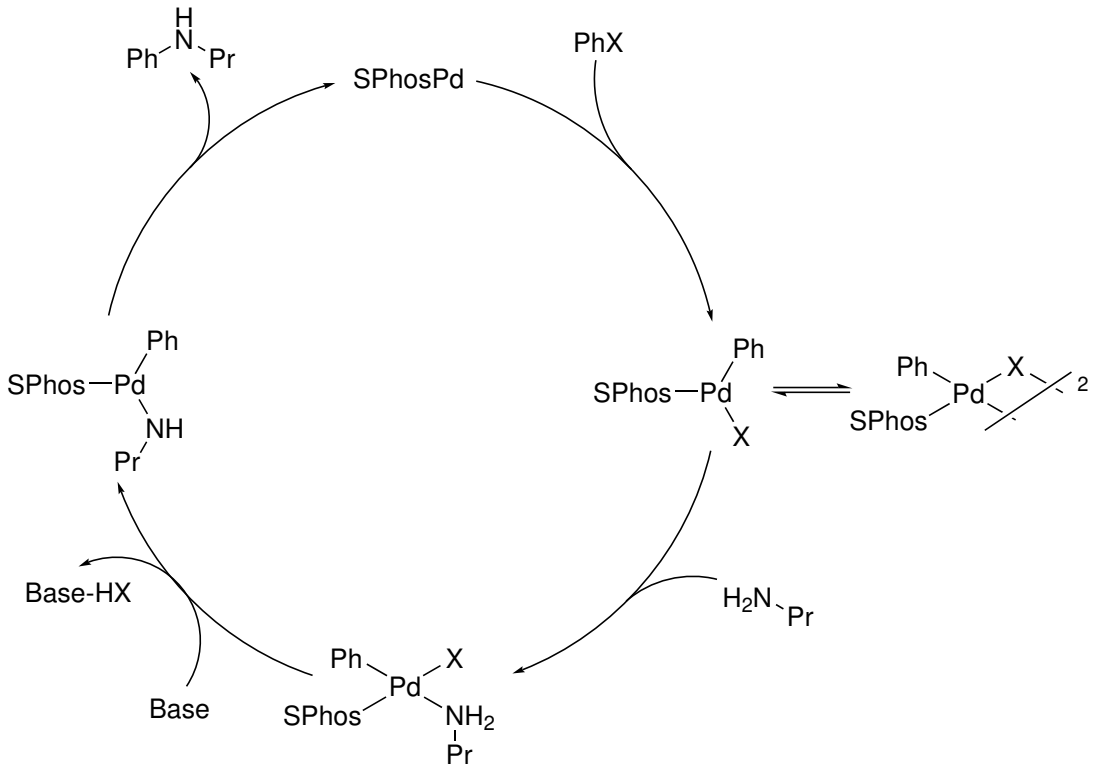

Scheme 1.4: Catalytic cycle of the Buchwald-Hartwig coupling

1.3.2 Structural determination

1.3.3 Device preparation

Photolithography

Photolithography is used to generate the geometry of the interdigital structure used in the preparation of OFETs. After a wafer is cleaned, hexamethyldisilazane is casted onto the wafer. The HMDS will react with the terminating hydroxyl groups of the silicon oxide layer of the wafer and leave a hydrophobic surface of trimethylsilyl groups which interact well with the photoresist, which is added next. The photoresist, which is a postive one in this work, is applied by spin-coating. A shadow mask is placed above the wafer which allows only illumination at the locations of the future interdigital structure. The wafer is then irridiated with a UV-lamp and the irradiated photoresist is removed with a developer solution to leave a negativ of the interdigital structure on the wafer. The electrode material (e.g. gold) is then accumulated by physical vapor deposition onto the wafer. After that the remaining photoresist is removed with the help of an ultrasonic bath. In this process the excess electrode material is removed as well leaving only the final interdigital electrode structure on the wafer.

Physical vapor deposition

Physical vapor deposition is one of the major methods to process organic molecular materials. In a vacuum chamber a crucible with the organic material is placed. The substrate containing the interdigial structure is placed on a turnable holder in certain distance above the crucible (figure 1.4). A quartz crystal oscillator is placed next to the substrate holder, which works as micro balance. In the beginning the substrate is turned away from the crucible so that no material can reach it. The chamber is then evacuated and upon reaching the required vacuum the crucible is heated, usually by a coil. A beam of material is generated through the sublimation and the given geometry of the deposition chamber. The beam hits the crystal oscillator and the substrate holder with the substrate still turned away. By the change in frequency of the crystal oscillator due to the deposited material the evaporation rate can be adjusted. When the required rate is obtained the substrate holder is turned so that the interdigital structure is exposed towards the material beam and a thin film is grown onto it.

Determination of thin film thickness

The thin film thickness is determined by the means of a quartz crystal micro balance. During physical vapor deposition a part of the material beam is deposited onto the crystal oscillator and the increase in mass is accompanied by an decrease in vibration frequency.

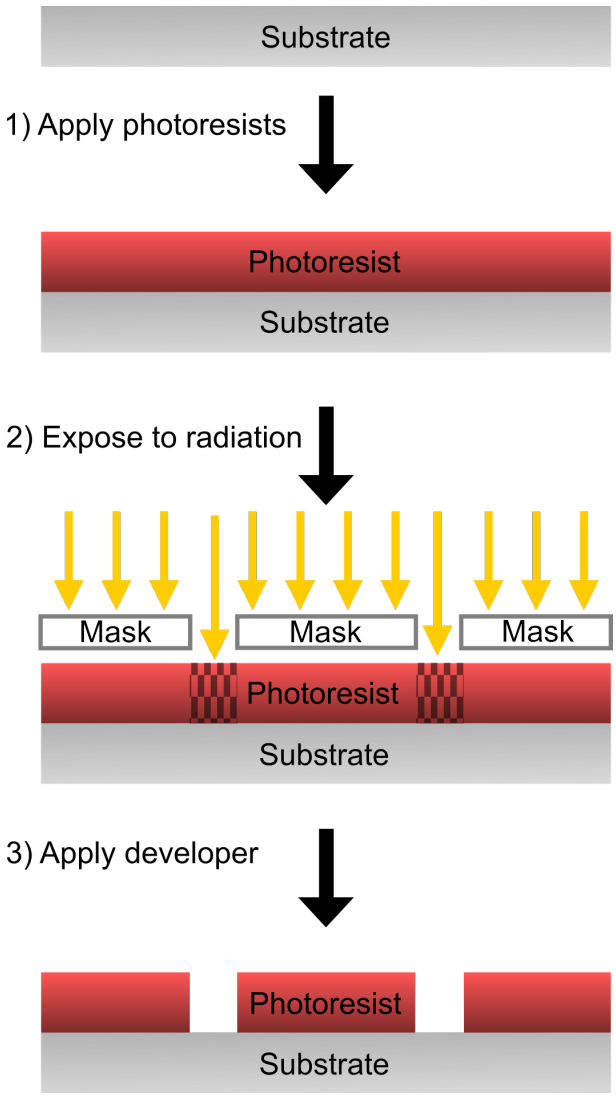

Figure 1.3: schematic photolithography

For a thin and rigid deposited layer this phenomenon can be expressed by the Sauerbrey equation which gives a linear dependency between the deposited mass Δm and the change in vibration frequency Δf.

$$\Delta f = -\frac{2f_0^2}{A\sqrt{\rho_q \mu_q}} \Delta m \tag{1.6}$$

f_0 is the resonance frequency of the fundamental mode and usually between 4 and 6 MHz. A is the piezoelectrically active crystal area. ρ_q denotes the density and μ_q the shear modulus of the crystal oscillator. In order to be able to extract the thin film thickness from this measurement, it is important to calibrate the micro balance. To do so the extinction coefficient for a material with known density, which also absorbs light in the visible range, is determined. The extinction coefficient is predicted by the combination of AFM and UV/Vis measurements of thin films created from the said material. This material is deposited on a glass substrate while the micro balance is in place and its film thickness is

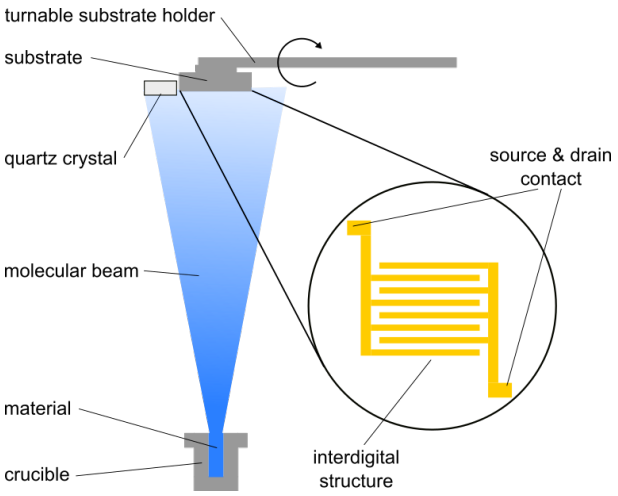

Figure 1.4: schematic of physical vapor deposition

then calculated from UV/Vis measurements. The film thickness and the density of the material can now be used to obtain a general factor c to calculate the thickness of a thin film depending on the change in frequency of the vibration.

$$\Delta f = c^* m = c^* V \rho_m = c^* A d_m \rho_m = c d_m \rho_m \tag{1.7}$$

The deposited mass m can be expressed by the density ρ_m of the material times the deposited volume V, which itself can be expressed by the covered area A and the film thickness d_m. The covered area is solely depending on setup of the PVD and will not change until the experimental setup is changed, which then of course requires a new calibration. Therefore the covered area A is incorporated into the factor c^* to obtain an experiment specific factor c to determine the film thickness for deposition experiments.

1.4 Idea and goal of the project

Very limited research in the field of organic electronics focuses on the investigation of early transition metal complexes, despite their low toxicity and abundance. Further, most of the research in this area resolves around phthalocyanines.[141] Another major class are square planar nickel(II) complexes.[62] Therefore the molecular structures investigated are most times planar or slightly distorted from planarity. The arrangement of such materials by dispersion forces often results in anisotropic crystal structures with the π-systems being stacked upon each other comparable to stacks of coins. In such an arrangement the charge carriers can only be transported in the direction of the stacking effectively. To move into a new direction the idea was to combine the early transition metals with an octahedral coordination sphere with two tridentate ligands with an extended π-system. The resulting complexes will then bear two π-systems perpendicular to each other and allow for a 2D molecular stacking motif. Additionally, the complexes should be neutral. First of all, counter anions might be arranged unfavorable within the crystal structure

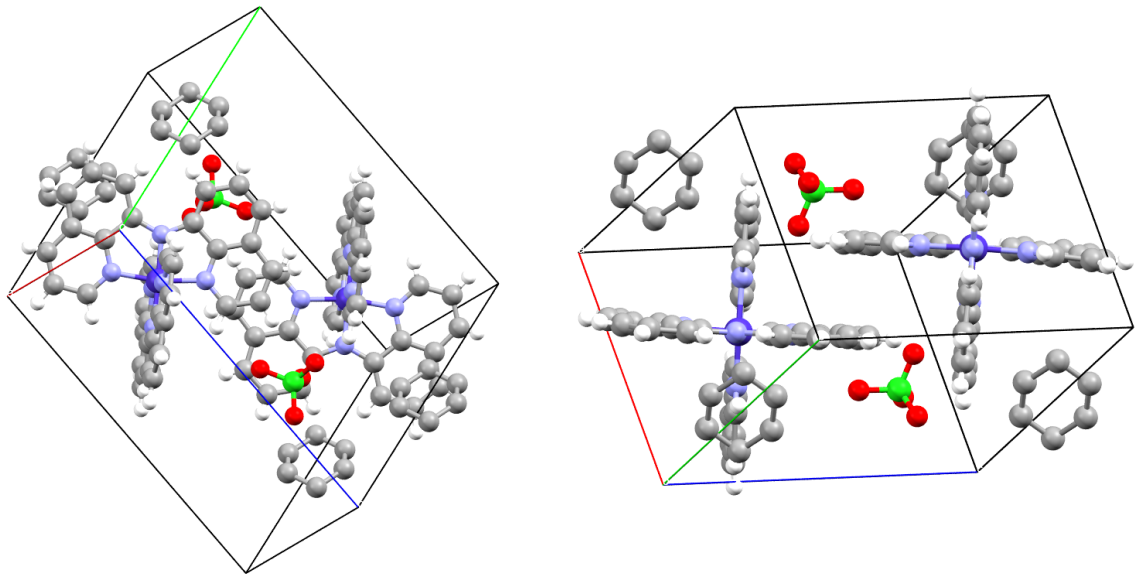

(a) *(b)*

Figure 1.5: Crystal structure of $Co(BQA)_2ClO_4$ viewed from different angles.[140]

and prevent π-systems from overlapping sufficiently. Second, neutral complexes are easier to sublime which allows the use of techniques like physical vapor deposition. A suitable candidate for a ligand was found quickly. *N*-8-Quinolinyl-8-quinolinamide has been used in various transition metal complexes, both neutral and charged.[139, 140, 142–144] But none of the studies investigated the electric properties of these materials. The neutral bis(bis(8-quinolinyl)amide)zinc(II) complex[142, 140] is already a good candidate for the investigation as an organic semiconductor as it combines all desired properties. Additionally, the crystal structure of $[Co(BQA)_2]ClO_4$[140] shows promising arrangement of the ligands with parallel displaced (figure 1.5a) and T-shaped (figure 1.5b) π–π-interactions despite the appearance of perchlorate anions within the crystal cells. The neutral $Fe(BQA)_2$ was accessible by the reduction of $[Fe(BQA)_2]BPh_4$ and an attempt towards its synthesis confirmed its availability but isolation had not been achieved yet.[143] Other octahedral and neutral complexes included cadmium(II), mercury(II)[142] or ruthenium(II).[143] But as these elements are rare and and in the cases of cadmium and mercury also toxic, their application was not in our interest. Other studies looked into square planar metal centers like copper(II)[145] or nickel(II), palladium(II), and platinum(II)[144], which did obviously also not meet the requirements for this investigation.

With these information gathered the objectives were set. First the neutral bis(bis(8-quinolinyl)amide)zinc(II) complex **1a** was meant to be synthesized by a literature procedure. Its counterparts containing Fe(II) **2a**, Cr(II) **3**, and Mn(II) **4** were then to be obtained next (see figure 1.6 for molecular structures). The molecular structure and the crystal packing should be then investigated, their redox properties and UV/Vis absorption measured and tested whether they might be used as organic materials in OFETs. After these initial tests were successful the scope of the project was expanded and as a next step a variety of ligand derivatives were designed. The 6-positions of the quinolinyl moieties seemed

to be the most suitable spots for substitution. It was synthetically easily accessible, a substitution in these positions should not interfere with π–π-stacking and the introduction of side chains orthogonal to the stacking direction was already proven as a working concept in organic electronics.

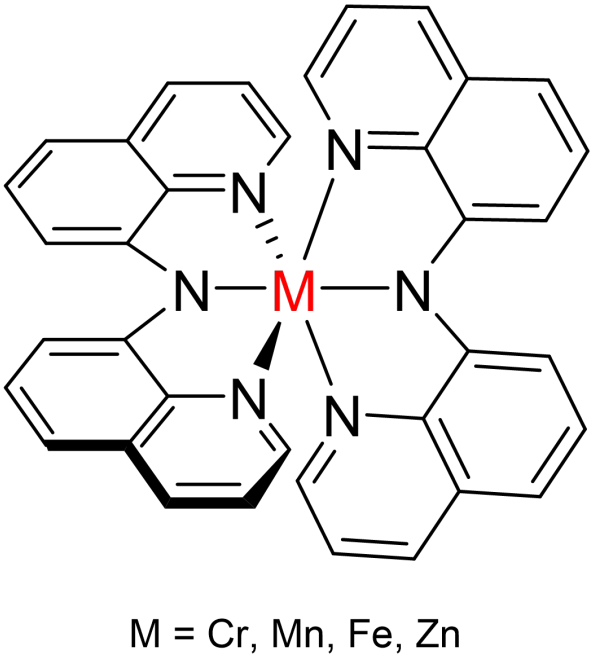

Figure 1.6: Proposed molecular structure for the target complexes

2 Results & discussion

*This project is part of a collaboration of the groups of Prof. Derck Schlettwein and Prof. Peter R. Schreiner. Some of the results presented here were submitted as a publication with Dr. Georg Albrecht and myself as the shared lead authors. During the project Dr. Georg Albrecht took care of device fabrication, thin film preparation and the interpretation of these results. He also prepared single crystals by sublimation. After his graduation he was succeeded by Pascal Schweitzer, who took over the aforementioned tasks. A broad number of people from the Schlettwein group, including Dr. Georg Albrecht, Pascal Schweiter, Thi Hai Quyen Nguyen, Sophie Göbel, and Clemens Geis measured cyclovoltammograms, UV/vis spectra and conducted AFM measurements, provided the data and suggested interpretation thereof. XRD structure determination was performed by Dr. Jonathan Becker. The synthesis of compound **5i** and its precursors was achieved by Paul Debes as part of his bachelor thesis under my supervision. Anna McCurry supported my efforts with synthetic work as an exchange students as a part of the Liebig-College program under my supervision. Mass specotrommetry, NMR- and IR-measurements were conducted by the analytical department of the Justus-Liebig-Universität Gießen. DFT calculations, design and execution of synthetic routes, preparation of single crystals from solution and the interpretation of all data with respect to the influence of the molecular structure of the constituents were performed by me unless stated otherwise.*

2.1 Synthesis

In the beginning of the project *N*-8-Quinolinyl-8-quinolinamine **5a** and its corresponding Zn-complex $Zn(BQA)_2$ **1a** were synthesized according to literature procedures.[142] The iron(II) complex was mentioned in literature but its purification was never acchieved.[143] Nevertheless, the synthesis of the iron(II) **2a**, chromium(II) **3**, and manganese(II) **4** complex was performed by deprotonating the ligand precursors **5a** with potassium *tert*-butoxide followed by the addition of the corresponding metal(II) chloride salt under the inert atmosphere of a nitrogen-filled glove box. The complexes were purified either by crystallization or extraction depending on their solubility. Successful synthesis was shown by mass spectrometry, IR spectroscopy and XRD-analysis of single crystals.

After the initial success of the bis(bis(8-quinolinyl)amide)metall(II) complexes, substituted versions of the complexes bearing addtional functional groups on the ligands seemed promising. In order to obtain these substituted ligand precursors **5a** – **h**, a synthetic scheme was applied that worked for most target structures including those, which were substituted with methoxy, fluro or alkyl groups. First both "halves", meaning the individual quinolinyl moiteity, of the ligand were synthesized and these were then combined by a

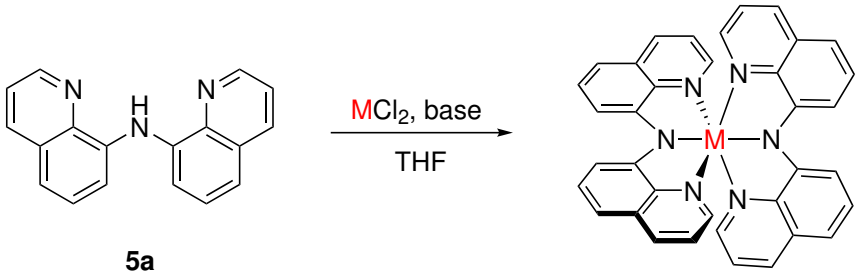

Scheme 2.1: Synthesis of the unsubstituted M(BQA)$_2$-complexes

Buchwald-Hartwig-coupling. Therefore one half had to contain an amine function, while the other contained a bromo substituent. The first step for each "half" is to create the quinoline moiety by a Skraup reaction. This reaction was known to be suitable for the generation of functionalized bromoquinolines[146, 147] and nitroquinolines[148]. To create the 8-bromo-substituted quinolines **6b** – **h**, 2-bromo-anilines are subjected to a reaction with glycerol, sodium 3-nitrobenzenesulfonate and iron(II) sulfate heptahydrate in methanesulfonic acid (scheme 2.2). Yields for this reaction ranged from fair to very good depending on the substrate.

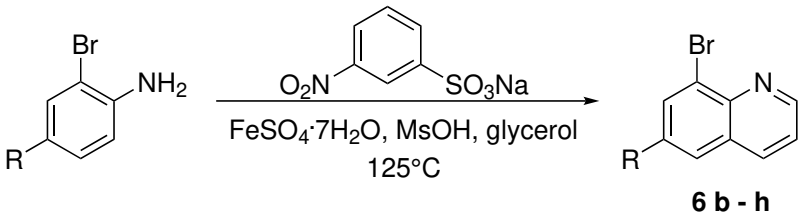

Scheme 2.2: Skraup synthesis towards 8-bromo-quinolines

The 8-amine subsituted quinolines were accessed from the corresponding nitroquinolines. Those were obtained by the means of Skraup reaction. To generate compounds **8b**, **8c** and **8e** – **h** 2-nitroanilines and glycerol were added to a mixture of 3-nitrobenzenesulfonate in diluted sulfuric acid. For compound **8c** the Skraup reaction was performed using sodium iodide and concentrated sulfuric acid.[149] Yields of the intermediate nitro compounds **8b** – **h** were mostly poor and sometimes at least fair. After purification of the material the nitro group is catalytically reduced by hydrogen with palladium on charcoal[150, 148] in methanol, which resulted in excellent yields of compounds **7b** – **h** (scheme 2.3).

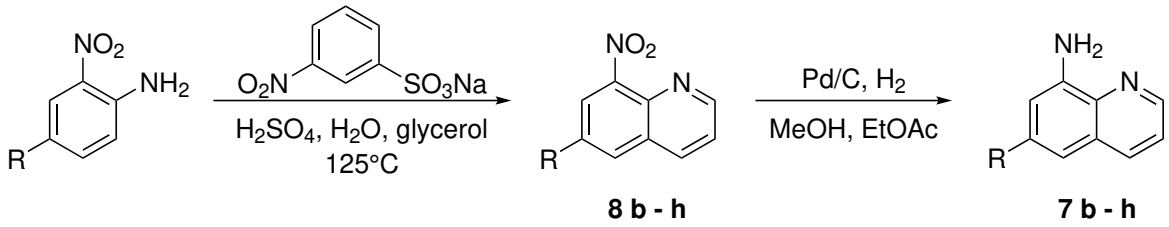

R = b) Me, c) Et, d) ^{i}Pr, e) ^{t}Bu, f) ^{n}Bu, g) F, h) OMe

Scheme 2.3: Synthetic steps towards 8-amino-quinolines

For the final step towards the ligand precursors **5a** − **h**, tris(dibenzylideneacetone) dipalladium(0) and *rac*-BINAP were dissolved in toluene and the corresponding bromo **6b** − **h** and amino **7b** − **h** quinolines were added as well as sodium *tert*-butoxide. These mixtures were heated to reflux for several days. After purification ligand precursors **5b** − **h** were obtained in a wide range of yields reaching from poor to very good depending on the substituents (scheme 2.4).

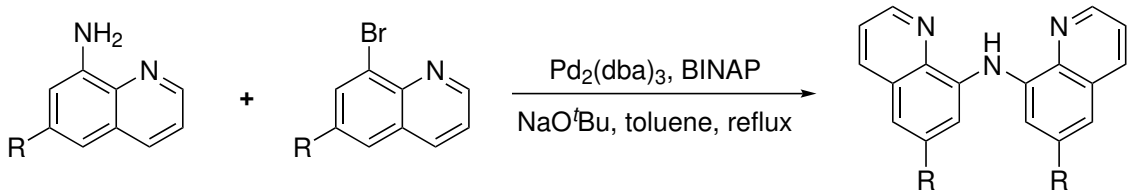

R = a) H b) Me c) Et d) ^{i}Pr e) ^{t}Bu f) ^{n}Bu g) F h) OMe

Scheme 2.4: Buchwald-Hartwig coupling to obtain the ligand precursor

Also the nitrile substituted ligand precursor was obtained, but as nitrile groups were sensitive to strong acids especially when increased temperatures were applied, the synthetic approach used so far was not suitable. A different synthetic route was applied instead (scheme 2.5). First 6-bromo-8-chloro-quinoline **9** was obtained by subjecting 4-bromo-2-chloro-aniline to Skraup reaction conditions. Therefore the aniline was mixed with glycerol, sodium 3-nitrobenzenesulfonate and iron(II) sulfate heptahydrate in methanesulfonic acid and the target material **9** was obtained in very good yield. In the next step the bromo group was substituted with cyanide originating from iron(II) hexacyanoferrate. The whole process was catalyzed by allylpalladium(II) chloride dimer and xantphos, which resulted in quantitative yields of the 8-chloro-6-quinolinecarbonitrile **10**. A part of the product **10** was transformed to the corresponding amine **11** by first performing a Buchwald-Hartwig-coupling with benzophenone imine catalyzed by palladium(II) acetate and xantphos. The intermediate product was then hydrolyzed with aqueous hydrochloric acid to obtain 8-amino-6-quinolinecarbonitrile **11** in good yield. At last, both corresponding quinoline compounds **10** and **11** were again subjected to a Buchwald-Hartwig-coupling with

palladium(II) acetate and *rac*-BINAP forming the catalyst *in situ*. The target compound **5i** was obtained in good yield.

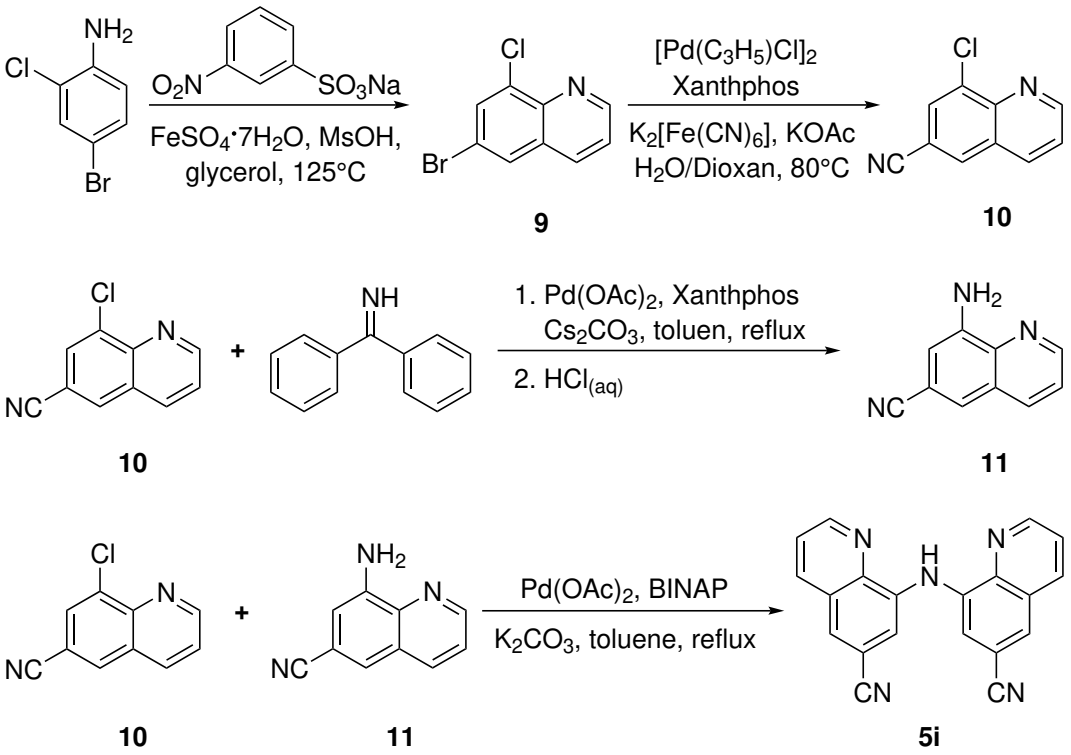

Scheme 2.5: Sythetic approach to obtain the nitrile substituted ligand precursor

As the $Zn(BQA)_2$ **1a** and $Fe(BQA)_2$ **2a** showed the most promising properties for electronic devices all following complex synthesis were performed using only iron and zinc salts, omitting the synthesis of additional chromium and manganese complexes. To achieve synthesis the ligand precursors **5b** – **i** were dissolved or suspended in THF and a base, either KO^tBu or NEt_3, was added. Subsequently, zinc(II) chloride or iron(II) chloride were added to the mixture. The materials were again purified by extraction or recrystallization depending on their solubility.

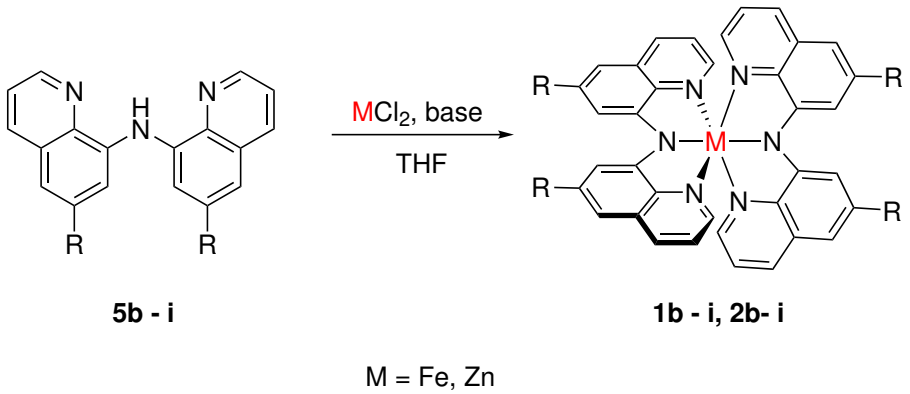

Scheme 2.6: Sythesis of the substituted iron(II) and zinc(II) complexes

2.2 Analysis of the unsubstituted Cr, Mn, Fe, and Zn-complexes

2.2.1 Crystal structure analysis

The packing of complex molecules within the crystal structures obtained is of the main interests in this study. The alignment of π-systems is predicted to be a major factor for charge carrier mobility in organic semiconductors and so the study of their arrangement might be linked to device performance. But it is also important to not over-interpret results. Materials in thin-film devices might be amorphous or their morphology might be very different from the one observed in crystals of them obtained from solution. Nevertheless the behavior in solution might give hints for the suitability and the necessary processing of materials for later use. For that reason some of the electric behavior of devices created from these materials is already mentioned here despite being discussed in detail later.

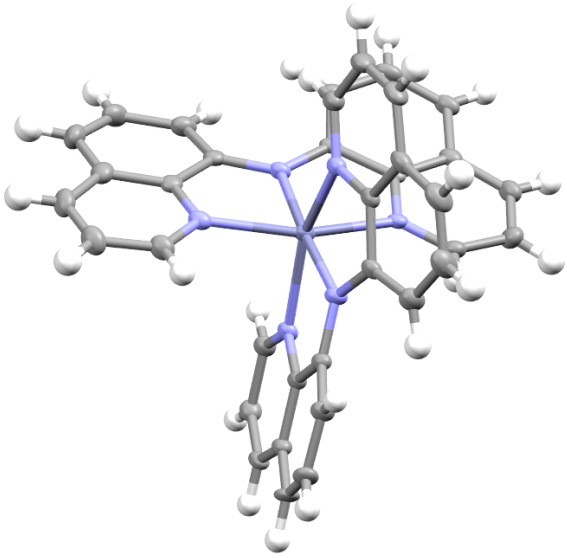

Figure 2.1: Molecular structure of $Zn(BQA)_2$ **1a**

When **1a** was crystallized from solution, a hexagonal cell with a = b = 20.965 and 13.596 Å was obtained (figure 2.2a). The space group was $P6_1$. Each unit cell contained six complex molecules, which were such arranged, that cavities formed channels within the crystal filled with solvent molecules. The ligands' π-systems did not occupy a co-planar alignment, suggesting that π–π-interactions were not the dominating factors for crystal growth and were comparable weak. Additionally, crystals were grown by sublimation in vacuum. This resulted in a monoclinic crystal cell with the dimension a = 19.562, b = 13.471 and c = 22.595 Å, β = 113.99° and the space group $C2/c$ (figure 2.2b). Ligands again did not occupy a co-planar alignment. The cavities that were prior formed and filled with solvents did not occur in this case.

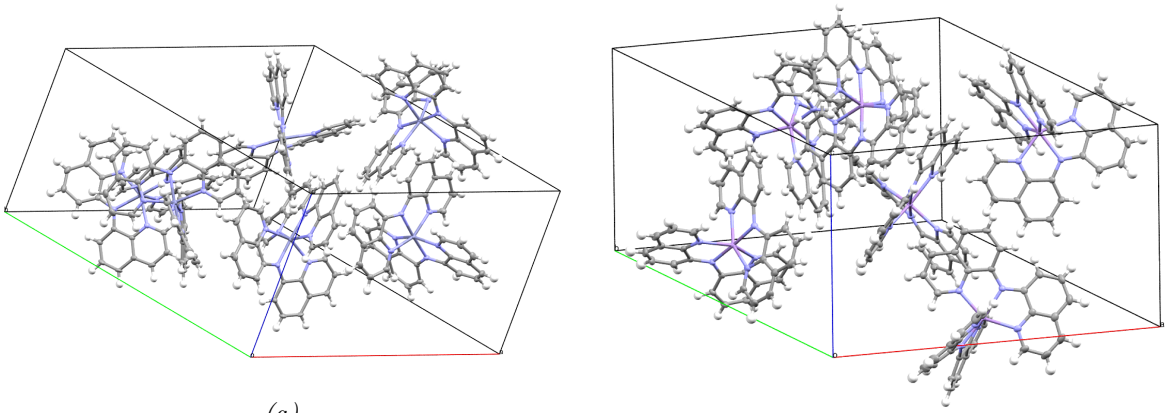

(a) *(b)*

Figure 2.2: Molecular structure of $Zn(BQA)_2$ **1a** obtained from a) solution or b) sublimation, solvent molecules omitted for clarity

The crystals obtained from the Fe-complex **2a** form a triclinic unit cell with the lengths a = 11.858, b = 12.237, c = 12.268 Å and the angles α = 90.36, β = 101.55, and γ = 116.95° (figure 2.3). In contrast to **1a** the π-systems have a co-planar alignment resulting in a combination of parallel displaced and T-shaped π–π-interactions due to the three-dimensional molecular structure. The complexes are ordered in such a fashion, that they form 2D-layers of π–π-interacting complexes. Between these layers electron density is measured, this is attributed to solvent molecules, which were not able to be refined for the structure analysis.

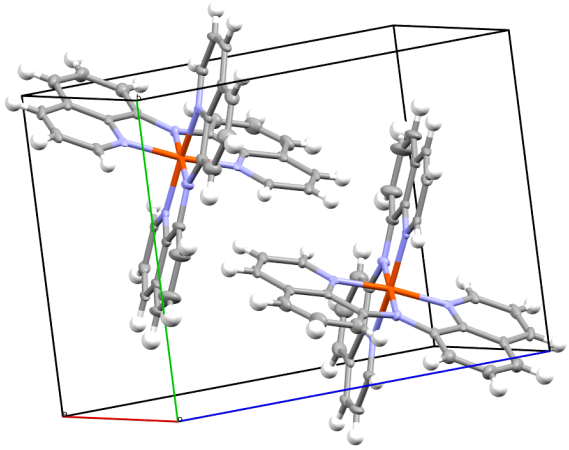

Figure 2.3: Molecular structure of $Fe(BQA)_2$ **2a**, solvent molecules omitted for clarity

When the Cr-complex **3** was processed with THF and crystals were grown from solution, crystals with a triclinic unit cell having the dimensions a = 9.072, b = 12.758, and c = 16.071 Å, α = 81.03, β = 75.69, and γ = 79.30° (figure 2.4a) were obtained. Six THF molecules can be found within the unit cell. Like in the case of the iron complex **2a** the π-systems of the ligands arrange, such that parallel displaced and T-shape configurations can be observed. Other than in the case of the iron complex **2a**, the chromium complex **3**

forms a three-dimensional network of π–π-interactions with the THF molecules filling voids between the individual complexes. When complex **3** was processed with DCM and crystals were grown, crystals containing the oxidized counterpart $[Cr(BQA)_2]Cl$ were obtained. These crystals were featured with a triclinic unit cell with the dimensions a = 10.774, b = 11.688, c = 15.329 Å and α = 80.558, β = 78.383, and γ = 68.265° (figure 2.4b). Although oxidized, the molecular structure of the complex stays intact and the chloride counter anions are located in vaccancies between the complex. Additionally, four molecules of DCM can be found within the unit cell. Like in case of the unoxidized species of **3**, a 3D-network of π–π-interactions is formed.

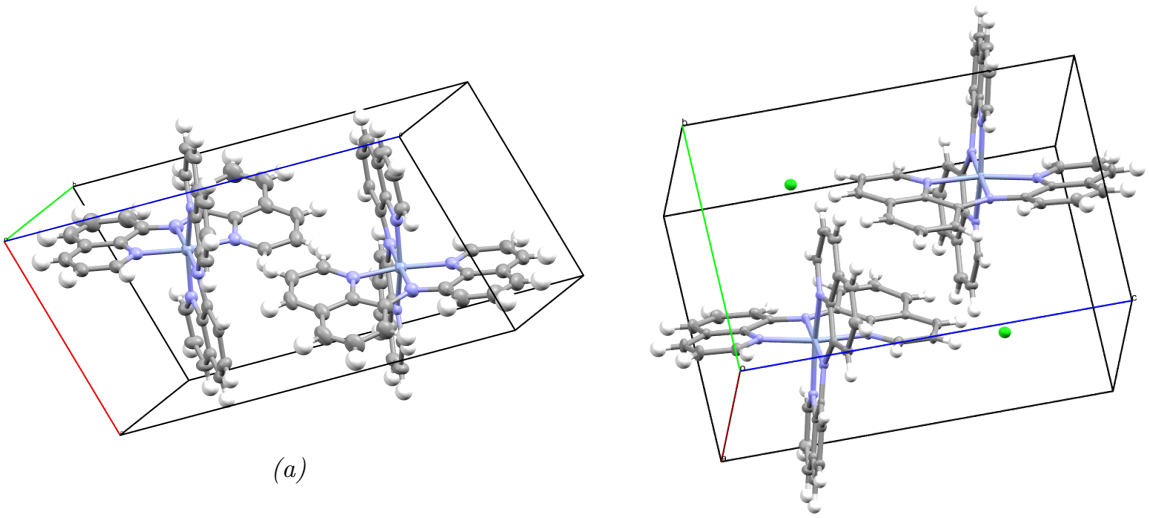

(a) *(b)*

Figure 2.4: Molecular structure of a) $Cr(BQA)_2$ **3** and b) $[Cr(BQA)_2]Cl$, solvent molecules omitted for clarity

4 formed crystals with hexagonal unit cell with the parameters a = b = 20.545, and c = 13.835 Å (figure 2.5). Six complex molecules were found within one unit cell and cavities in the form of channels were shaped. This arrangement resembled the unit cell of the crystals of **1a** obtained from solution. Also there was no co-planar arrangement of π-systems in this case as well.

2.2.2 Comparing computed structural features with measured ones

The molecular structure of the different transition metal complexes **1a**, **2a**, **3**, and **4** looked similar at the first glance. As intended, the metal center was coordinated octahedrically by two *N*-8-Quinolinyl-8-quinolinamide ligands (figure 2.1). At a closer look the structures varied by the sizes of the metal centers resulting in different metal nitrogen bond lengths. The metal centers size was influenced by its spin state, as unpaired electrons require a higher number of orbitals to be occupied, which increased the space needed. As a consequence with larger metal centers the hydrogen atoms at position 7 and 7' repulsed each other, so that the quinolinyl moieties of the individual ligands were not coplanar. To

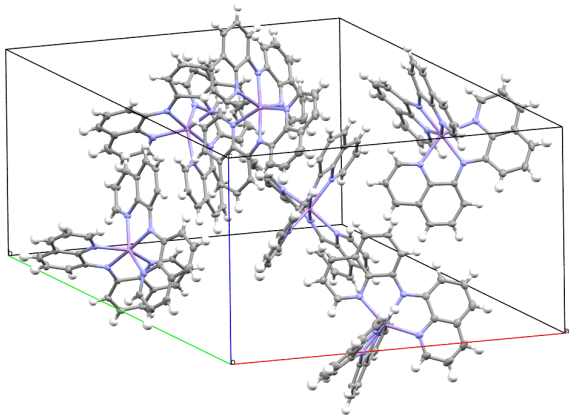

Figure 2.5: Molecular structure of $Mn(BQA)_2$ **4**, solvent molecules omitted for clarity

express this distortion from perfect planarity the dihedral angle between both moeities were taken as a measure. Therefore the dihedral angle obtained from calculating the geometries of the complexes depending on the spin state set for the calculation were compared with the actual dihedral angles. The zinc center in **1a** had completely filled d-orbitals and is therefore large in size. The calculated dihedral angle matched the measured one well (found 23.7°, calc. 25.4°). The small angle measured for the Fe-complex **2a** (found: 5.2°, calc.: 9.7°) suggests the occurrence of d_6 low spin state. For the chromium complex **3** one of the ligands only showed a small dihedral angle (found: 7.9°), while the other ligand was more distorted (found: 19.0°). The angle obtained from theory is somewhere inbetween (calc.: 15.7°), which made predictions quite useless. The manganese complex **4** supposedly had a d_5 high spin system considering the largest dihedral angle to be found in this complex (found 25.8°, calc.: 28.9° for the sextet, 16.8° for the quartet state).

2.2.3 UV/Vis absorption and TDDFT computations

As expected the central metal has a strong influence on the electronic structure of the complexes and the position and strength of the absorption bands. The ligand precursor **5a** shows a strong band at 400 nm, when measured in DMF, which is assigned to a π–π^* transition. A comparable transition is also present for the corresponding transition metal complexes, but it is shifted to higher wavelengths. A correlation between the red-shift of this band (**2a** > **3** > **4** > **1a**) and the decrease in dihedral angle between the quinolyl moieties (**1a** ≈ **4** > **3** > **2a**) can be observed, which is explained by the increased orbital delocalization due to a higher planarity. In the case of the zinc complex **1a** the ligand centered band is located at 500 nm and no bands with even higher wavelengths are present, as there are no possible *d*–*d* transitions as all these orbitals are filled for zinc(II). The manganese complex **4** has a comparable spectrum to that of **1a** below 600 nm. Above that wavelength a domain of weak transitions in the range from 600 to 900 nm is visible, which can be assigned to the spin-forbidden transitions of the *d*-orbitals of the high-spin complex. The chromium complex **3** also shows *d*-*d* transitions but with even weaker intensities for the long wavelengths between 700 and 900 nm. The transitions are not

spin-forbidden in this case as there are only four *d*-electrons present in chromium(II), so the low intensities still lack an explanation. There are two ligand centered transitions for **3** at 450 nm and 580 nm. The iron complex **2a** displays way stronger intensities for the absorption above 600 nm with an absorption maximum at 700 nm. Computations were performed to simulate the transitions of the complexes but failed to achieve sufficient accuracy.

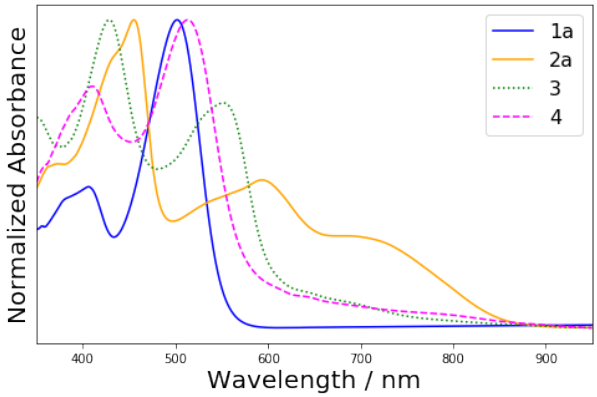

Figure 2.6: UV/Vis absorbance spectra of compounds **1a**, **2a**, **3**, and **4**

Additionally, thin films of these complexes were prepared on glass substrates by vapor deposition. UV/Vis measurements of these films were conducted at various thicknesses from 1 to 20 nm (see figure 2.7), allowing to predict the growth mode of these materials. A red-shift of the spectra was observed for the manganese **4**, iron **2a**, and zinc **1a** complexes compared to the solution, which increased with rising film thickness. A blue-shift was observed for the chromium complex **3** comparing the thin films to the solution, but thicker films were red-shifted compared to thinner ones. Such shifts are caused by changes in the dielectric environment, which, of course, is quite different between solution and a solid film. In general the occurring red-shift for thicker films is the result of the influence of the packing of the materials on the surface. At low surface coverage, with an average film thickness of 1 nm, mainly isolated molecules interact with the surface, while at higher film thicknesses intermolecular interactions dominate. With increasing thickness the band more and more reaches its bulk value.

If a layered growth type is present the peak energy E of an absorption band is dependant on the inverse of the film thickness $1/d$, which can be described by the following equation, which holds true for a dense, closed film with a coverage of more than a monolayer.

$$E(d) = E_{bulk} + \Delta E \cdot \frac{d_{int}}{d} \tag{2.1}$$

Herein ΔE describes the difference in transition energy between interface and bulk molecules. d_{int} denotes the thickness of an optically different interface layer.[151, 152] It is assumed, that the interactions between molecules are highly isotropic, which is reasonable for these highly symmetric complexes. Also the thickness of the films should be proportional to the deposited molecules, which was established *via* a quartz micro

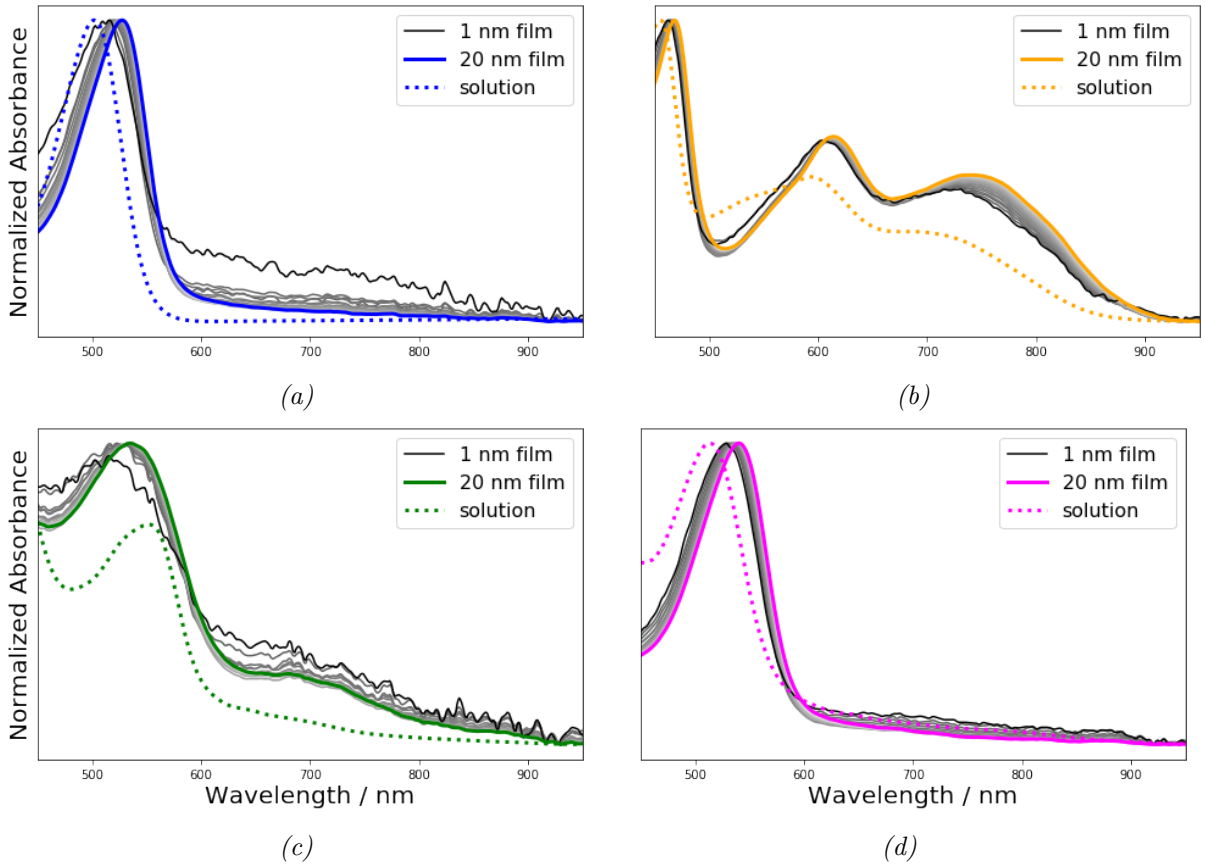

Figure 2.7: UV/Vis absorbance of thin films of a) **1a**, b) **2a**, c) **3**, and d) **4**. Measurements were taken subsequently while deposing the materials. The solution spectrum is plotted for comparison

balance. Therefore roughly a dependence of the transition energy from the inverse of the film thickness d should be visible. By plotting the data (figure 2.8) two regimes are visible for all the complexes, wherein this relation holds true and a hyperbolic fit matches each. Plotting a hyperbolic function for the whole data does result in a worse fit. The first of regimes mentioned before can be explained by the decreasing influence of isolated molecules. The second one is characterized by the changing ratio between interface and bulk molecules. A kink between these two regimes is observed, which marks a change in growth mode, presumably caused by the full coverage of the surface. It occurs at a thickness of 5 nm for the zinc **1a**, iron **2a**, and manganese **4** complex. For the chromium complex **3** this kink occurs already at roughly 2 nm. For the iron complex **2a** and the chromium complex **3** the thickness, at which a measurable current between the electrodes when preparing an OFET sets in, matches the value obtained for full coverage here. This will be presented in the next part in detail.

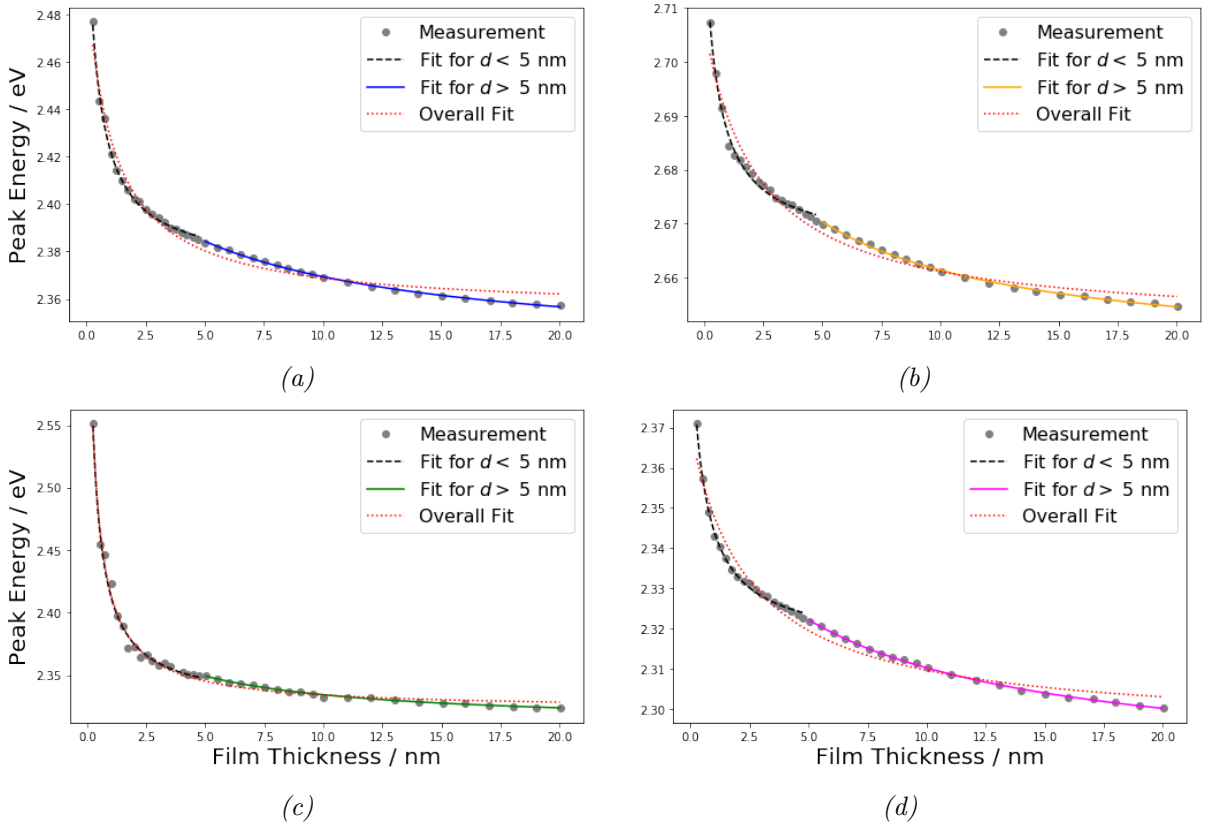

Figure 2.8: Plot of the peak energy against the film thickness of materials a) **1a**, b) **2a**, c) **3**, and d) **4**. A separate hyperbolic fit for low and high film thicknesses returns better results than a fit for the whole range.

2.2.4 Preliminary device fabrication

Device fabrication was solely conducted by the Schlettwein group. None of the results here are due to my own work. They are presented as the project is part of a collaboration and their presentation puts the synthesis and characterization of the discussed materials into a bigger picture.

As a first measure to investigate the suitability of the materials **1a**, **2a**, **3**, and **4** as organic semiconductors is to apply their thin films in a basic bottom gate bottom contact field-effect transistor setup. A straightforward architecture was chosen consisting of a silicon wafer with a thermally grown oxide insulator layer and two interdigitated Gold electrodes. The current between these electrodes was measured while monitoring the thin film thickness during its deposition. For **1a** and **4** no measurable current was observed during device preparation. For **2a** a current set in at roughly 5 nm (see figure 2.9a). It increased linearly up to around 10 nm, after which the current started to flatten out. When applying a linear fit to the region between 6 and 9 nm and extrapolating the fit, the thickness for the current inset is determined to be 5.5 nm. These results can be combined with the ones from the UV/vis analysis of the thin films to generate the following hypothesis. First islands grow on the surface, which are then fully connected at an average

thickness of around 5.5 nm, at which the current flow sets in. After that the remaining gaps between the islands are filled with additional material until the film is fully closed at an average thickness of around 15 nm. Now new island start to grow on top of the existing film, which themselves take no part in charge carrier propagation, which explains the flattening out of the current at the end of the deposition. For the chromium complex **3** the current flow started at a thickness around 2.5 nm. The current increased no-linearly from that point with increasing film thickness and did not reach any plateau. This is also in accordance with the UV/Vis data, because compared to the other complexes, **3** showed a much more uniform growth reaching a closed film already at around 2 nm, which fits the device data.

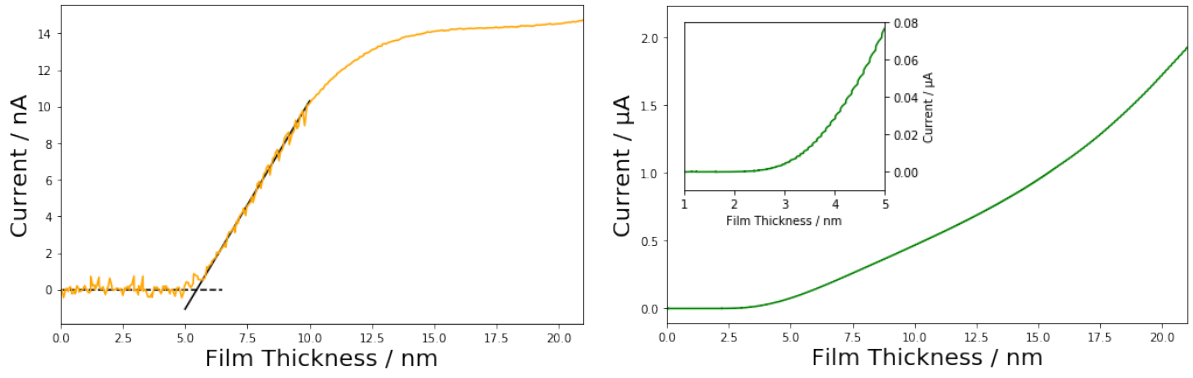

(a) *(b)*

Figure 2.9: Current between the electrodes plotted against the thin film thickness while deposing the material for a) the iron complex **2a**, a fit is applied to linear region between 6 and 9 nm to obtain the minimum thickness of measuring a current b) the chromium complex **3**, a focus on the region around 2.5 nm is added additionally.

For the zinc complex **1a** only small currents in the range of 0 – 100 nA can be observed for negative gate voltages along its films (see figure 2.10). Therefore the material is a p-type semiconductor. The material's conductivity is estimated at $V_G = 0$ V to be $9.5 \cdot 10^{-8}$ S m^{-1}, which is significantly lower than 10^{-4} S m^{-1}, the usual magnitude for organic semiconductors.[153] The charge carrier mobility of **1a** was extracted from the linear regime at 20 V and determined to be $8.2 \cdot 10^{-7}$ cm^2 V^{-1} s^{-1}, which is a quite low value. [62] One possible explanation for these low values might be the absence of parallel aligned quinolyl moieties as was observed in the crystal structure, which results in an unfavorable electron hoping process. The threshold voltage $V_{th} = -30.1$ V suggests the presence of hole trapping states at the semiconductor insulator interface for this device.

The iron complex **2a** outperforms its zinc counterpart in its conducting properties. Currents up to 2.5 µA are reached (see figure 2.11a). The corresponding charge carrier mobility extracted from the linear regime at −50 V equals $7.5 \cdot 10^{-5}$ cm^2 V^{-1} s^{-1}, a value comparable to that of iron(II) phthalocyanine,[154] which is probably the most noted iron(II) species in organic electronics. The increase in performance of the iron complex **2a** compared to the zinc complex **1a** might be explained by the parallel alignment of the molecules' π-systems seen in the crystal structure analysis. In the case of **2a** the threshold voltage

$V_{th} = -6.5$ V is negative, implying the presence of hole trappings states at the inferface layer. An increase in the current is the consequence of exposing the devices with **2a** as the semiconductor to air at 1 mbar. This increase is accompanied with a strongly reduced influence of the gate voltage, which renders the device useless for OFET operation (see figure 2.11b). The cause of this increase is likely the doping of the thin film through the oxidation of the iron(II) to iron(III) complexes by O_2 molecules in air. As the material is hole conducting the oxidation creates additional holes and therefore charge carriers, which in consequence increases the concentration of the later to a value, that is high enough to allow a current flow without an applied gate voltage. To further avoid any complications through air exposure a gate valve was used to transport the material from the glove box to the PVD chamber. This improved handling increased the On/Off ratio to 218 compared to 82 beforehand. The charge carrier mobility stayed in the same realm with a value of $1.0 \cdot 10^{-5}$ $cm^2\,V^{-1}\,s^{-1}$, while the threshold voltage was raised to -11.1 V suggesting a purer film.

Thin films of the chromium complex **3** show a high conductivity directly after deposing them. The gate voltage does nearly have no influence on the source-drain current. Comparable to the iron complex **2a** the chromium complex **3** shows parallel aligned quinolyl moieties in its crystal structure. Also thinking about the absence of this kind of alignment in the zinc **1a** and manganese **4** complexes, this might be one of the causes of the high conductivity of **3**. Exposing the films of material **3** to air even for short times and at low pressure, results in the complete and irreversible loss of conductivity.

For the manganese complex **4** no current was measured at any gate voltage. Also exposure to air does not result in a measurable current. As the material has a similar molecular geometry, crystal behavior and thin film growth like the zinc counterpart **1a**, its semiconducting properties are presumably just not pronounced enough having in mind that also **1a** showed quite poor semiconducting behavior.

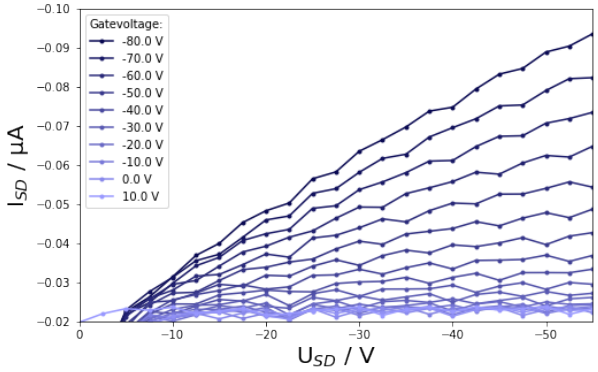

Figure 2.10: Output characteristics of an OFET created with the zinc complex **1a** as the semiconducting layer

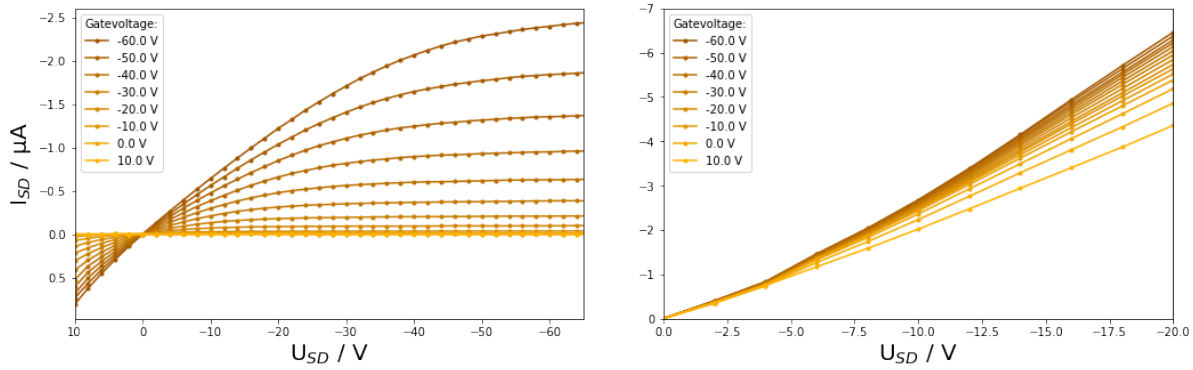

Figure 2.11: a) Output characteristics of an OFET created with iron complex **2a** as the semiconducting layer, b) Output characteristics of the same device after air exposure.

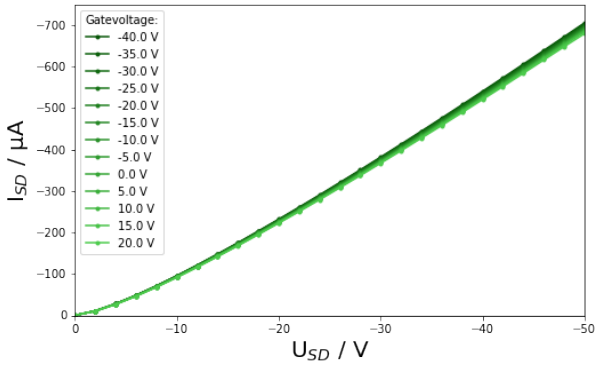

Figure 2.12: Output characteristics of a device created with chromium complex **3** as the semiconducting layer

2.3 Crystal structure analysis of substituted complexes

2.3.1 Substituted zinc complexes

Telling from the crystal structures obtained so far and the measurements from the preliminary devices the compounds showing distinct π–π-interactions, compounds **2a** and **3** resulted in higher currents. Despite other factors being possibly responsible for these findings, for example larger crystal sizes in the thin films and better charge carrier injection, it is interesting to observe how changes in the molecular structure will affect packing of the resulting crystal structure and the electronic behavior. For the rest of the study manganese was dismissed as a central metal as the manganese complex **4** did not show any interesting electronic properties. Chromium was dismissed as complex **3** was very air sensitive, which made processing difficult and the devices made of the complex did only barely show an influence of the gate voltage. It was possible to create OFETs from the zinc **1a** and iron complex **2a**, although the device performance was rather low.

Complex **1b** forms a tetragonal unit cell with the cell lengths a = b = 8.739 and c = 20.149 Å. The molecules form 2D-layers by π–π-stacking and each layer is rotated by 45° towards its neighboring layers. The methyl groups fill all potential vacancies between the layers, which could be occupied by solvent molecules. The zinc-nitrogen bond lengths deviate a bit from the original complex **1a**. They are increased for the zinc-amide bond (2.112 Å compared to 2.074 Å in average for **1a**) and slightly decreased for the zinc-quinolinyl-nitrogen bond (2.149 Å compared to 2.179 in average for **1a**, (see electronic attachment). Following this trend there is also a small dihedral angle of 5.3° between the two quinolinyl moieties of an individual ligand observed. The whole structure looks straightened and one might hypothesize whether these conformational changes paired with the apparently well-ordered stacking motif will result in a well-performing material.

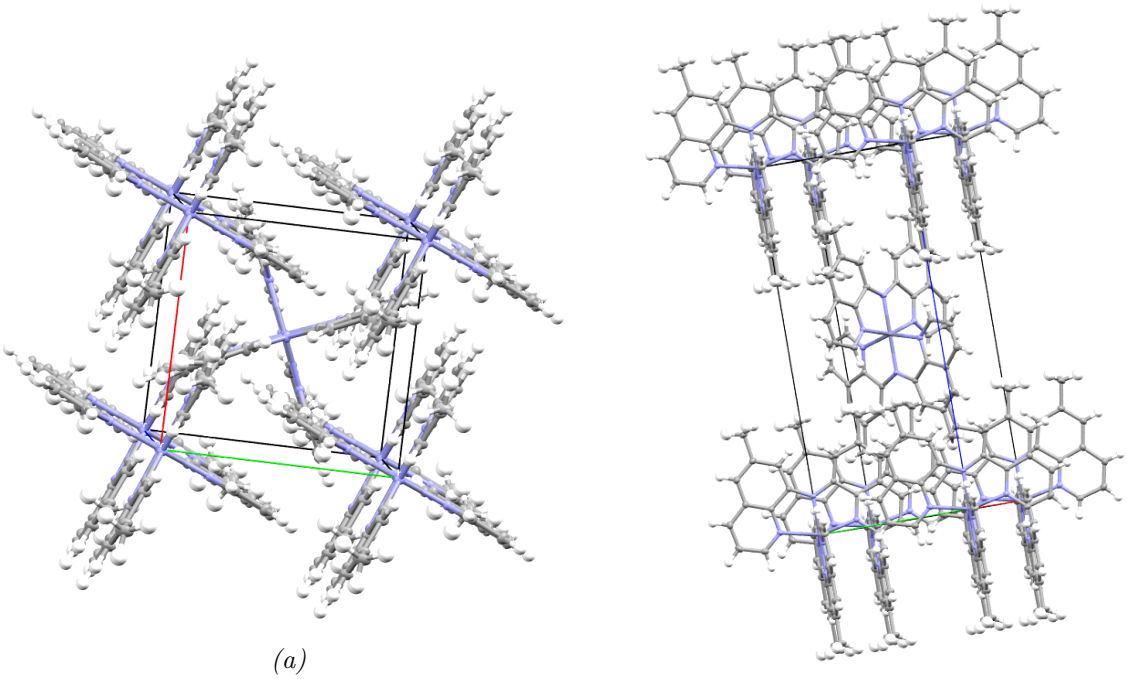

(a) *(b)*

Figure 2.13: Molecular structure of Zn-complex **1b** from different angles

When Zn-complex **1c** was recrystallized from THF/*n*-hexane a monoclinic cell with a = 12.274, b = 29.581, c = 12.403 Å and β = 90.04° was obtained. The structure has some analogies to that of **1b**. 2D-layers are formed, which have parallel aligned π-systems but their overlap is quite limited observing only some T-shaped stacking and no parallel displaced overlap (figure 2.14a). The ethyl groups arrange between the aforementioned 2D-layers.

Instead when **1c** was recrystallized form $CDCl_3$ layered with *n*-hexane it resulted in a tetragonal unit cell with a = b = 16.456 and c = 13.365 Å. In this structure the π-systems form a three dimensional network of interacting complexes (figure 2.14b). There are no distinct layers visible like in crystals obtained from the THF solution. The ethyl groups occupy vaccancies between the quinolyl moieties. A possible hypothesis is, that the

structure obtained from the deuterated chloroform solution might result in better electronic properties. It is an interesting question how the morphology behaves in thin-films and what the result will be for device performance.

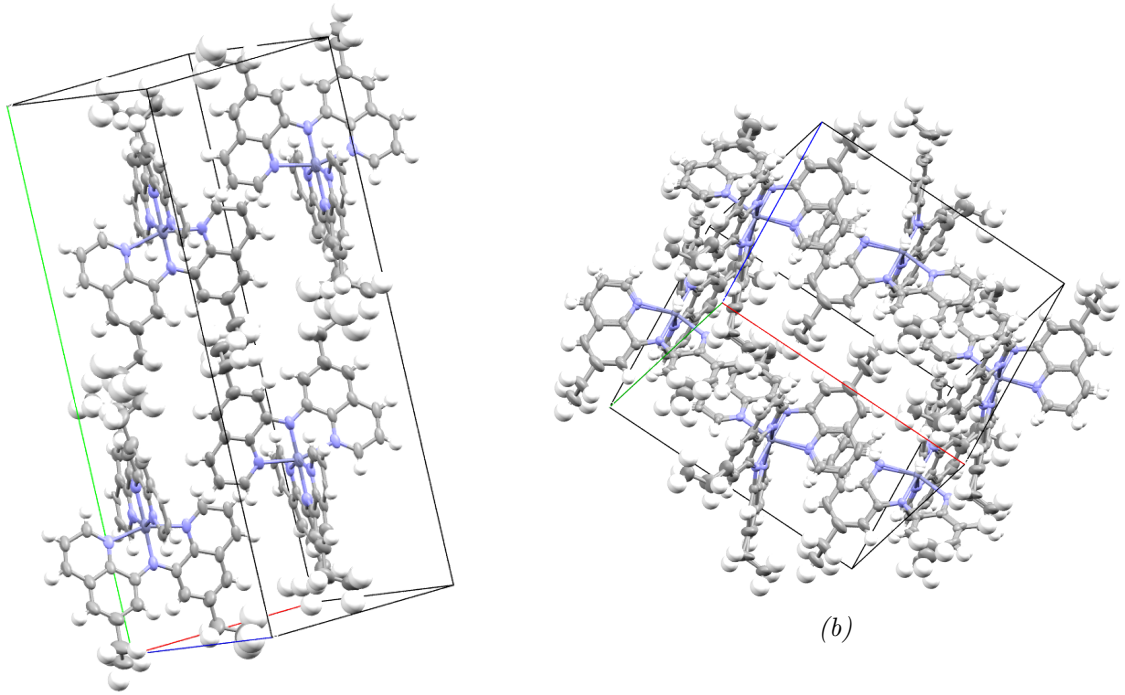

(a) *(b)*

Figure 2.14: Molecular structure of Zn-complex **1c** obtained from a) THF solution and b) $CDCl_3$ solution, solvent molecules omitted for clarity

Zn-complex **1d** formed crystals with a monoclinic cell with the parameters a = 12.321, b = 15.595, c = 12.399 Å and β = 92.02°. Again the complexes form two-dimensional layers with the π-systems aligned co-planar. Edge-to-face stacking can be observed for all quinolyl moities, but parallel displaced interactions are only present in one direction of the formed network. The steric hindrance of the quite large isopropyl groups seem to prevent a closer arrangment and four THF molecules are found in every unit cell within the formed cavities.

A triclinic unit cell was found in the case of zinc complex **1e** with cell dimensions a = 16.952, b = 17.463, c = 17.895 Å and α = 103.90, β = 92.66, γ = 102.10°. Also in this case 2D-layers of complex molecules are formed with co-planar aligment of the qinolinyl groups in only one direction. In the second direction there is only very minor overlap of the π-systems visible in form of a T-shaped interaction. The reason for that seems to be the steric hindrances of the large *tert*-butyl groups, which do not allow further co-planar orientation. The large alkyl groups also result in larger distances between the separate layers, which creates cavities which are filled with THF molecules. Ten of them can be found in each unit cell, which contains four of the complexes.

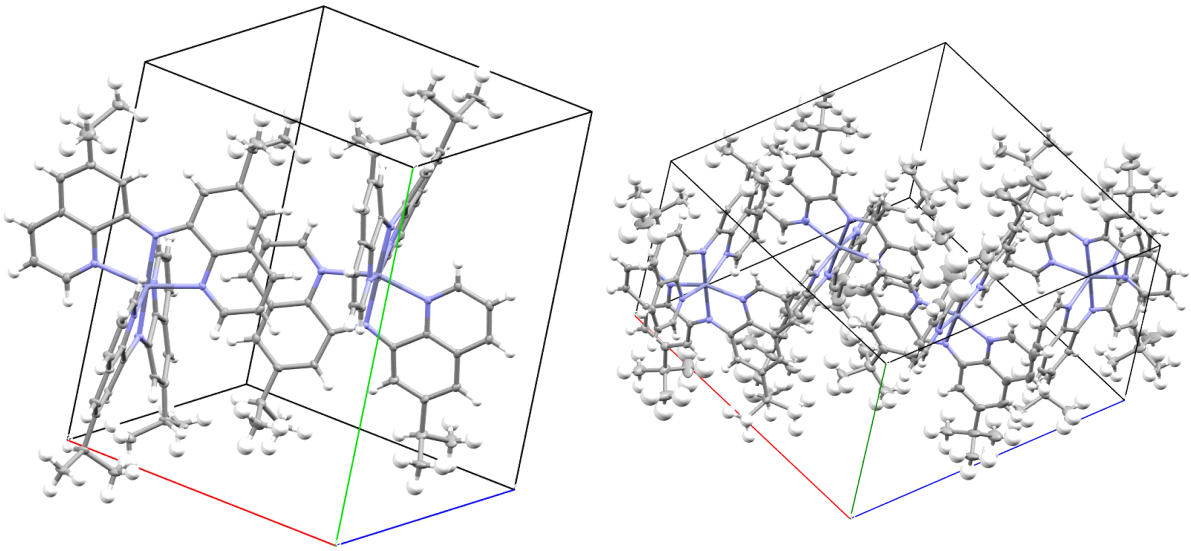

(a) (b)

Figure 2.15: Molecular structure of Zn-complexes a) **1d** and b) **1e**, solvent molecules omitted for clarity

A tetragonal unit cell was found for the butylated complex **1f** with the cell lengths a = b = 12.565 and c = 13.224 Å (figure 2.16a). There are again 2D-layers of complex but in this instance besides the co-planar arrangment of the π-systems only some T-shaped π–π-stacking can be observed. The long n-butyl groups are a arrangend between the quinolinyl moieties and hinder further π–π-interactions. The packing seems to be very dense and no solvent molecules are filling vacancies. But for the limited interactions of the quinolyl systems it is questionable whether this material will perform well as an organic semiconductor.

Complex **1g** crystallizes in a monoclinic unit cell with the parameters a = 19.766, b = 16.340, c = 8.685 Å and β = 97.85° (figure 2.16b). For this complex no distinct π–π-interactions are apparent. The structure is densely packed as no vacancies filled with solvent molecules are found. One of the ligands on each complex shows a nearly completely flat conformation. This structure is an outlier of all the substituted zinc complexes, as it is the only one, which does not show a co-planar arrangement of the π-systems. It will be interesting to see the performance of the material as an organic semiconductor.

Zn-complex **1h** forms a trichlinic unit cell with the dimensions a = 8.720, b = 14.496, c = 17.337 Å and α = 65.71, β = 82.50, γ = 78.20° (figure 2.17a). Also in this case the complex form 2D-layers of π–π-interacting complexes. Comparable with the methylated variant **1b** the two quinolinyl moieties of each ligand are nearly completely co-planar. The methoxy backbones overlap but the carbon-oxygen distance with 3.8 Å is too large for usual C–H$\cdots$O hydrogen bonds, which have a distances of 3.2 Å or less.[155] Vaccancies resulting from this arrangement are filled with DCM molecules and four of them can be found in one unit cell.

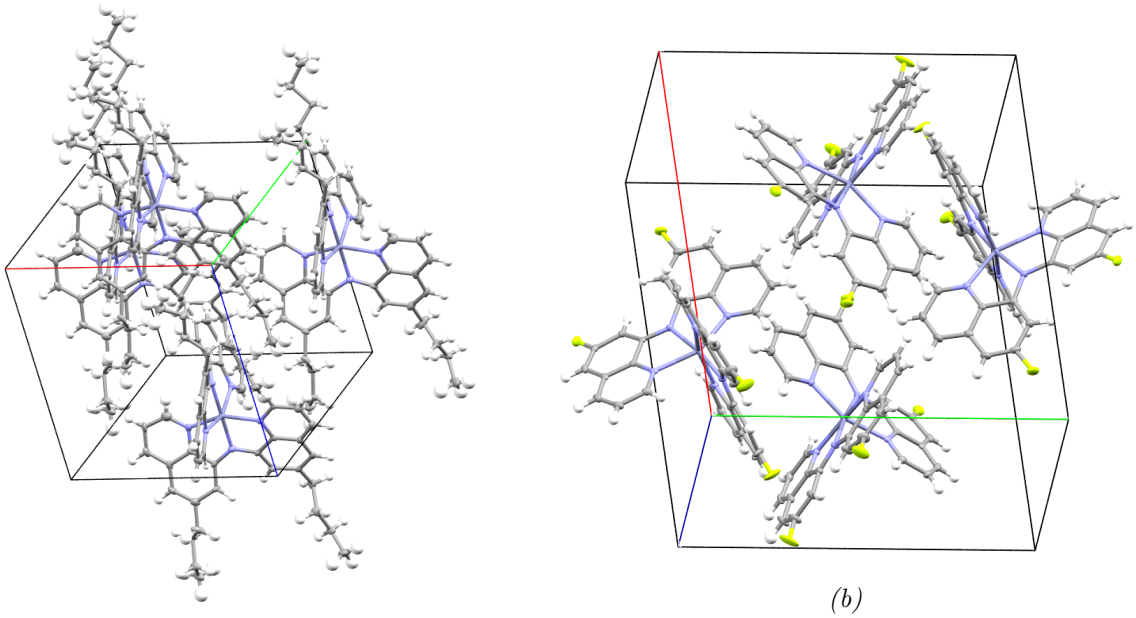

(a) *(b)*

Figure 2.16: Molecular structure of Zn-complexes a) **1f** and b) **1g**, solvent molecules omitted for clarity

Crystal of the Zn-complex **5i** form a monoclinic unit cell with the lengths a = 15.451, b = 15.255, c = 17.020 Å and the angle $\beta = 98.04°$. Again the two dimensional layers of complexes can be observed (figure 2.17b). But despite the observations in all other cases, there is only very limited co-planar alignment of π-systems visible so that some pairs of π–π-stacked complexes form. But overall there is no chain or layer of well aligned complexes. The nitrile groups just seem to be to stiff and too long to allow a closer packing of the molecules. Quite huge cavities are formed, which are filled with *n*-hexane molecules and four of them can be found in every unit cell.

In summary the crystal structure of the methyl substituted complex **1b** seems to be the most promising for the construction of a device. It shows no inclusion of solvent molecules and the π-systems interact favorably. Larger alkyl group substitutions, as it is the case for **1c** − **f**, result in a deviation from that beneficial alignment probably by being too bulky. Fluoro substitution as in **1g** eventuates in a crystal packing without any clear alignment of π-systems. In the case of substitution with methoxy groups, complex **1h** shows co-planar alignment of the quinolyl moieties and a clearly visible stacking motif, but solvent molecules get included into the cell. Nitrile substitution results in a behavior comparable to a large alkyl group and is therefore also not favorable. In summary, the best electric performance of all these zinc complexes is expected for complex **1b**.

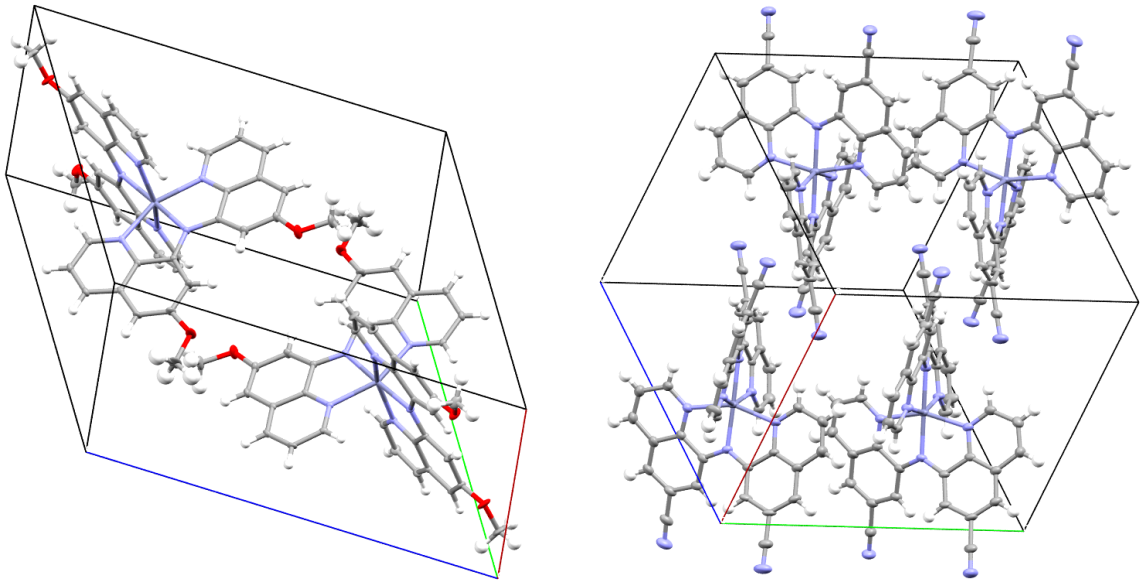

(a) *(b)*

Figure 2.17: Molecular structure of Zn-complexes a) **1h** and b) **1i**, solvent molecules omitted for clarity

2.3.2 Substituted iron complexes

For the methyl substituted iron complex **2b** only a preliminary structure was obtained, only a small and disordered crystal was obtained. Although the data gained is not sufficient to clearly determine the structure, it will be discussed here. Despite its zinc counterpart **2a**, the molecules of **2b** are not arranged in layers where the quinolyl moieties interact *via* π–π interactions (figure 2.18). The arrangement of the complex molecules within the crystal is rather comparable to **1a**, where channel-like cavities are formed, which are occupied by solvent molecules, while there is no co-planar alignment of the π-systems. This is a quite counter-intuitive finding, as the iron complex **1b** showed a high degree of parallel alignment.

For the ethyl substituted complex **2c** no suitable crystals for X-ray analysis were obtained at all and unfortunately this structure cannot be discussed at the moment.

Crystal of the isopropyl substituted complex **2d** are found to be triclinic with the cell dimensions a = 12.094, b = 12.610, c = 16.489 Å and $\alpha = 88.66$, $\beta = 73.19$, $\gamma = 87.45°$ (figure 2.19). Two complex molecules are in each unit cell accompanied by two molecules of THF. Also, in this case it is observed that the complexes form 2D-layers, which have a network of parallel displaced and T-shaped π–π-interactions. These layers are separated from each other by their isopropyl groups and the vacancies between the alkyl groups are occupied by the aforementioned THF molecules. This crystal packing actually resembles that of its zinc counterpart **1d**.

Complex **2e** crystallized in a triclinic cell with a = 17.447, b = 17.630, c = 18.096 Å and $\alpha = 63.23$, $\beta = 79.22$, $\gamma = 88.90°$. The packing is similar to its zinc counterpart **1e**. Two

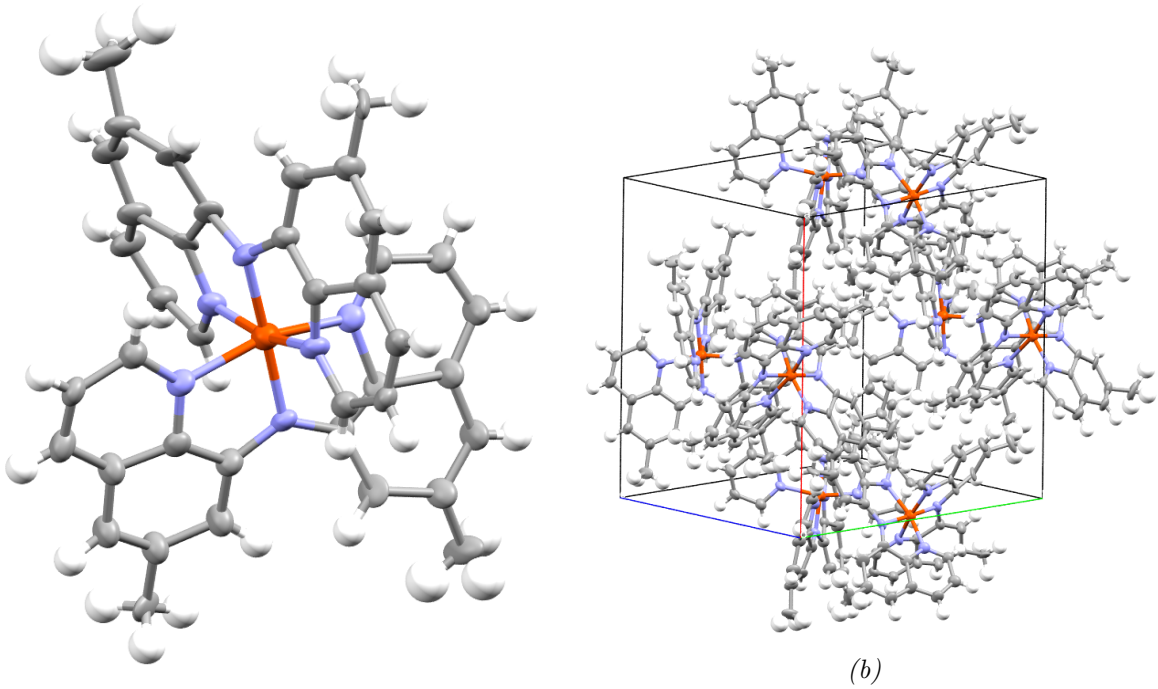

(a) *(b)*

Figure 2.18: Molecular structure of the methyl-substituted Fe-complexe **2b** a) molecular structure b) packing behavior within the unit cell, solvent molecules omitted for clarity. Only a preliminary structure was obtained.

dimensional layers of the complexes are formed. In one direction the π-system stack in prallel displaced and T-shaped fashion. In the other direction only a T-shaped interaction are observable as the alignment of π-systems is not co-planar anymore, due to the steric repulsion of the large *tert*-butyl groups. The vacancies resulting from this arrangement and each unit cells contains four complex molecules as well as eight THF molecules.

The crystals of Fe-complex **2f** form a triclinic cell with a = 12.854, b = 13.122, c = 13.272 Å and $\alpha = 81.72$, $\beta = 74.46$, $\gamma = 75.05°$. The whole structure behaves similar the corresponding Zn-complex **1f**. Also in this case the complexes arrange in layers wherein π-systems arrange co-planar but with only limited T-shaped π–π-stacking. The large alkyl groups prevent a further approaching of the quinolyl moieties. As of this its semiconducting properties might be rather inferior to the other versions of the complex.

A tetragonal cell was found for the fluorinated iron complex **2g** with the parameters a = b = 21.610 and c = 21.401 Å. No parallel alignment of the quinolyl moieties is found in this case. Like for its zinc counterpart **1g**, it is probably caused by the repulsion between the fluoro groups. The complexes are arranged, such that channel-like cavities form. These cavities are filled with solvent molecules and an unidentified species, which seems to be of inorganic origin. As the the crystal structure contains these additional chemicals, its morphology after physical vapor deposition should be quite different from this one.

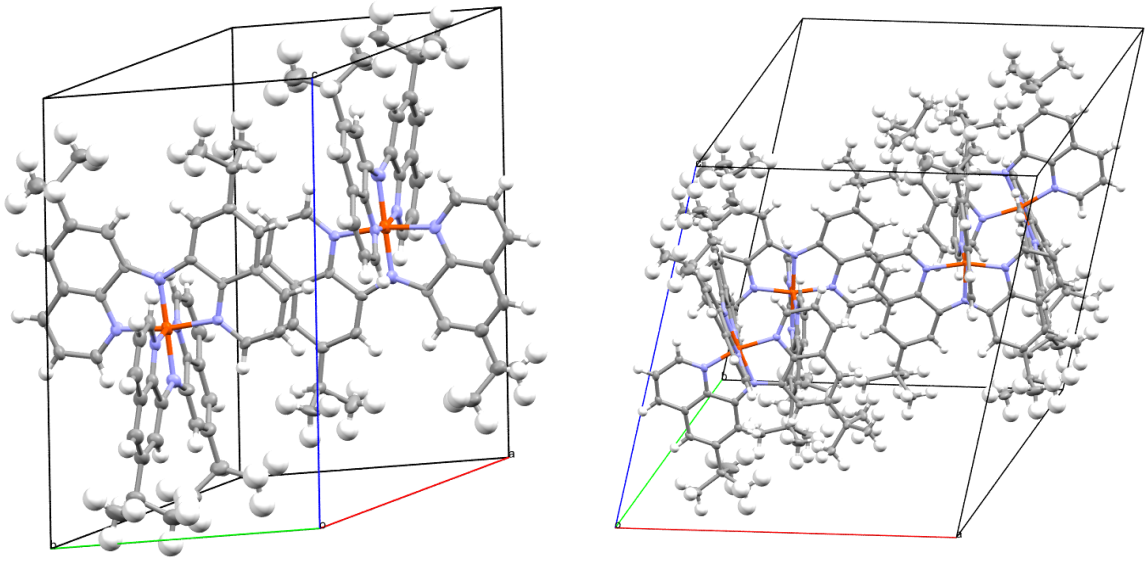

(a) *(b)*

Figure 2.19: Molecular structure of Fe-complexes with a) isopropyl substitution **2d** and b) *tert*-butyl substitution **2e**, solvent molecules omitted for clarity

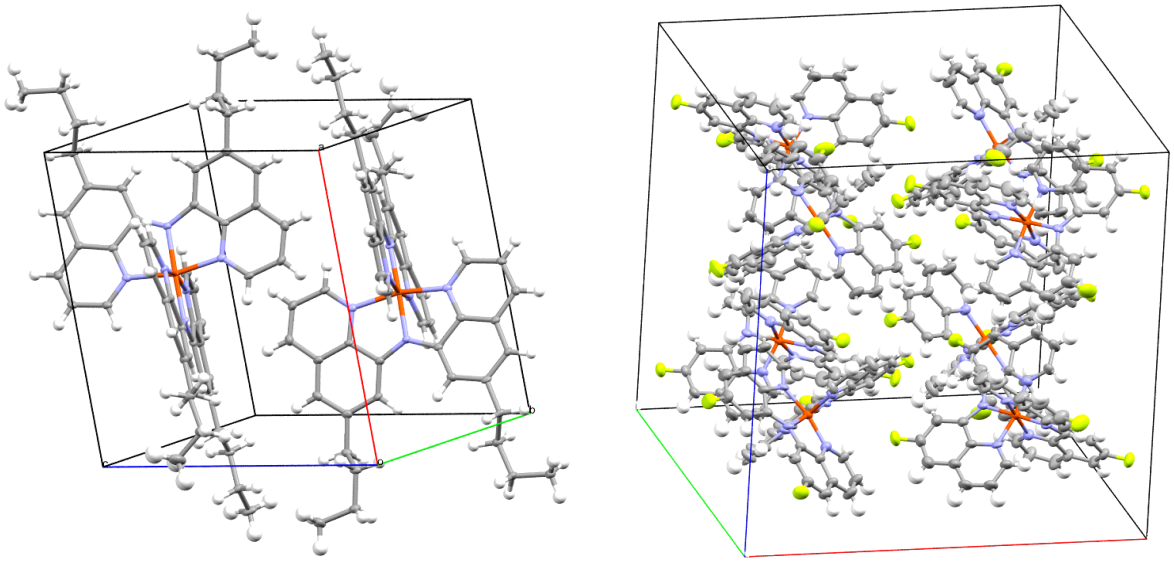

(a) *(b)*

Figure 2.20: Molecular structure of a) complex **2f**, and b) complex **2g**, solvent molecules omitted for clarity

Summary of the crystal structure discussion

In summary alkyl substitution is a useful measure to address the packing of the complexes within the crystal structure. Larger alkyl groups like the isopropyl groups and onwards

tend to have the same effect on zinc and iron complexes. The quinoyl moieties tend towards a coplanar arrangement, but the large size of the groups does not allow that completely. These substitution patterns seem therefore to be not favorable for organic semiconducting devices. Small alkyl groups lead to favorable packing within the realm of the zinc complexes. Especially the methyl substituted complex resulted in a crystal packing with the π-systems aligned parallel with dense layers of π–π interacting complexes. For the case of the iron complexes only a preliminary structure was obtained for the methyl substituted one. This structures differs quite a lot from its zinc counterpart and shows not the desired alignment of the quinolyl moieties.

The substitution with different functional groups resulted in a variety of packing motifs for the zinc and iron complexes. Fluoro substitution resulted in a packing with no co-planar aligments of the π-systems for both, iron and zinc complexes. This is probably caused by the repulsion between the negatively polarized fluoro substituents, which would be in close proximity to each other in a co-planar alignment. Substitution with methoxy groups results in parallel oriented quinolyl moieties for the zinc complex. When nitrile groups are applied to the Zn-complex, only limited π–π interactions of the quinolyl moieties are visible, probably due to the size and stiffness of the nitrile groups, which prevent further approaching.

3 Conclusion & Outlook

3.1 Conclusion

In summary, complexes containing two amide ligands and various metal centers, Cr(II), Mn(II), Fe(II) and Zn(II) were synthesized and their molecular structure and crystal packing was investigated. UV/Vis absorbance was measured in solution and as a thin film. The absorbance behavior of increasingly thick films were used to make statements about the growth mode. It is supposed that first islands grow onto the substrate followed by filling the gaps between the island with additional material until a complete film is obtained. Hereby the zinc **1a**, iron **2a** and manganese **4** complexes behave quite similar, the thin films are red-shifted compared to the solution and a fully closed film is reached at an average film thickness of 5 nm. The chromium complex **3** behaves different. Its thin film is blue-shifted compared to the solution and a fully closed film is already reached at a thickness of 2 nm. OFET devices with these materials as semiconductors were constructed with completely different results based on the central transition metal. The Zinc complex **1a** was a material with quite low charge carrier mobility, but OFETs could be constructed using it. The iron complex **2a** showed a better performance with increased charge carrier mobility, but the devices were sensitive to air. Air exposure led to an increase in conductivity, but due to the high amount of charge carriers present, caused by this kind of doping, the influence of the gate voltage was diminished and the device did not function as an OFET anymore. The chromium complex **3** showed relatively high conductivity but the gate voltage had nearly no influence on the currents measured. The material was very sensitive to oxidation in general and even slight air exposure completely shut down any current. The manganese complex **4** was not useful as a semiconductor at all and showed no interesting electric properties.

Based on these initial findings, manganese was dismissed as a useless central element and chromium was dismissed as being too sensitive to oxidation. Therefore a series of zinc and iron complexes with ligand derivatives were created. The derivatisation always targeted the 6- and 6'- positions of the amide ligand and alkyl groups with varying size and functional groups were introduced. The alkyl groups included methyl, ethyl, isopropyl, *n*-butyl and *tert*-butyl groups. The functional groups involved methoxy, fluoro, and nitrile groups. The crystal structure of these new complexes were investigated and the results were compared in terms of the alignment of the quinolyl moieties.
For the series of the zinc complexes **1b** – **1i** the substitution with alkyl groups in general resulted in a parallel or close to parallel alignment and is therefore an improvement compared to the parent complex **1a**. The methylated version of **1a**, the complex **1b**, was the most promising one with a complete co-planar alignment of the π-systems and the absence of any voids in the crystal structure, that could be filled with solvent molecules. If

larger alkyl substituents were present, the steric hindrance prevented a complete co-planar alignment of the π-systems and voids were created, that were filled with solvent molecules. The substitution with functional groups had varying effects depending on the size and polarity, but none of them resulted in a really promising molecular arrangement.
For the substituted iron complexes **2b** – **2i** not all crystal structure could be obtained yet, unfortunately. These include the structures for the complexes **2b** and **2c** containing methyl and ethyl groups, as well as the structure of **2h** and **2i** containing methoxy and nitrile groups respectively. So far the substitution of ligands with larger alkyl groups has a comparable effect on the arrangement within the crystal structure as observerd for the zinc complexes. The larger alkyl groups lead to deviation from the co-planar alignment of the quinolyl moieties seen for the unsubstituted iron complex **2a**, accompanied by the formation of solvent-filled voids. The fluoro substituted complex **2g** shows the absence of any co-planar alignment of the π-systems like its zinc counterpart **1g**, probably because of the repulsion between negatively polarized fluoro groups. Crystals for the other iron complexes substituted with functional groups were not obtained. The major outlier is the preliminary crystal structure of the methyl groups containing complex **2b**, which, despite its zinc counterpart, does not show parallel alignment of the quinolyl moieties.

3.2 Outlook

As some of the crystal structures for the iron complexes are missing, these data should be acquired first. Then a real comparison between the zinc and the iron series of the substituted complexes should allow to get an idea, how a beneficial arrangement of such complexes is obtained. This might answer the question, how the packing of the crystal structure is influenced best. Also it might be interesting to investigate additional possible metal centers. Candidates are the alkaline earth metals, as they are usually found in the desired oxidation state. The absence of any *d*-orbitals might give insights in the requirements for organometallic species used in electronics.
Next organic field-effect transistors should be created from all the available materials. This will involve the investigation of the growth mode and thin film thickness dependant measurements. So far no advanced methods for device preparation were used. As presented in the introduction the pretreatment of the substrate with alkyl silanes for example can improve the formation of well-ordered thin film. Also heating the substrate while depositing the material followed by slow cooling can improve the crystallinity. As such techniques are crucial for a well-performing device it is necessary to investigate this issue in the future.
Also doping is worth a try in this case. Usually, the inclusion of dopants result in change of the morphology as they do not fit into the lattice of the parent material. But in this case, the different central metals allow the incorporation of possible dopants, that should have only a minor influence on the morphology as the ligands mainly determine the molecular size and shape of the complexes. Therefore, the chromium complex **3** might still be useful as a dopant, that readily gives away an electron, although a device incorporating that material might be still very air sensitive.

Overall this work can be seen as a first step into a new class of materials with a multitude of possible further research. Future researchers will find out, whether these materials, using all the methodes available, will perform on the top level.

4 Experimental

4.1 General

Chemicals and solvents were purchased by commercial suppliers and used as received. All organic compounds were prepared under air unless stated otherwise. Complex preparations were performed in an inert nitrogen atmosphere within a glovebox. High resolution mass spectrometry (HRMS) spectra were recorded on an ESI-MS FinniganLCQ–DUO. Nuclear Magnetic Resonance (NMR) spectra were measured with a Bruker Advance III HD spectrometer at 400 MHz. IR Spectra were recorded on a Bruker Vertex 70 as thin films on BaF_2. IR intensities are denominated as strong (s), moderate (m) and weak (w). Full molecular geometry optimizations at the DFT level of theory were performed using the PBE[156] functional combination as implemented in the Gaussian16 Revision B.01 software package. No symmetry restrictions were applied. Unless mentioned otherwise, we employed a Def2TZVP[157, 158] basis set, which was found to give satisfactory results for the electronic structure computations of transition metal complexes[159].

4.2 Crystallography

Crystallographic data were collected at low temperatures (100 K) using ϕ- and ω-scans on a BRUKER D8 Venture system equipped with dual IμS microfocus sources, a PHOTON100 detector and an OXFORD CRYOSYSTEMS 700 low temperature system. Mo-Kα radiation with wavelength 0.71073 Å or Cu-Kα radiation with wavelength 1.54178 Å and a collimating Quazar multilayer mirror were used. Semi-empirical absorption corrections from equivalents were applied using SADABS-2016/2.[160] The space groups were determined by systematic absences using XPREP and the structures were solved by direct methods using SHELXT.[161] Refinement for all structures was performed against F2 on all data by full-matrix least squares using SHELXL. [162] All non-hydrogen atoms were refined anisotropically and C-H hydrogen atoms were positioned at geometrically calculated positions and refined using a riding model. The isotropic displacement parameters of all hydrogen atoms were fixed to 1.2x or 1.5x (CH3 hydrogens), the Ueq value of the atoms they are linked to. The crystallographic data were deposited at the Cambridge Crystallographic Data Centre as CCDC 1897889-1897893 and can be obtained free of charge. [163]

4.3 Device preparation

In a cleanroom with class ISO 6 a silicon wafer with a thickness of 250 to 300 µm and an silicon oxide layer of 300 nm was cleaned with a stream of dry nitrogen followed by rinsing the wafer at 3000 rpm on a Delta 6 RC spin-coater from Süss Mircotech with acetone and isopropyl alcohol for 45 s. After that the wafer was heated to 180°C at a heating plate for 5 min. HMDS (700 µl) was placed on the middle of the wafer and kept there for 30 s. Then the wafer was again placed on the spin-coater for 45 s at 3000 rpm. The wafer was placed on the heating plate for 60 s at 100°C. Positive photoresist ma-P-1215 (700 µl) was placed on the middle of the wafer and put on the spin-coater for 30 s at 3000 rpm once more. The wafer was placed on the heating plate for 90 s at 100°C. The wafer was then exposed to UV-radiation for 14 s by a MA 56 mask-aligner while a chrome-shadow-mask from Rose Fotomasken was placed on top of it. The wafer was swiveled in ma-D-331 developer solution for 30 to 40 s. This process was stopped by washing the wafer with water and drying it with a stream of dry nitrogen. The quality of the wafer was inspected under an optical microscope.
The following steps were then performed outside the cleanroom. The wafer was placed into a Univex 300 electron-beam evaporator from Leybold. The deposition chamber was evacuated until a pressure of $6.0{\cdot}10^{-5}$ mbar was reached. The target was heated by electron bombardment for 2 min. Then a layer of gold (50 to 60.5 nm) was evaporated onto the wafer with a rate of 1.2 to 1.7 5 $\mathrm{nm\,s^{-1}}$. The evaporation chambered was vented. The wafer was layered with acetone for 45 s, while being placed in an ultrasonic bath. Short pulse of ultrasound (2 to 5 s) were applied to remove surplus gold from the formed interdigital structure. After that, the wafer was placed into fresh acetone and the procedure was repeated until the interdigital structure was fully visible. The wafer was rinsed with isopropyl alcohol and dried with a stream of nitrogen. The quality of the wafer was inspected under an optical microscope and the wafer was tested for short circuits. The particular interdigital structure were then cut out of the wafer.
For the physical vapor deposition interdigital structures with a channel length of 5 µm and a gap width of 15 mm, or structures with a channel length of 10 µm and a gap width of 30 mm were used. One of these interdigital structures were placed into the evaporation chamber. A boron nitride crucible from Lesker was placed in an ultrasonic bath filled with acetone or isopropyl alcohol for 5 min each. The crucible was dried with a stream of nitrogen and heated until being red-hot with a blow-torch. Within a glove box the crucible was filled with the metal-organic material. The crucible was placed into a gate valve and the valve was attached to the evaporation chamber. The chamber was evacuated until a pressure of $1.0{\cdot}10^{-6}$ mbar was reached. The crucible was heated with a heating coil with the exact temperature depending on the used material. It was aimed to achieve a deposition rate of 0.5 ± 0.2 $\mathrm{nm\,s^{-1}}$. This rate was measured indirectly with the support of a quartz crystal micro balance.
The quartz crystal micro balance had previously been calibrated by depositing thin films of CuPc on a glass substrate and using UV/Vis measurements to determine the actual thickness of the thin films.

4.4 Synthesis

Preparation of BQAH and Zn(BQA)$_2$ N-8-quinolinyl-8-quinolinamine (BQAH) and Zn(BQA)$_2$ **1a** were synthesized following literature procedures[139]. Crystals suitable for X-ray structural analysis were grown by vapor diffusion of *n*-hexane into a concentrated solution of Zn(BQA)$_2$ in tetrahydrofuran (THF). Also, crystals were obtained by sublimation at 220 °C and $\sim 10^{-2}$ mbar.

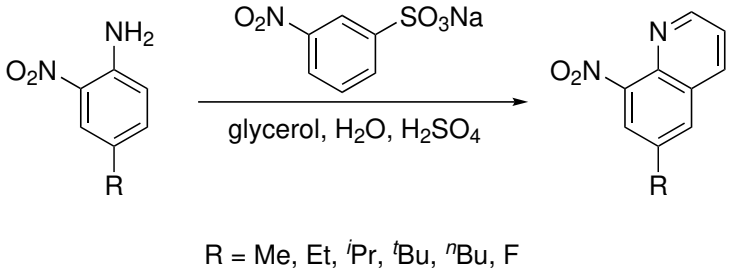

Scheme 4.1: Skraup synthesis of 8-nitroquinolines

6-methyl-8-nitro-quinoline 8b
Sodium 3-nitrobenzenesulfonate (19.3 g, 85.6 mmol, 1.3 equiv.) is mixed with water (16.5 ml) and sulfuric acid (21.0 ml) and this mixture is heated to 100 °C while stirring. Then 4-methyl-2-nitroaniline (10.0 g, 65.7 mmol, 1.0 equiv.) and glycerol (17.3 ml, 237 mmol, 3.6 equiv.) are added. The mixture is further heated to 125 °C and is stirred overnight at this temperature. After cooling to r. t., the mixture is poured into water (400 ml) and the mixture is basified with conc. ammonia solution. The mixture is filtered and the residue is dried, taken up in DCM and filtered over silica. The filtrate is evaporated to dryness and the residue is purified by column chromatography (SiO_2, EtOAc,/Hexane: 10/90 to 25/75) to obtain the target compound (3.08 g, 25 % yield). **IR (ATR):** ν = 3048 (w), 2916 (w), 1520 (s), 1425 (m), 1384 (m) 1358 (m), 1329 (m), 1038 (w), 871 (s), 786 (s), 761 (s), 625 (m) cm^{-1}; **^{1}H-NMR (400 MHz, $CDCl_3$):** δ[ppm] = 9.01 (dd, J = 4.2, 1.7 Hz, 1H), 8.17 (dd, J = 8.3, 1.7 Hz, 1H), 7.90 (d, J = 1.9 Hz, 1H), 7.83 – 7.77 (m, 1H), 7.52 (dd, J = 8.4, 4.2 Hz, 1H), 2.61 (s, 3H); **^{13}{^{1}H}-NMR (100 MHz, $CDCl_3$):** δ[ppm] = 151.8, 148.0, 138.2, 135.8, 135.5, 130.9, 129.1, 125.9, 122.8, 21.4; **MS [ESI]:** m/z = 243.9734 $[M+Na]^+$ (calc. m/z = 243.9732);

6-ethyl-8-nitro-quinoline 8c
Sodium 3-nitrobenzenesulfonate (17.6 g, 78.2 mmol, 1.3 equiv.) is mixed with water (32.6 ml) and sulfuric acid (24.8 ml) and this mixture is heated to 100 °C while stirring. Then 4-ethyl-2-nitroaniline (10.0 g, 60.2 mmol, 1.0 equiv.) and glycerol (13.7 ml, 187 mmol, 3.1 equiv.) are added. The mixture is further heated to 125 °C and is stirred overnight at this temperature. After cooling to r. t., the mixture is poured into water (400 mL) and the mixture is basified with conc. ammonia solution. DCM (100 ml) was added and the layers were separated. The aqueous phase was extracted with DCM (2 × 100 ml). The combined organic phases were dried with Na_2SO_4, the solvent was evaporated and the residue was purified by column chromatography (SiO_2 / DCM) to obtain the target compound (2.22 g,

18 % yield). **IR (ATR):** ν = 3050 (w), 2973 (m), 2938 (w), 2875 (w), 1631 (w), 1591 (m), 1523 (s), 1494 (s), 1459 (m) 1359 (m), 1332 (m), 879 (s), 785 (m), 755 (m). 639 (m), 619 (m) cm^{-1}; **^{1}H-NMR (400 MHz, $CDCl_3$):** δ[ppm] = 9.00 (dd, J = 4.2, 1.7 Hz, 1H), 8.19 (dd, J = 8.4, 1.7 Hz, 1H), 7.92 (d, J = 1.9 Hz, 1H), 7.81 (m, 1H), 7.52 (dd, J = 8.4, 4.2 Hz, 1H), 2.90 (q, J = 7.6 Hz, 2H), 1.37 (t, J = 7.6 Hz, 3H); **$^{13}\{^1$H$\}$-NMR (100 MHz, $CDCl_3$):** δ[ppm] = 151.8, 148.1, 141.9, 138.3, 135.7, 129.6, 129.1, 124.9, 122.7, 28.6, 15.0; **MS [ESI]:** m/z = 225.0633 $[M+Na]^+$ (calc. m/z = 225.0634);

6-(1-methylethyl)-8-nitro-quinoline 8d
Glycerol (5.5 ml, 74.9 mmol, 2.7 equiv.) was heated to 160 °C for 1 h. Then it was cooled to 110 °C. 4-(1-methylethyl)-2-nitroaniline (4.71 g, 27.7 mmol, 1.0 equiv.) and NaI (0.830 g, 5.54 mmol, 0.20 equiv.) were added. The mixture was heated to 150 °C, sulfuric acid (3.84 ml, 63.7 mmol, 2.3 equiv.) was added dropwise and the mixture was stirred for 1 h. After cooling to r.t., water (20 ml) and DCM (20 ml) were added and filtered through a pad of celite. The pad was washed with DCM (2 × 20 ml). The layers were separated and the aqueous phase was extracted with DCM (2 × 30 ml). The combined organic phase were dried over Na_2SO_4. The solvent was removed and the obtained material was purified by column chromatography (SiO_2, EtOAc,/Hexane: 5/95 to 20/80) to obtain the target material (3.20 g, 53 % yield). **IR (ATR):** ν = 3030 (w), 2956 (w), 2928 (w), 2870 (w), 1634 (w), 1593 (w), 1518 (s), 1381 (m), 1360 (s), 1252 (m), 1039 (m), 883 (s), 783 (s), 755 (m), 655 (w), 620 (w) cm^{-1}; **^{1}H-NMR (400 MHz, $CDCl_3$):** δ[ppm] = 9.02 (dd, J = 4.2, 1.7 Hz, 1H), 8.21 (dd, J = 8.4, 1.7 Hz, 1H), 7.98 (d, J = 2.0 Hz, 1H), 7.83 (d, J = 2.0 Hz, 1H), 7.53 (dd, J = 8.4, 4.2 Hz, 1H), 3.17 (hept, J = 6.9 Hz, 1H), 1.38 (d, J = 7.0 Hz, 6H); **$^{13}\{^1$H$\}$-NMR (100 MHz, $CDCl_3$):** δ[ppm] = 151.9, 148.2, 146.6, 138.5, 135.8, 129.1, 128.3, 123.7, 122.7, 34.1, 23.6; **MS [ESI]:** m/z = 239.0789 $[M+Na]^+$ (calc. m/z = 239.0791);

6-(1,1-dimethylethyl)-8-nitro-quinoline 8e
Sodium 3-nitrobenzenesulfonate (13.5 g, 59.9 mmol, 1.3 equiv.) is mixed with water (11.6 ml) and sulfuric acid (14.7 ml) and this mixture is heated to 100 °C while stirring. Then 4-(1,1-dimethylethyl)-2-nitroaniline (8.30 g, 46.1 mmol, 1.0 equiv.) and glycerol (12.1 ml, 166 mmol, 3.6 equiv.) are added. The mixture is further heated to 125 °C and is stirred overnight at this temperature. After cooling to r. t., the mixture is poured into water (300 ml) and the mixture is basified with conc. ammonia solution. The mixture is filtered and the residue is dried, taken up in DCM and filtered over silica. The filtrate is evaporated to dryness and the residue is purified by column chromatograpy (SiO_2, EtOAc,/Hexane: 15/85) to obtain a brownish oil. The oil was taken up in acetonitrile and was precipitated with water, filtered off and washed with methanol/water (1:1) to obtain the target material as a yellow solid (4.19 g, 39 % yield). **IR (ATR):** ν = 3076 (w), 2959 (w), 1592 (w), 1525 (s), 1394 (w), 1367 (m), 1262 (m), 1193 (m), 1037 (w), 883 (s), 789 (s), 745 (m), 694 (w), 659 (w), 617 (m) cm^{-1}; **^{1}H-NMR (400 MHz, $CDCl_3$):** δ[ppm] = 9.01 (dd, J = 4.2, 1.7 Hz, 1H), 8.23 (dd, J = 8.4, 1.7 Hz, 1H), 8.14 (d, J = 2.1 Hz, 1H), 7.95 (d, J = 2.1 Hz, 1H), 7.53 (dd, J = 8.3, 4.2 Hz, 1H), 1.45 (s, 9H); **$^{13}\{^1$H$\}$-NMR (100 MHz, $CDCl_3$):** δ[ppm] = 152.0, 149.0, 148.1, 138.1, 136.2, 128.9, 127.2, 123.0, 122.7, 35.3, 31.0; **MS [ESI]:** m/z = 253.0945 $[M+Na]^+$ (calc. m/z = 253.0947);

6-butyl-8-nitro-quinoline 8f
Sodium 3-nitrobenzenesulfonate (5.27 g, 23.4 mmol, 1.3 equiv.) is mixed with water (4.5 ml) and sulfuric acid (5.8 ml) and this mixture is heated to 100 °C while stirring. Then 4-butyl-2-nitroaniline (3.50 g, 18.0 mmol, 1.0 equiv.) and glycerol (4.8 ml, 65.7 mmol, 3.6 equiv.) are added. The mixture is further heated to 125 °C and is stirred overnight at this temperature. After cooling to r. t., the mixture is poured into water (250 ml) and the mixture is basified with conc. ammonia solution. DCM (100 ml) is added and the mixture is filtered. The phases are separated. The aqueous phase is extracted with DCM (2 × 50 ml) and the combined organic phases are dried over Na_2SO_4. After evaporation of the solvent the target material is obtained (2.16 g, 52 % yield) and used without further purification. **IR (ATR):** ν =2957 (w), 2930 (w), 2861 (w), 1596 (w), 1529 (s), 1494 (w), 1561 (w), 1355 (m), 1126 (w), 1039 (w), 881 (m), 790 (m), 765 (w), 623 (w) cm^{-1}; **^{1}H-NMR (400 MHz, $CDCl_3$):** δ[ppm] = 9.01 (dd, J = 4.2, 1.7 Hz, 1H), 8.19 (dd, J = 8.4, 1.7 Hz, 1H), 7.92 (d, J = 1.9 Hz, 1H), 7.80 (m, 1H), 7.52 (dd, J = 8.4, 4.2 Hz, 1H), 2.73 (t, J = 7.8 Hz, 1H), 1.79 – 1.66 (m, 2H), 1.41 (dq, J = 14.6, 7.3 Hz, 2H), 0.97 (t, J = 7.4 Hz, 3H); **^{13}\{^{1}H\}-NMR (100 MHz, $CDCl_3$):** δ[ppm] = 151.72, 148.00, 140.71, 138.22, 135.68, 130.33, 129.06, 125.12, 125.10, 122.69, 35.21, 32.99, 22.21, 13.82; **MS [ESI]:** m/z = 253.0946 $[M+Na]^+$ (calc. m/z = 253.0947);

6-fluoro-8-nitro-quinoline 8g
Sodium 3-nitrobenzenesulfonate (15.0 g, 66.5 mmol, 1.3 equiv.) is mixed with water (12.9 ml) and sulfuric acid (16.4 ml) and this mixture is heated to 100 °C while stirring. Then 4-fluoro-2-nitroaniline (8.00 g, 51.2 mmol, 1.0 equiv.) and glycerol (13.5 ml, 65.7 mmol, 3.6 equiv.) are added. The mixture is further heated to 125 °C and is stirred overnight at this temperature. After cooling to r. t., the mixture is poured into water (500 ml) and the mixture is basified with conc. ammonia solution. The mixture is filtered and the residue is dried, taken up in DCM and filtered over silica. After evaporation of the solvent the crude material was recrystallized from MeOH to obtain the target material as orange crystals (3.1 g, 31 % yield). **IR (ATR):** ν = 3076 (w), 1630 (w), 1601 (w), 1530 (s), 1352 (m), 1336 (m), 1236 (m), 1126 (w), 1039 (w), 968 (w), 888 (s), 870 (s), 783 (s), 765 (s) 717 (w), 626 (m) cm^{-1}; **^{1}H-NMR (400 MHz, $CDCl_3$):** δ[ppm] = 9.05 (dd, J = 4.3, 1.7 Hz, 1H), 8.23 (dd, J = 8.4, 1.7 Hz, 1H), 7.86 (dd, J = 7.5, 2.8 Hz, 1H), 7.70 (dd, J = 8.1, 2.8 Hz, 1H), 7.59 (dd, J = 8.4, 4.2 Hz, 1H); **^{13}\{^{1}H\}-NMR (100 MHz, $CDCl_3$):** δ[ppm] = 159.34, 156.83, 151.99 (d, J = 2.8 Hz), 136.80 (d, J = 1.8 Hz), 135.54 (d, J = 5.3 Hz), 129.65 (d, J = 9.5 Hz), 123.56, 115.14 (d, J = 21.1 Hz), 114.63 (d, J = 30.3 Hz); **MS [ESI]:** m/z = 215.0229 $[M+Na]^+$ (calc. m/z = 215.0227);

8-amino-6-methyl-quinoline 7b
6-methyl-8-nitro-quinoline **8b** (1.50 g, 7.97 mmol, 1.0 equiv.) and palladium on charcoal (5.0 % w/w, 0.400 g, 0.188 mmol, 0.024 equiv.) were suspended in methanol (30 ml) under a nitrogen atmosphere. A balloon filled with hydrogen gas was attached and the mixture was stirred until TLC showed complete conversion. The mixture was filtered over celite and the filtrate was evaporated to obtain the target material as a yellow-brownish oil, which was used without further purification (1.21 g, 96 % yield). **IR (ATR):** ν = 3420 (w), 3380 (w), 3285 (w), 3094 (w), 2912 (w), 2852 (w), 1619 (m), 1588 (m), 1504 (s), 1441 (m), 1376 (s), 1336 (m), 1248 (w), 1163 (w), 1120 (w), 1036 (w), 871 (w), 830 (s), 794 (m),

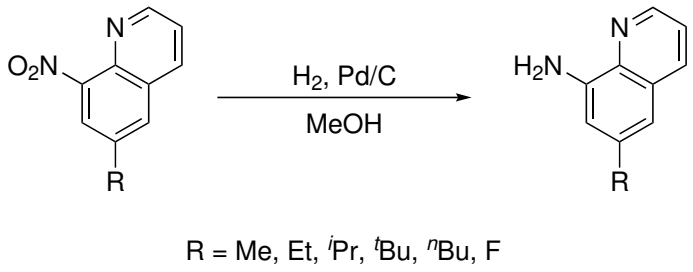

Scheme 4.2: Synthesis of 8-aminoquinolines

778 (m), 692 (m), 637 (m) cm^{-1}; **^{1}H-NMR (400 MHz, $CDCl_3$):** δ[ppm] = 8.68 (dd, J = 4.2, 1.7 Hz, 1H), 7.96 (dd, J = 8.3, 1.7 Hz, 1H), 7.31 (dd, J = 8.3, 4.2 Hz, 1H), 7.08 – 6.87 (m, 1H), 6.78 (d, J = 1.8 Hz, 1H), 4.90 (s, 2H), 2.43 (s, 3H); **^{13}{^{1}H}-NMR (100 MHz, $CDCl_3$):** δ[ppm] = 146.6, 143.5, 137.4, 137.2, 135.3, 129.0, 121.4, 115.4, 112.2, 22.0; **MS [ESI]:** m/z = 159.0920 $[M+H]^+$ (calc. m/z = 159.0917);

8-amino-6-ethyl-quinoline 7c

6-ethyl-8-nitro-quinoline **8c** (2.22 g, 11.0 mmol, 1.0 equiv.) and palladium on charcoal (5.0 % w/w, 0.594 g, 0.279 mmol, 0.025 equiv.) were suspended in methanol (30 ml) under a nitrogen atmosphere. A balloon filled with hydrogen gas was attached and the mixture was stirred until TLC showed complete conversion. The mixture was filtered over celite and the filtrate was evaporated to obtain the target material as a yellow-brownish oil, which was used without further purification (1.79 g, 94 % yield). **IR (ATR):** ν = 3463 (w), 3346 (w), 3028 (w), 2962 (w), 2930 (w), 2869 (w), 1618 (m), 1587 (s), 1501 (s), 1431 (m), 1379 (s), 1242 (w), 1161 (w), 1120 (w), 1037 (w), 883 (w), 843 (s), 788 (s), 617.9 (w) cm^{-1}; **^{1}H-NMR (400 MHz, $CDCl_3$):** δ[ppm] = 8.67 (dd, J = 4.2, 1.7 Hz, 1H), 7.95 (dd, J = 8.3, 1.7 Hz, 1H), 7.28 (dd, J = 8.3, 4.2 Hz, 1H), 6.96 – 6.88 (m, 1H), 6.77 (d, J = 1.7 Hz, 1H), 4.93 (s, 2H), 2.69 (q, J = 7.6 Hz, 2H), 1.27 (t, J = 7.6 Hz, 3H); **^{13}{^{1}H}-NMR (100 MHz, $CDCl_3$):** δ[ppm] = 146.7, 143.7, 143.7, 137.5, 135.5, 129.0, 121.4, 114.0, 111.2, 29.3, 15.4; **MS [ESI]:** m/z = 195.0895 $[M+Na]^+$ (calc. m/z = 195.0892);

8-amino-6-(1-methylethyl)-quinoline 7d

6-(1-methylethyl)-8-nitro-quinoline **8d** (1.50 g, 7.97 mmol, 1.0 equiv.) and palladium on charcoal (5.0 % w/w, 0.400 g, 0.188 mmol, 0.024 equiv.) were suspended in methanol (30 ml) under a nitrogen atmosphere. A balloon filled with hydrogen gas was attached and the mixture was stirred until TLC showed complete conversion. The mixture was filtered over celite and the filtrate was evaporated to obtain the target material as a yellow-brownish oil, which was used without further purification (1.21 g, 96 % yield). **IR (ATR):** ν = 3468 (w), 3363 (w), 3031 (w), 2957 (m), 2867 (w), 1620 (m), 1588 (s), 1502 (s), 1458 (m), 1429 (m), 1376 (s), 1346 (m), 1299 (w), 1244 (w), 1183 (w), 1118 (w), 1079 (w), 1029 (w), 958 (w), 894 (w), 844 (s), 783 (s), 747 (w), 669 (w), 626 (m) cm^{-1}; **^{1}H-NMR (400 MHz, $CDCl_3$):** δ[ppm] = 8.61 (dd, J = 4.2, 1.7 Hz, 1H), 7.91 (dd, J = 8.3, 1.7 Hz, 1H), 7.23 (dd, J = 8.3, 4.1 Hz, 1H), 6.89 (d, J = 1.8 Hz, 1H), 6.77 (d, J = 1.8 Hz, 1H), 4.85 (s, 2H), 2.88 (hept, J = 6.9 Hz, 1H), 1.22 (d, J = 6.9 Hz, 6H); **^{13}{^{1}H}-NMR (100 MHz, $CDCl_3$):** δ[ppm] = 148.2, 146.8, 143.7, 137.7, 135.7, 128.9, 121.3, 112.7, 109.9, 34.5, 23.9; **MS [ESI]:** m/z = 187.1232 $[M+H]^+$ (calc. m/z = 187.1230);

8-amino-6-(1,1-dimethylethyl)-quinoline 7e
6-(1,1-dimethylethyl)-8-nitro-quinoline **8e** (2.00 g, 8.69 mmol, 1.0 equiv.) and palladium on charcoal (5.0 % w/w, 0.470 g, 0.221 mmol, 0.025 equiv.) were suspended in methanol (30 ml) under a nitrogen atmosphere. A balloon filled with hydrogen gas was attached and the mixture was stirred until TLC showed complete conversion. The mixture was filtered over celite and the filtrate was evaporated to obtain the target material as a brownish oil, which was used without further purification (1.71 g, 98 % yield). **IR (ATR):** ν = 3466 (w), 3370 (w), 3035 (w), 2952 (m), 2903 (w), 2866 (w), 1619 (m), 1587 (m), 1502 (s), 1425 (w), 1378 (s), 1239 (w), 1137 (w), 1107 (w), 889 (w), 846 (s), 783 (m), 620 (m) cm^{-1}; **^{1}H-NMR (400 MHz, $CDCl_3$):** δ[ppm] = 8.70 (dd, J = 4.2, 1.7 Hz, 1H), 8.03 (dd, J = 8.4, 1.7 Hz, 1H), 7.33 (dd, J = 8.3, 4.2 Hz, 1H), 7.10 (d, J = 2.0 Hz, 1H), 7.04 (d, J = 2.0 Hz, 1H), 4.90 (s, 2H), 1.38 (s, 9H); **^{13}{^{1}H}-NMR (100 MHz, $CDCl_3$):** δ[ppm] = 150.4, 147.0, 143.3, 137.4, 136.0, 128.6, 121.3, 111.8, 109.3, 34.9, 31.2; **MS [ESI]:** m/z = 201.1384 $[M+Na]^+$ (calc. m/z = 201.1386);

8-amino-6-butyl-quinoline 7f
6-butyl-8-nitro-quinoline **8f** (2.16 g, 9.38 mmol, 1.0 equiv.) and palladium on charcoal (5.0 % w/w, 1.63 g, 0.760 mmol, 0.081 equiv.) were suspended in methanol (20 ml) under a nitrogen atmosphere. A balloon filled with hydrogen gas was attached and the mixture was stirred until TLC showed complete conversion. The mixture was filtered over celite and the filtrate was evaporated to obtain the target material as a brownish oil, which was used without further purification (1.55 g, 82 % yield). **IR (ATR):** ν = 3473 (w), 3373 (w), 2955 (w), 2927 (m), 2856 (w), 1619 (m), 1589 (m), 1502 (s), 1464 (w), 1432 (w), 1380 (s), 1339 (w), 1247 (w), 1162 (w), 1121 (w), 1036 (w), 841 (m), 794 (m), 739 (w), 619 (w) cm^{-1}; **^{1}H-NMR (400 MHz, $CDCl_3$):** δ[ppm] = 8.69 (dd, J = 4.2, 1.7 Hz, 1H), 7.99 (dd, J = 8.3, 1.7 Hz, 1H), 7.32 (dd, J = 8.3, 4.2 Hz, 1H), 6.97 – 6.92 (m, 1H), 6.81 (d, J = 1.7 Hz, 1H), 4.49 (s, 2H), 2.77 – 2.62 (m, 2H), 1.78 – 1.58 (m, 2H), 1.38 (h, J = 7.4 Hz, 2H), 0.94 (t, J = 7.3 Hz, 3H); **^{13}{^{1}H}-NMR (100 MHz, $CDCl_3$):** δ[ppm] = 146.64, 143.60, 142.31, 137.49, 135.45, 128.91, 121.33, 114.84, 111.55, 36.06, 33.39, 22.45, 14.01.; textbfMS [ESI]: m/z = 223.1206 $[M+Na]^+$ (calc. m/z = 223.1205);

8-amino-6-fluoro-quinoline 7g
6-fluoro-8-nitro-quinoline **8g** (2.95 g, 15.3 mmol, 1.0 equiv.) and palladium on charcoal (5.0 % w/w, 0.816 g, 0.383 mmol, 0.025 equiv.) were suspended in methanol (50 ml) and EtOAc (15 ml) under a nitrogen atmosphere. A balloon filled with hydrogen gas was attached and the mixture was stirred until TLC showed complete conversion. The mixture was filtered over celite and the filtrate was evaporated to obtain the target material as a brownish oil, which was used without further purification (2.41 g, 97 % yield). **IR (ATR):** ν = 3473 (w), 3364 (w), 1620 (s), 1591 (s), 1505 (s), 1470 (w), 1433 (m), 1380 (s), 1340 (w), 1239 (w), 1206 (w), 1132 (s), 984 (m), 895 (w), 830 (s), 793 (m), 755 (w), 643 (m) cm^{-1}; **^{1}H-NMR (400 MHz, $CDCl_3$):** δ[ppm] = 8.68 (dd, J = 4.2, 1.7 Hz, 1H), 7.98 (dd, J = 8.3, 1.6 Hz, 1H), 7.36 (dd, J = 8.3, 4.2 Hz, 1H), 6.73 (dd, J = 9.3, 2.6 Hz, 1H), 6.66 (dd, J = 10.6, 2.6 Hz, 1H), 5.14 (s, 2H); **^{13}{^{1}H}-NMR (100 MHz, $CDCl_3$):** δ[ppm] = 161.67 (d, J = 243.9 Hz), 146.40 (d, J = 2.7 Hz), 146.27 (d, J = 13.3 Hz), 135.74, 135.46 (d, J = 5.8 Hz), 129.45 (d, J = 12.4 Hz), 122.24, 99.32 (d, J = 29.2 Hz), 98.58 (d, J = 22.5 Hz); **MS [ESI]:** m/z = 163.0666 $[M+H]^+$ (calc. m/z = 163.0666);

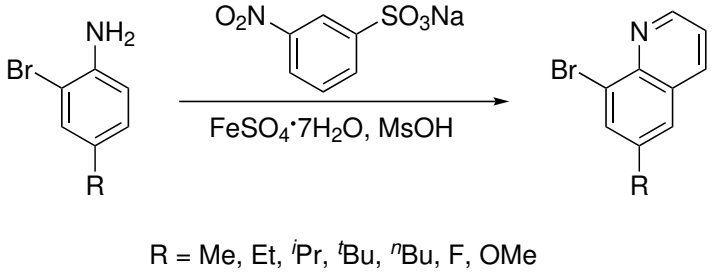

Scheme 4.3: Skraup-synthesis of 8-bromoquinolines

8-bromo-6-methyl-quinoline 6b
Sodium 3-nitrobenzenesulfonate (11.6 g, 51.6 mmol, 1.2 equiv.), $FeSO_4 \cdot 7H_2O$ (0.639 g, 2.30 mmol,0.053 equiv.) and 2-bromo-4-methylaniline (8.00 g, 43.0 mmol, 1.0 equiv.) are mixed with methanesulfonic acid (59 ml) and this mixture is heated to 125 °C while stirring. Then glycerol (17.3 ml, 237 mmol, 3.6 equiv.) is added. The mixture is further stirred at this temperature overnight. After cooling to r. t., the mixture is poured into aqueous NaOH solution (36.5 g, 913 mmol in 300 ml water) while cooling with an ice bath. The mixture war filtered and the residue was dried, taken up in DCM and filtered over silica. The filtrate was evaporated to dryness and the target material was obtained as an orange oil (7.38 g, 77 % yield) and was used without further purification. **IR (ATR):** ν = 3029 (w), 2914 (w), 1615 (w), 1595 (m), 1477 (s), 1438 (m), 1356 (m), 1319 (m), 1219 (w), 1037 (w), 983 (m), 904 (s), 858 (s), 824 (m), 778 (s), 743 (m), 626 (s) cm^{-1}; **^{1}H-NMR (400 MHz, $CDCl_3$):** δ[ppm] = 8.97 (dd, J = 4.2, 1.7 Hz, 1H), 8.06 (dd, J = 8.2, 1.7 Hz, 1H), 7.91 (d, J = 1.8 Hz, 1H), 7.56 – 7.52 (m, 1H), 7.41 (dd, J = 8.3, 4.2 Hz, 1H), 2.51 (s, 3H); **^{13}\{^{1}H\}-NMR (100 MHz, $CDCl_3$):** δ[ppm] = 150.4, 143.9, 137.2, 135.9, 135.2, 129.5, 126.7, 124.3, 121.9, 21.2; **MS [ESI]:** m/z = 243.9734 $[M+Na]^+$ (calc. m/z = 243.9732);

8-bromo-6-ethyl-quinoline 6c
Sodium 3-nitrobenzenesulfonate (11.5 g, 51.0 mmol, 1.2 equiv.), $FeSO_4 \cdot 7H_2O$ (0.633 g, 2.28 mmol, 0.053 equiv.) and 2-bromo-4-ethyl-aniline (8.50 g, 42.5 mmol, 1.0 equiv.) are mixed with methanesulfonic acid (58 ml) and this mixture is heated to 125 °C while stirring. Then glycerol (17.3 ml, 237 mmol, 3.6 equiv.) is added. The mixture is further stirred at this temperature overnight. After cooling to r. t., the mixture is poured into aqueous NaOH solution (39.0 g, 975 mmol in 400 ml water) while cooling with an ice bath. DCM (200 ml) was added and the biphasic mixture was filtered and the layers were separated afterwards. The aqueous phase was extracted with DCM (2 × 100 ml) and the combined organic phases were dried over Na_2SO_4. The solvent was reduced to a volume of roughly 50 mL and the solution was then filtered over silica. The filtrate was evaporated to dryness and the target material was obtained as an orange oil (7.42 g, 74 % yield) and was used without further purification. **IR (ATR):** ν = 3030 (w), 2964 (m), 2930 (w), 2871 (w), 1614 (w), 1595 (m), 1478 (s), 1355 (m), 1325 (m), 1216 (w), 1160 (w), 997 (w), 962 (m), 872 (s), 826 (m), 781 (s), 735 (m), 650 (w), 623 (m) cm^{-1}; **^{1}H-NMR (400 MHz, $CDCl_3$):** δ[ppm] = 8.79 (dd, J = 4.2, 1.7 Hz, 1H), 7.85 (dd, J = 8.3, 1.7 Hz, 1H), 7.72 (d, J = 1.9 Hz, 1H), 7.35 – 7.27 (m, 1H), 7.20 (dd, J = 8.3, 4.2 Hz, 1H), 2.59 (q, J = 7.6 Hz,

2H), 1.13 (t, J = 7.6 Hz, 3H); **^{13}\{^{1}H\}-NMR (100 MHz, $CDCl_3$):** δ[ppm] = 149.20, 142.79, 142.16, 134.94, 133.03, 128.33, 124.27, 123.24, 120.70, 27.36, 14.01; **MS [ESI]:** m/z = 257.9886 $[M+Na]^+$ (calc. m/z = 257.9889);

8-bromo-6-(1-methylethyl)-quinoline 6d
Sodium 3-nitrobenzenesulfonate (10.5 g, 46.5 mmol, 1.2 equiv.), $FeSO_4 \cdot 7H_2O$ (0.578 g, 2.08 mmol, 0.053 equiv.) and 2-bromo-4-(1-methylethyl)-aniline (8.30 g, 38.7 mmol, 1.0 equiv.) are mixed with methanesulfonic acid (53 ml) and this mixture is heated to 125 °C while stirring. Then glycerol (8.5 ml, 116 mmol, 3.0 equiv.) is added. The mixture is further stirred at this temperature overnight. After cooling to r. t., the mixture is poured into aqueous NaOH solution (39.0 g, 975 mmol in 400 ml water) while cooling with an ice bath. The mixture is filtered and the residue is dried, extracted with DCM and filtered over silica. The filtrate is evaporated to dryness to obtain the target compound as an orange oil (7.09 g, 73 % yield), which was used without further purification. **IR (ATR):** ν = 3030 (w), 2960 (m), 2869 (w), 1616 (w), 1593 (m), 1479 (s), 1358 (m), 1323 (m), 1218 (w), 1175 (w), 1035 (w), 979 (m), 914 (m), 875 (s), 824 (m), 780 (s), 721 (m), 658 (w), 622.8 (m) cm^{-1}; **^{1}H-NMR (400 MHz, $CDCl_3$):** δ[ppm] = 8.95 (dd, J = 4.3, 1.7 Hz, 1H), 8.05 (dd, J = 8.3, 1.7 Hz, 1H), 7.95 (d, J = 1.9 Hz, 1H), 7.54 (d, J = 1.9 Hz, 1H), 7.37 (dd, J = 8.2, 4.2 Hz, 1H), 3.02 (hept, J = 6.9 Hz, 1H), 1.30 (d, J = 7.0 Hz, 6H); **^{13}\{^{1}H\}-NMR (100 MHz, $CDCl_3$):** δ[ppm] = 150.4, 147.9, 144.1, 136.2, 133.0, 129.5, 124.5, 124.0, 121.8, 33.9, 23.7; **MS [ESI]:** m/z = 250.0228 $[M+Na]^+$ (calc. m/z = 250.0226);

8-bromo-6-(1,1-dimethylethyl)-quinoline 6e
Sodium 3-nitrobenzenesulfonate (9.47 g, 42.1 mmol, 1.2 equiv.), $FeSO_4 \cdot 7H_2O$ (0.521 g, 1.88 mmol, 0.054 equiv.) and 2-bromo-4-(1,1-dimethylethyl)-aniline (8.00 g, 35.1 mmol, 1.0 equiv.) are mixed with methanesulfonic acid (48 ml) and this mixture is heated to 125 °C while stirring. Then glycerol (7.7 ml, 105 mmol, 3.0 equiv.) is added. The mixture is further stirred at this temperature overnight. After cooling to r. t., the mixture is poured into aqueous NaOH solution (30.8 g, 770 mmol in 400 ml water) while cooling with an ice bath. The mixture war filtered and the residue was dried, taken up in DCM and filtered over silica. The filtrate was evaporated to dryness and the target material was obtained as a yellowish solid (4.73 g, 51 % yield) and was used without further purification. **IR (ATR):** ν = 2960 (m), 1866 (w), 1617 (w), 1588 (w), 1477 (s), 1369 (m), 1318 (w), 1261 (m), 1207 (w), 1183 (w), 975 (m), 888 (s), 830 (w), 784 (s), 703 (m), 665 (w), 617 (m) cm^{-1}; **^{1}H-NMR (400 MHz, $CDCl_3$):** δ[ppm] = 8.99 (dd, J = 4.3, 1.7 Hz, 1H), 8.18 – 8.09 (m, 2H), 7.70 (d, J = 2.1 Hz, 1H), 7.43 (dd, J = 8.2, 4.2 Hz, 1H), 1.42 (s, 9H); **^{13}\{^{1}H\}-NMR (100 MHz, $CDCl_3$):** δ[ppm] = 150.7, 150.4, 143.9, 136.6, 132.3, 129.2, 124.4, 122.9, 121.9, 35.0, 31.1; **MS [ESI]:** m/z = 286.0205 $[M+Na]^+$ (calc. m/z = 286.0202);

8-bromo-6-butyl-quinoline 6f
Sodium 3-nitrobenzenesulfonate (4.14 g, 18.4 mmol, 1.2 equiv.), $FeSO_4 \cdot 7H_2O$ (0.228 g, 0.820 mmol, 0.054 equiv.) and 2-bromo-4-butyl-aniline (3.50 g, 15.3 mmol, 1.0 equiv.) are mixed with methanesulfonic acid (20 ml) and this mixture is heated to 125 °C while

stirring. Then glycerol (3.5 ml, 47.8 mmol, 3.1 equiv.) is added. The mixture is further stirred at this temperature overnight. After cooling to r. t., the mixture is poured into aqueous NaOH solution (12.5 g, 313 mmol in 200 ml water) while cooling with an ice bath. The mixture war filtered and the residue was dried, taken up in DCM and filtered over silica. The filtrate was evaporated to dryness and the target material was obtained as a yellowish oil (2.70 g, 67 % yield) and was used without further purification. **IR (ATR):** ν = 3030 (w), 2954 (m), 2927 (m), 2857 (w), 1616 (w), 1594 (w), 1478 (s), 1356 (m), 1317 (w), 1212 (w),1037 (w), 978 (w), 912 (m), 865 (m), 827 (w), 781 (s), 725 (w), 651 (w), 626 (m) cm^{-1}; **^{1}H-NMR (400 MHz, $CDCl_3$):** δ[ppm] = 8.98 (dd, J = 4.2, 1.7 Hz, 1H), 8.09 (dd, J = 8.2, 1.7 Hz, 1H), 7.93 (d, J = 1.9 Hz, 1H), 7.58 – 7.52 (m, 1H), 7.42 (dd, J = 8.3, 4.2 Hz, 1H), 2.83 – 2.69 (m, 2H), 1.76 – 1.61 (m, 2H), 1.49 – 1.32 (m, 2H), 0.96 (t, J = 7.3 Hz, 3H); **^{13}\{^{1}H\}-NMR (100 MHz, $CDCl_3$):** δ[ppm] = 150.4, 144.0, 142.1, 136.1, 134.6, 129.5, 126.1, 124.4, 121.8, 35.2, 33.2, 22.3, 13.9; **MS [ESI]:** m/z = 286.0204 $[M+H]^+$ (calc. m/z = 286.0202);

8-bromo-6-fluoro-quinoline 6g
Sodium 3-nitrobenzenesulfonate (11.4 g, 50.5 mmol, 1.2 equiv.), $FeSO_4 \cdot 7H_2O$ (0.624 g, 2.25 mmol, 0.054 equiv.) and 2-bromo-4-fluoro-aniline (8.00 g, 42.1 mmol, 1.0 equiv.) are mixed with methanesulfonic acid (56 ml) and this mixture is heated to 125 °C while stirring. Then glycerol (9.2 ml, 126 mmol, 3.0 equiv.) is added. The mixture is further stirred at this temperature overnight. After cooling to r. t., the mixture is poured into aqueous NaOH solution (36.0 g, 900 mmol in 300 ml water) while cooling with an ice bath. The mixture war filtered and the residue was dried, taken up in DCM and filtered over silica. The filtrate was evaporated to dryness and the target material was obtained as greyish powder (8.28 g, 87 % yield) and was used without further purification. **IR (ATR):** ν = 3061 (w), 1729 (w), 1624 (m), 1596 (m), 1561 (w), 1489 (m), 1455 (m), 1415 (w), 1358 (m), 1326 (m), 1222 (m), 1141 (m), 1119 (m), 1034 (w), 990 (m), 921 (s), 874 (s), 862 (s), 778 (s), 752 (s), 625 (s) cm^{-1}; **^{1}H-NMR (400 MHz, $CDCl_3$):** δ[ppm] = 8.95 (dd, J = 4.3, 1.6 Hz, 1H), 8.07 (dd, J = 8.3, 1.7 Hz, 1H), 7.82 (dd, J = 8.1, 2.7 Hz, 1H), 7.43 (dd, J = 8.3, 4.2 Hz, 1H), 7.38 (dd, J = 8.3, 2.7 Hz, 1H); **^{13}\{^{1}H\}-NMR (100 MHz, $CDCl_3$):** δ[ppm] = 159.4 (d, J = 251.6 Hz), 150.5 (d, J = 2.9 Hz), 142.7 (d, J = 1.5 Hz), 136.1 (d, J = 5.5 Hz), 129.3 (d, J = 10.2 Hz), 126.2 (d, J = 10.6 Hz), 123.7 (d, J = 28.3 Hz), 122.6, 110.8 (d, J = 21.1 Hz); **MS [ESI]:** m/z = 247.9483 $[M+Na]^+$ (calc. m/z = 247.9481);

8-bromo-6-methoxy-quinoline 6h
Sodium 3-nitrobenzenesulfonate (10.7 g, 47.5 mmol, 1.2 equiv.), $FeSO_4 \cdot 7H_2O$ (0.587 g, 2.11 mmol, 0.054 equiv.) and 2-bromo-4-fluoro-aniline (8.00 g, 39.6 mmol, 1.0 equiv.) are mixed with methanesulfonic acid (50 ml) and this mixture is heated to 125 °C while stirring. Then glycerol (8.7 ml, 118 mmol, 3.0 equiv.) is added. The mixture is further stirred at this temperature overnight. After cooling to r. t., the mixture is poured into aqueous NaOH solution (33.0 g, 825 mmol in 400 ml water) while cooling with an ice bath. The mixture war filtered and the residue was dried, taken up in DCM and filtered over silica. The filtrate was evaporated to dryness and the target material was obtained as a brownish powder (5.83 g, 72 % yield) and was used without further purification. **IR (ATR):** ν = 3021 (w), 2985 (w), 1604 (m), 1473 (m), 1415 (m), 1366 (m), 1328 (m),

1232 (s), 1199 (m), 1149 (s), 1122 (m), 1041 (m), 1020 (s), 977 (m), 915 (w), 867 (w), 840 (s), 773 (s), 739 (m), 634 (m) cm^{-1}; **^{1}H-NMR (400 MHz, $CDCl_3$):** δ[ppm] = 8.88 (dd, J = 4.2, 1.6 Hz, 1H), 8.04 (dd, J = 8.3, 1.7 Hz, 1H), 7.75 (d, J = 2.7 Hz, 1H), 7.40 (dd, J = 8.3, 4.2 Hz, 1H), 7.05 (d, J = 2.7 Hz, 1H), 3.92 (s, 3H); **^{13}{^{1}H}-NMR (100 MHz, $CDCl_3$):** δ[ppm] = 157.4, 148.7, 141.4, 135.4, 129.9, 125.8, 125.5, 122.1, 105.4, 55.8; **MS [ESI]:** m/z = 259.9678 $[M+Na]^+$ (calc. m/z = 259.9681);

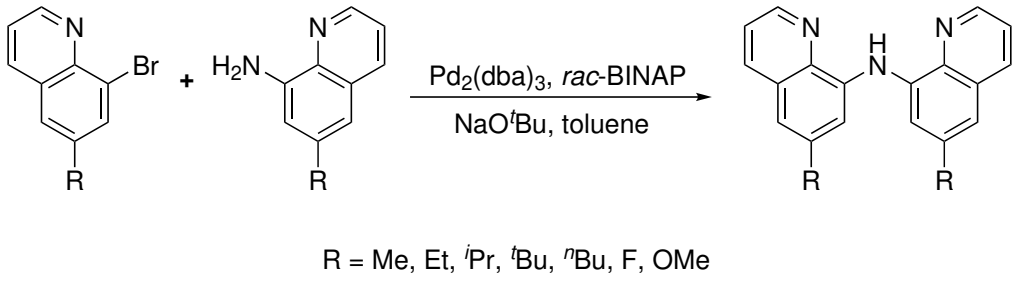

Scheme 4.4: Buchwald-Hartwig coupling to obtain the ligand precursors

6-Methyl-N-(6-methyl-8-quinolinyl)-8-quinolinamine 5b
$Pd_2(dba)_3$ (0.140 g,0.153 mmol, 0.02 equiv.) and *rac*-BINAP (0.190 g, 0.305 mmol, 0.04 equiv.) were dissolved in toluene (65 ml) under a nitrogen atmosphere and stirred for 15 min. Then 8-bromo-6-methyl-quinoline **6b** (1.70 g, 7.64 mmol, 1.0 equiv.) in toluene (10 ml), 8-amino-6-methyl-quinoline **7b** (1.21 g, 7.64 mmol, 1.0 equiv.) in toluene (5 ml) and sodium *tert*-butoxide (0.879 g, 9.14 mmol, 1.2 equiv.) were added. The mixture was heated to reflux for 1.5 d. After cooling to r.t., the mixture was filtered and the residue was washed with DCM (3 × 10 ml). The filtrate was evaporated to dryness and the residue was purified by column chromatography (SiO_2, DCM) to obtain a brownish oil, to which methanol (6 ml) was added. A solid formed which was filtered off and washed with methanol (6 × 3 ml). The target compound was yielded as a yellow solid (1.42 g, 62 % yield). **IR (ATR):** ν = 3242 (w), 2913 (w), 1625 (w), 1569 (m), 1532 (s), 1487 (m), 1450 (m), 1429 (s), 1380 (s), 1331 (m), 1232 (w), 1200 (w), 1153 (w), 1116 (w), 1034 (w), 975 (w), 892 (w), 823 (s), 793 (s), 774 (s), 728 (m), 660 (w), 609 (s) cm^{-1}; **^{1}H-NMR (400 MHz, $CDCl_3$):** δ[ppm] = 10.54 (s, 1H), 8.87 (dd, J = 4.2, 1.7 Hz, 2H), 8.02 (dd, J = 8.2, 1.7 Hz, 2H), 7.72 (d, J = 1.6 Hz, 2H), 7.39 (dd, J = 8.2, 4.2 Hz, 2H), 7.12 – 7.06 (m, 2H), 2.56 (s, 6H); **^{13}{^{1}H}-NMR (100 MHz, $CDCl_3$):** δ[ppm] = 147.2, 138.9, 138.5, 137.0, 135.4, 129.0, 121.7, 116.9, 112.0, 22.6; **MS [ESI]:** m/z = 300.1492 $[M+H]^+$ (calc. m/z = 300.1495);

6-Ethyl-N-(6-ethyl-8-quinolinyl)-8-quinolinamine 5c
$Pd_2(dba)_3$ (0.181 g, 0.197 mmol, 0.02 equiv.) and *rac*-BINAP (0.246 g, 0.394 mmol, 0.04 equiv.) were dissolved in toluene (85 ml) under a nitrogen atmosphere and stirred for 15 min. Then 8-bromo-6-ethyl-quinoline **6c** (2.33 g, 9.87 mmol, 1.0 equiv.) in toluene (10 ml), 8-amino-6-ethyl-quinoline **7c** (1.70 g, 9.87 mmol, 1.0 equiv.) in toluene (5 ml) and sodium *tert*-butoxide (1.14 g, 11.8 mmol, 1.2 equiv.) were added. The mixture was heated to reflux for 3 d. After cooling to r.t., the mixture was filtered and the residue was washed with DCM (3 × 10 ml). The filtrate was evaporated to dryness and the residue was purified by column chromatography (SiO_2, DCM/hexane: 50/50 to 95/5) to obtain

the target compound as a yellow solid (1.72 g, 53 % yield). **IR (ATR):** ν = 3265 (w), 2954 (w), 2925 (w), 2926 (w), 2868 (w), 1625 (w), 1569 (m), 1530 (s), 1485 (m), 1451 (m), 1424 (s), 1384 (m), 1334 (m), 1236 (w), 1196 (w), 1146 (w), 1116 (w), 1057 (w), 886 (w), 869 (w), 815 (s), 780 (m), 746 (m), 680 (w), 609 (m) cm^{-1}; **^{1}H-NMR (400 MHz, $CDCl_3$):** δ[ppm] = 10.45 (s, 1H), 8.88 (dd, J = 4.2, 1.7 Hz, 2H), 8.06 (dd, J = 8.2, 1.7 Hz, 2H), 7.78 (d, J = 1.7 Hz, 2H), 7.40 (dd, J = 8.2, 4.2 Hz, 2H), 7.12 (s, 2H), 2.85 (q, , J = 7.6 Hz , 4H), 1.39 (t, J = 7.6 Hz, 6H); **^{13}{^{1}H}-NMR (100 MHz, $CDCl_3$):** δ[ppm] = 147.3, 143.2, 139.1, 138.7, 135.6, 129.1, 121.6, 115.6, 111.2, 29.7, 15.5; **MS [ESI]:** m/z = 328.1805 $[M+Na]^+$ (calc. m/z = 328.1808);

6-(1-methylethyl)-N-(6-(1-methylethyl)-8-quinolinyl)-8-quinolinamine 5d
$Pd_2(dba)_3$ (0.154 g, 0.168 mmol, 0.02 equiv.) and *rac*-BINAP (0.209 g, 0.336 mmol, 0.04 equiv.) were dissolved in toluene (80 ml) under a nitrogen atmosphere and stirred for 15 min. Then 8-bromo-6-(1-methylethyl)-quinoline **6d** (2.10 g, 8.38 mmol, 1.0 equiv.) in toluene (10 ml), 8-amino-6-(-methylethyl)-quinoline **7d** (1.56 g, 8.38 mmol, 1.0 equiv.) in toluene (10 ml) and sodium *tert*-butoxide (0.966 g, 10.1 mmol, 1.2 equiv.) were added. The mixture was heated to reflux for 3 d. After cooling to r.t., the mixture was filtered and the residue was washed with DCM (3 × 10 ml). The crude material was purified by column chromatography (SiO_2, EtOAc,/Hexane: 5/95 to 10/90) to obtain the target material as a yellow solid (2.56 g, 86 % yield) **IR (ATR):** ν = 3330 (w), 2956 (m), 2866 (w), 1624 (w), 1568 (m), 1527 (s), 1492 (m), 1449 (m), 1423 (s), 1380 (m), 1341 (w), 1299 (w), 1235 (w), 1117 (w), 1033 (w), 964 (w), 847 (m), 785 (m), 662 (w), 609 (m) cm^{-1}; **^{1}H-NMR (400 MHz, $CDCl_3$):** δ[ppm] = 10.34 (s, 1H), 8.87 (dd, J = 4.2, 1.7 Hz, 2H), 8.07 (dd, J = 8.3, 1.7 Hz, 2H), 7.85 (d, J = 1.8 Hz, 2H), 7.40 (dd, J = 8.2, 4.2 Hz, 2H), 7.14 (d, J = 1.9 Hz, 2H), 3.09 (hept, J = 6.9 Hz, 2H), 1.40 (d, J = 6.9 Hz, 12H); **^{13}{^{1}H}-NMR (100 MHz, $CDCl_3$):** δ[ppm] = 147.65, 147.39, 139.25, 138.78, 135.75, 129.07, 121.60, 114.42, 109.86, 34.78, 24.00; **MS [ESI]:** m/z = 356.2121 $[M+H]^+$ (calc. m/z = 356.2121);

6-(dimethylethyl)-N-(6-(dimethylethyl)-8-quinolinyl)-8-quinolinamine 5e
$Pd_2(dba)_3$ (0.156 g, 0.170 mmol, 0.02 equiv.) and *rac*-BINAP (0.212 g, 0.341 mmol, 0.04 equiv.) were dissolved in toluene (80 ml) under a nitrogen atmosphere and stirred for 15 min. Then 8-bromo-6-(1,1-dimethylethyl)-quinoline **6e** (2.25 g, 8.53 mmol, 1.0 equiv.), 8-amino-6-(1,1-dimethylethyl)-quinoline **7e** (1.71 g, 8.53 mmol, 1.0 equiv.) in toluene (10 ml) and sodium *tert*-butoxide (0.981 g, 10.2 mmol, 1.2 equiv.) were added. The mixture was heated to reflux for 2 d. After cooling to r.t., the mixture was filtered and the residue was washed with DCM (3 × 10 ml). The filtrate was evaporated to dryness and the residue was taken up in DCM and filtered over silica. The filtrate was evaporated to dryness and an oil which was crystallized by adding methanol. The solid was filtered off and washed with methanol (3 × 5 ml). The material was further purified by column chromatography and the obtained compound was recrystallized from EtOAc/MeOH to obtain the target material as yellow crystals (1.14 g, 35 % yield). **IR (ATR):** ν = 3291 (w), 2948 (m), 2901 (w), 2864 (w), 1622 (w), 1569 (m), 1530 (s), 1488 (m), 1419 (s), 1378 (m), 1260 (w), 1237 (w), 1196 (w), 1120 (m), 837 (m), 783 (s), 696 (m), 659 (m), 609 (s) cm^{-1}; **^{1}H-NMR (400 MHz, $CDCl_3$):** δ[ppm] = 10.26 (s, 1H), 8.89 (dd, J = 4.2, 1.7 Hz, 2H), 8.11 (dd, J = 8.3, 1.7 Hz, 2H), 8.06 (d, J = 1.9 Hz, 2H), 7.42 (dd, J = 8.2, 4.2

Hz, 2H), 7.27 (d, J = 1.9 Hz, 2H), 1.47 (s, 18H); **^{13}{^{1}H}-NMR (100 MHz, $CDCl_3$):** δ[ppm] = 149.9, 147.6, 138.9, 138.5, 136.1, 128.7, 121.6, 113.3, 109.4, 35.2, 31.4; **MS [ESI]:** m/z = 384.2436 $[M+H]^+$ (calc. m/z = 384.2434);

6-Butyl-N-(6-butyl-8-quinolinyl)-8-quinolinamine 5f
$Pd_2(dba)_3$ (0.137 g, 0.150 mmol, 0.02 equiv.) and *rac*-BINAP (0.187 g, 0.300 mmol, 0.04 equiv.) were dissolved in toluene (75 ml) under a nitrogen atmosphere and stirred for 15 min. Then 8-bromo-6-butyl-quinoline **6f** (1.98 g, 7.49 mmol, 1.0 equiv.), 8-amino-6-butyl-quinoline **7f** (1.50 g, 7.49 mmol, 1.0 equiv.) and sodium *tert*-butoxide (0.861 g, 8.96 mmol, 1.2 equiv.) were added. The mixture was heated to reflux for 3 d. After cooling to r.t., the solvent was evaporated. The residue was taken up in DCM and filtered over silica. After evaporation of the solvent the material was purified by column chromatography (SiO_2, DCM) The obtained material was washed in MeOH to yield the target compound as a yellow solid (1.92 g, 67 % yield). **IR (ATR):** ν = 3265 (w), 2952 (w), 2922 (w), 2855 (w), 1625 (w), 1568 (m), 1532 (s), 1487 (m), 1447 (m), 1427 (s), 1387 (s), 1334 (w), 1256 (w), 1235 (w), 1153 (w), 1116 (w), 972 (w), 844 (s), 749 (m), 750 (w), 728 (w), 609 (s) cm^{-1}; **^{1}H-NMR (400 MHz, $CDCl_3$):** δ[ppm] = 10.38 (s, 1H), 8.87 (dd, J = 4.2, 1.7 Hz, 2H), 8.05 (dd, J = 8.2, 1.7 Hz, 2H), 7.76 (d, J = 1.7 Hz, 2H), 7.40 (dd, J = 8.2, 4.2 Hz, 2H), 7.10 (d, J = 1.8 Hz, 2H), 2.81 (t, J = 7.6 Hz, 4H), 1.80 – 1.67 (m, 4H), 1.44 (h, J = 7.4 Hz, 4H), 0.98 (t, J = 7.4 Hz, 6H); **^{13}{^{1}H}-NMR (100 MHz, $CDCl_3$):** δ[ppm] = 147.3, 141.8, 139.1, 138.6, 135.6, 129.0, 121.6, 116.5, 111.6, 36.4, 33.5, 22.4, 14.1.; **MS [ESI]:** m/z = 384.2437 $[M+H]^+$ (calc. m/z = 384.2434);

6-fluoro-N-(6-fluoro-8-quinolinyl)-8-quinolinamine 5g
$Pd_2(dba)_3$ (0.137 g, 0.150 mmol, 0.02 equiv.) and *rac*-BINAP (0.187 g, 0.300 mmol, 0.04 equiv.) were dissolved in toluene (75 ml) under a nitrogen atmosphere and stirred for 15 min. Then 8-bromo-6-fluoro-quinoline **6g** (1.98 g, 7.49 mmol, 1.0 equiv.), 8-amino-6-fluoro-quinoline **7g** (1.50 g, 7.49 mmol, 1.0 equiv.) and sodium *tert*-butoxide (0.861 g, 8.96 mmol, 1.2 equiv.) were added. The mixture was heated to reflux for 3 d. After cooling to r.t., the solvent was evaporated The residue was taken up in DCM and filtered over silica. After evaporation of the solvent the material was recrystallized from toluene/hexane. After drying the material was obtained as a yellow crystalline powder (1.92 g, 67 % yield). **IR (ATR):** ν = 3308 (w), 1626 (m), 1606 (m), 1574 (s), 1536 (s), 1501 (s), 1469 (m), 1433 (s), 1379 (s), 1340 (m), 1252 (w), 1210 (m), 1188 (m), 1139 (m), 1127 (m), 1041 (m), 1011 (m), 990 (m), 887 (w), 864 (w), 822 (s), 786 (s), 687 (m), 673 (m), 601 (m) cm^{-1}; **^{1}H-NMR (400 MHz, $CDCl_3$):** δ[ppm] = 10.94 (s, 1H), 8.90 (dd, J = 4.2, 1.7 Hz, 2H), 8.10 (dd, J = 8.3, 1.7 Hz, 2H), 7.59 (dd, J = 11.1, 2.6 Hz, 2H), 7.49 (dd, J = 8.3, 4.2 Hz, 2H), 6.98 (dd, J = 8.9, 2.6 Hz, 2H); **^{13}{^{1}H}-NMR (100 MHz, $CDCl_3$):** δ[ppm] = 161.28 (d, J = 244.7 Hz), 147.28 (d, J = 2.7 Hz), 139.91 (d, J = 13.0 Hz), 137.32, 135.71 (d, J = 5.9 Hz), 129.36 (d, J = 12.1 Hz), 122.65, 101.14 (d, J = 22.4 Hz), 100.54 (d, J = 31.1 Hz); **MS [ESI]:** m/z = 330.0814 $[M+Na]^+$ (calc. m/z = 330.0813);

6-methoxy-N-(6-methoxy-8-quinolinyl)-8-quinolinamine 5h
$Pd_2(dba)_3$ (0.115 g, 0.126 mmol, 0.02 equiv.) and *rac*-BINAP (0.157 g, 0.252 mmol, 0.04 equiv.) were dissolved in toluene (66 ml) under a nitrogen atmosphere and stirred for 15 min. Then 8-bromo-6-methoxy-quinoline **6h** (1.50 g, 6.30 mmol, 1.0 equiv.), 8-amino-6-

methoxy-quinoline **7h** (1.10 g, 6.30 mmol, 1.0 equiv.) and sodium *tert*-butoxide (0.725 g, 7.54 mmol, 1.2 equiv.) were added. The mixture was heated to reflux for 4 d. After cooling to r.t., the mixture was filtered over a silica plug and eluted with DCM. The filtrate was concentrated by removing DCM in vacuo and was then cooled to -20 °C. The formed solid was collected by filtration and washed with toluene (2 × 20 ml) and hexane (20 ml). The target material was obtained as an orange solid (1.66 g, 80 % yield) **IR (ATR):** ν = 3282 (w), 2935 (w), 2828 (w), 1621 (m), 1573 (m), 1526 (s), 1494 (m), 1451 (m), 1424 (m), 1387 (m), 1246 (w), 1205 (s), 1163 (s), 1077 (w), 1028 (m), 892 (w), 822 (s), 786 (s), 736 (m), 701 (w), 662 (w), 615 (m) cm^{-1}; **^{1}H-NMR (400 MHz, $CDCl_3$):** δ(s) = 10.69 (s, 1H), 8.79 (dd, J = 4.2, 1.7 Hz, 2H), 8.01 (dd, J = 8.2, 1.7 Hz, 2H), 7.53 (d, J = 2.4 Hz, 2H), 7.40 (dd, J = 8.2, 4.2 Hz, 2H), 6.62 (d, J = 2.5 Hz, 2H), 3.94 (s, 6H); **^{13}{^{1}H}-NMR (100 MHz, $CDCl_3$):** δ[ppm] = 158.7, 145.7, 139.39, 136.9, 134.9, 129.8, 122.1, 102.9, 95.9, 55.4; **MS [ESI]:** m/z = 332.1396 $[M+H]^+$ (calc. m/z = 332.1394);

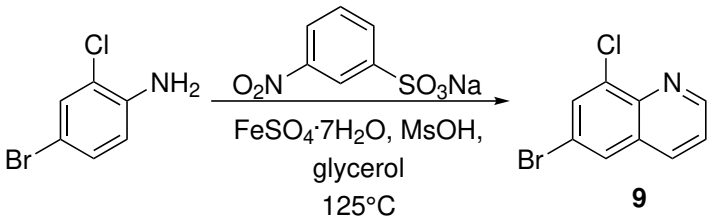

Scheme 4.5: Skraup synthesis of 6-bromo-8-chloro-quinoline **9**

6-bromo-8-chloro-quinoline 9
4-bromo-2-chloro-aniline (17.6 g, 84.1 mmol, 1.0 equiv.), sodium 3-nitrobenzenesulfonate (22.8 g, 101 mmol, 1.2 equiv.) and $FeSO_4 \cdot 7H_2O$ (1.18 g, 4.20 mmol, 0.05 equiv.) were suspended in methanesulfonic acid (100 ml) and heated to 125 °C. Upon reaching the temperature glycerol (19.0 mL, 252 mmol, 3.0 equiv.) were added and the mixture was stirred for 16 h at this temperature. After cooling to r.t., the mixture was poured into aqueous NaOH solution (78.0 g, 1.95 mol in 650 ml water) while cooling with an ice bath. The mixture was filtered and the residue was dried, taken up in DCM and filtered over silica. The filtrate was evaporated to dryness and the residue was washed in boiling MeOH. After drying the product was obtain as a yellowish solid (16.7 g, 82 % yield). **IR (KBR):** ν = 3059 (w). 1740 (w), 1588 (w), 1552 (w), 1471 (m), 1350 (m), 1308 (m), 1205 (w), 1186 (w), 1078 (w), 1038 (w), 978 (m), 858 (s), 825 (m), 778 (s), 629 (s) cm^{-1}; **^{1}H-NMR (400 MHz, $CDCl_3$):** δ[ppm] = 9.04 (dd, J = 4.2, 1.7 Hz, 1H), 8.10 (dd, J = 8.4, 1.7 Hz, 1H), 7.95 (d, J = 2.1 Hz, 1H), 7.92 (d, J = 2.1 Hz, 1H), 7.50 (dd, J = 8.3, 4.2 Hz, 1H); **^{13}{^{1}H}-NMR (100 MHz, $CDCl_3$):** δ[ppm] = 151.23, 143.30, 135.56, 134.76, 132.64), 130.20, 129.03), 122.79, 119.46; **MS [ESI]:** m/z = 241.9362 $[M+H]^+$ (calc. m/z = 241.9367);

8-chloro-6-quinolinecarbonitrile 10
Potassium acetate (0.608 g, 6.20 mmol, 0.5 equiv.) was dissolved in water (13 ml) and 1,4-dioxane (13 ml). Nitrogen was bubbled through the solution for 10 min. 6-bromo-8-chloro-quinoline **9** (3.02 g, 12.5 mmol, 1.0 equiv.), {K4[Fe(CN)6]}· $3H_2O$ (2.61 g,

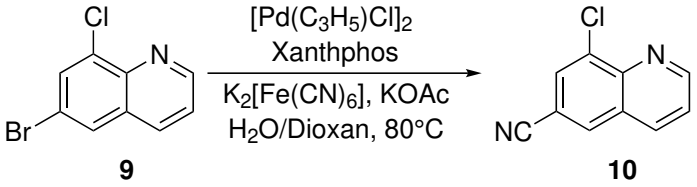

Scheme 4.6: Catalytic cyanation towards 8-chloro-6-quinolinecarbonitrile **10**

6.19 mmol, 0,5 equiv.), $[Pd(C_3H_5)Cl]_2$ 0.228 g, 0.624 mmol, 0.05 equiv.) and xantphos (0.358 g, 0.619 mmol, 0.05 equiv.) were added under a nitrogen atmosphere. The mixture was stirred for 1 h at 95 °C. After cooling to r.t., sat. NaCl solution (250 mL) and EtOAc (200 mL) were added, the layers were separated and the aqueous phase was extracted with EtOAc (3 × 120 mL). The combined organic phases were washed with sat. NaCl solution and dried over Na_2SO_4. The solvent was removed and the residue was taken up in a small amount of EtOAc and filtered over silica. The filtrate was evaporated to dryness and the target material was obtained as a colorless solid (2.34 g, 100 % yield). **IR (ATR):** ν = 3038 (w), 2233 (m, $\nu_{\text{-C}\equiv\text{N}}$), 1855 (w), 1750 (w), 1612 (w), 1592 (m), 1480 (s), 1413 (w), 1361 (m), 1315 (m), 1218 (m), 1155 (m), 1041 (m), 997 (s), 930 (m), 912 (s), 882 (m), 869 (s), 805 (m), 785 (vs), 736 (m), 637 (w), 624 (m), 602 (m) cm^{-1}; **^{1}H-NMR (400 MHz, $CDCl_3$):** δ[ppm] = 9.20 (dd, J = 4.3, 1.7 Hz, 1H), 8.29 (dd, J = 8.3, 1.7 Hz, 1H), 8.18 (d, J = 1.7 Hz, 1H), 8.01 (d, J = 1.8 Hz, 1H), 7.65 (dd, J = 8.3, 4.3 Hz, 1H); **^{13}{^{1}H}-NMR (100 MHz, $CDCl_3$):** δ[ppm] = 153.77, 145.77, 137.03, 135.58, 132.93, 129.91, 128.71, 123.56, 117.31, 110.64; **MS [ESI]:** m/z = 211.0031 $[M+Na]^+$ (calc. m/z = 211.0033);

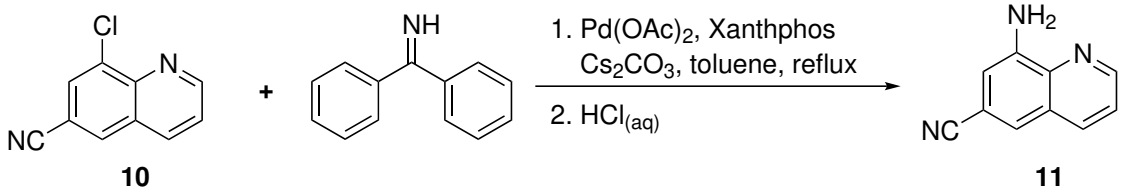

Scheme 4.7: Two step synthesis of 8-amino-6-quinolinecarbonitrile **11**

8-amino-6-quinolinecarbonitrile 11

8-chloro-6-quinolinecarbonitrile **10** (2.51 g, 13.31 mmol, 1.0 equiv.), benzophenone imine (3.13 g, 17.3 mmol, 1.3 equiv.), $Pd(OAc)_2$ (0.298 g, 1.33 mmol, 0.1 equiv.), xantphos (1.536 g, 2.65 mmol, 0.2 equiv.) and caesium carbonate (5.62 g, 17.3 mmol, 1.3 equiv.) were suspended in toluene (8.3 mL) and refluxed for 23 h. After cooling to r.t., the mixture was filtered over celite and the filter was washed with DCM. The filtrate was evaporated to dryness. To the residue water (150 mL) and THF (150 mL) were added. The pH-value was adjusted to pH 1 with 1 M aqueous hydrochloric acid and the mixture was stirred for 3 h. The mixture was basified by the addition of $NaHCO_3$. The mixture was extracted with DCM (4 × 100 mL) and the combined organic phases were washed with sat. NaCl solution and dried over Na_2SO_4. The solvent was removed and the residue was purified by column chromatography (SiO_2, DCM). The product was obtained as a yellow solid (1.78 g,

79 % yield). **IR (ATR):** ν = 3434 (m), 3334 (m), 2294 (w), 2227 (m), 1627 (s), 1603 (m), 1569 (m), 1504 (s), 1425 (m), 1383 (s), 1332 (m), 1283 (m), 1246 (m), 1148 (w), 1116 (w), 1038 (w), 984 (w), 926 (w), 890 (m), 856 (m), 834 (m), 785 (vs), 745 (w), 620 (m) cm^{-1}; **^{1}H-NMR (400 MHz, $CDCl_3$):** δ[ppm] = 8.87 (dd, J = 4.2, 1.7 Hz, 1H), 8.11 (dd, J = 8.3, 1.7 Hz, 1H), 7.50 (d, J = 1.9 Hz, 1H), 7.49!!! (m, 1H), 6.99 (d, J = 1.7 Hz, 1H), 5.24 (s, 2H); **^{13}\{^{1}H\}-NMR (100 MHz, $CDCl_3$):** δ[ppm] = 149.97, 145.05, 139.28, 136.42, 128.01, 122.85, 121.45, 119.26, 110.91, 109.35; **MS [ESI]:** m/z = 170.0713 $[M+H]^+$ (calc. m/z = 170.0713);

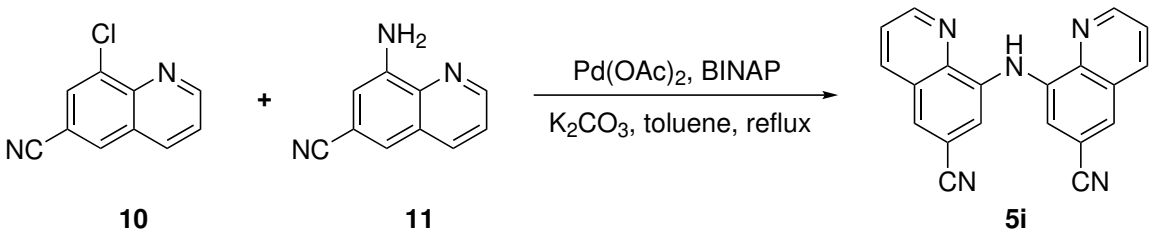

10 **11** **5i**

Scheme 4.8: Buchwald-Hartwig coupling to obtain the ligand precursor **5i**

8-((6-Cyanoquinoline-8-yl)amino)quinoline-6-carbonitrile 5i
8-amino-6-quinolinecarbonitrile **11** (1.73 g, 10.2 mmol, 1.0 equiv.), 8-chloro-6-quinolinecarbonitrile **10** (1.93 g, 10.2 mmol, 1.0 equiv.), potassium carbonate (2.13 g, 15.4 mmol, 1.5 equiv.), $Pd(OAc)_2$ (0.070 g, 0.31 mmol, 0,03 equiv.) and *rac*-BINAP (0.384 g, 0.617 mmol, 0.06 equiv.) were suspended in toluene (344 mL) and heated to reflux for 24 h while stirring. After cooling to r.t., the mixture was filtered over celite and residue was washed with DCM (4 l). The filtrate was reduced in volume to roughly 150 mL and the resulting precipitate was filtered off and washed with DCM and MeOH and dried under reduced pressure. The product was obtained as an orange solid (2.37 g, 72 % yield). **IR (ATR):** ν = 3316 (w), 3090 (w), 2920 (w), 2851 (w), 2229 (m), 1725 (w), 1670 (w), 1612 (w), 1590 (m), 1571 (s), 1532 (s), 1492 (s), 1450 (m), 1423 (s), 1379 (s), 1333 (m), 1261 (w), 1230 (w), 1198 (m), 1156 (w), 1128 (m), 1037 (m), 973 (w), 905 (w), 891 (w), 858 (s), 842 (s), 783 (s), 653 (m), 626 (m), 611 (s) cm^{-1}; **^{1}H-NMR (400 MHz, $CDCl_3$):** δ[ppm] = 10.93 (s, 1H), 9.09 (dd, J = 4.3, 1.7 Hz, 2H), 8.24 (dd, J = 8.4, 1.7 Hz, 2H), 7.91 (d, J = 1.6 Hz, 2H), 7.80 (d, J = 1.6 Hz, 2H), 7.63 (dd, J = 8.2, 4.3 Hz, 2H); **^{13}\{^{1}H\}-NMR (100 MHz, $CDCl_3$):** δ[ppm] = 151.36, 141.21, 139.19, 137.36, 128.56, 125.35, 123.88, 119.31, 111.39, 110.44; **MS [ESI]:** m/z = 344.0907 $[M+Na]^+$ (calc. m/z = 344.0907);

Zinc complex 1b (methyl substituents)
6-Methyl-N-(6-methyl-8-quinolinyl)-8-quinolinamine **5b** (169.1 mg, 0.565 mmol, 2.0 equiv.) was dissolved in THF (3 mL) and potassium *tert*-butoxide (63.4 mg, 0.565 mmol, 2.0 equiv.) was added. The mixture was stirred for 30 min, then $ZnCl_2$ (38.5 mg, 0.282 mmol, 1.0 equiv) was added. The mixture was stirred for 2 d and then filtered. The residue was washed with THF (2 × 1 mL) and was subsequently continuously extracted with DCM (12.5 mL). The extract was layer with *n*-hexane (12.5 mL) and after standing overnight the obtained solid was filtered off, washed with *n*-hexane (3 × 1 mL) and dried to obtain the target material as a red powder (105.1 mg, 56% yield). Crystals suitable for x-ray analysis were grown

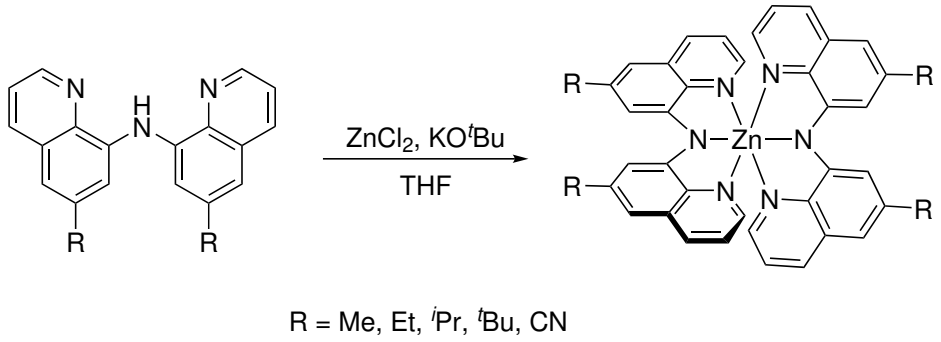

Scheme 4.9: Synthesis to obtain the Zinc complexes **1b** − **e** and **1i**

by layering a solution of the material in THF with *n*-hexane. **IR (ATR):** ν = 1600 (w), 1556 (m), 1478 (w), 1445 (m), 1415(s), 1383 (s), 1366 (s), 1328 (s), 1272 (m), 1225 (m), 1201 (m), 1171 (m), 1148 (m), 1120 (m), 977 (w), 901 (w), 815 (m), 782 (s), 676 (w), 618 (m) cm^{-1}; **^{1}H-NMR (400 MHz, $CDCl_3$):** δ[ppm] = 7.97 (d, J = 1.6 Hz, 4H), 7.84 (dd, J = 4.3, 1.7 Hz, 4H), 7.73 (dd, J = 8.2, 1.7 Hz, 4H), 6.82 (dd, J = 8.2, 4.4 Hz, 4H), 6.69 (s, 4H), 2.54 (s, 12H); **^{13}\{^{1}H\}-NMR (100 MHz, $CDCl_3$):** δ[ppm] = 146.27, 143.09, 139.89, 138.75, 136.08, 129.96, 121.05, 111.27, 111.20, 22.98; **MS [ESI]:** m/z = 661.2055 $[M+H]^+$ (calc. m/z = 661.2053);

Zinc complex 1c (ethyl substituents)
6-Methyl-N-(6-methyl-8-quinolinyl)-8-quinolinamine **5c** (130.7 mg, 0.399 mmol, 2.0 equiv.) was dissolved in THF (3 mL) and potassium *tert*-butoxide (44.8 mg, 0.399 mmol, 2.0 equiv.) was added. The mixture was stirred for 30 min, then $ZnCl_2$ (27.2 mg, 0.200 mmol, 1.0 equiv) was added. The mixture was stirred for 2 d and then filtered. The residue was washed with THF (2 × 1 mL). The residue was given into an extraction vessel and DCM (12.5 mL) was added to the vessel. The solid was continuously extracted for 1 d. The extracts were reduced in volume to approx. 4 mL and layered with *n*-hexane (4 mL). The solid formed was filtered off and dried to obtain the target material as a red powder (27.4 mg, 19% yield). Crystals suitable for x-ray analysis were grown by layering a solution of the material in THF with *n*-hexane. **IR (ATR):** ν = 2960.7 (w), 1597.3 (w), 1555.7 (m), 1474.8 (m), 1443.9 (m), 1422.0 (s), 1387.1 (s), 1281.9 (m), 1200.3 (m), 1143.3 (m), 1062 (m), 1005.5 (m), 899.3 (w), 873.4 (m), 769.4 (m), 683.4 (m), 630,3 (w) cm^{-1}; **^{1}H-NMR (400 MHz, $CDCl_3$):** δ[ppm] = 8.03 (d, J = 1.7 Hz, 4H), 7.85 (dd, J = 4.4, 1.7 Hz, 4H), 7.75 (dd, J = 8.2, 1.7 Hz, 4H), 6.82 (dd, J = 8.2, 4.4 Hz, 4H), 6.70 (d, J = 1.6 Hz, 4H), 2.827 (q, J = 7.6 Hz, 8H), 1.42 (t, J = 7.6 Hz, 12H); **^{13}\{^{1}H\}-NMR (100 MHz, $CDCl_3$):** δ[ppm] = 146.48, 144.92, 143.30, 140.09, 136.27, 129.95, 121.00, 110.22, 109.75, 30.15, 15.57; **MS [ESI]:** m/z = 717.2676 $[M+H]^+$ (calc. m/z = 717.2679);

Zinc complex 1d (1-methylethyl substituents)
From a stock solution of 6-(1-methylethyl)-N-(6-(1-methylethyl)-8-quinolinyl)-8-quinolinamine **5d** (373.0 mg, 1.05 mmol) a volume of 1.85 mL (0.333 mmol, 2.0 equiv.) was taken and potassium *tert*-butoxide (37.4 mg, 0.333 mmol, 2.0 equiv.) was added. The mixture was stirred for 30 min, then $ZnCl_2$ (22.7 mg, 0.167 mmol, 1.0 equiv.) was added. The mixture was stirred for 2 d. The reaction mixture was given into an extractor

and the reaction vessel was washed with THF (3 × 1 mL) and the washes were added to the extractor as well. Additional THF (6 mL) was added to the extractor and the material was extracted overnight. The extract was reduced in volume to 1.5 mL under reduced pressure and was layered with *n*-hexane (7 mL) and cooled to -30°C. After 3 d the precipitate was filtered off and was washed with *n*-hexane (3 × 1 mL) and then dried. The target material was obtained as a red powder (11.5 mg, 9% yield). **IR (ATR):** ν = 2953.3 (w), 1596.2 (w), 1561.5 (m), 1474.0 (m), 1444.2 (s), 1423.0 (s), 1391.0 (s), 1298.0 (m), 1282.4 (m), 1224.8 (m), 1201.4 (m), 1121.3 (m), 1121.3 (m), 1076.4 (m), 962.4 (w), 911.3 (w), 833.3 (s), 792.0 (w), 777.0 (s), 662.6 (w), 636.1 (m), 619.7 (m) cm^{-1}; **^{1}H-NMR (400 MHz, $CDCl_3$):** δ[ppm] = 8.10 (d, J = 1.8 Hz, 4H), 7.86 (dd, J = 4.4, 1.7 Hz, 4H), 7.78 (dd, J = 8.3, 1.7 Hz, 4H), 6.83 (dd, J = 8.2, 4.3 Hz, 4H), 6.72 (d, J = 1.6 Hz, 4H), 3.06 (hept, J = 6.8 Hz, 4H), 1.43 (d, J = 6.9 Hz, 24H); **^{13}{^{1}H}-NMR (100 MHz, $CDCl_3$):** δ[ppm] = 149.42, 146.60, 143.52, 140.18, 136.42, 129.85, 120.97, 108.71, 108.39, 35.20, 24.21; **MS [ESI]:** m/z = 773.3307 $[M+H]^+$ (calc. m/z = 773.3310);

Zinc complex 1e (1,1-dimethylethyl substituents)
6-(1,1-dimethylethyl)-N-(6-(1,1-dimethylethyl)-8-quinolinyl)-8-quinolinamine **5e** (215.0 mg, 0.561 mmol, 2.0 equiv.) was dissolved in THF (3 mL) and potassium *tert*-butoxide (62.9 mg, 0.565 mmol, 2.0 equiv.) was added. The mixture was stirred for 30 min, then $ZnCl_2$ (38.2 mg, 0.280 mmol, 1.0 equiv.) was added. The mixture was stirred for 3 d and then filtered. The residue was washed with THF (2 × 1 mL). The combined filtrates were layered with *n*-hexane (6 mL). After standing for 2 d at -30°C the formed solid was filtered off and washed with *n*-hexane (3 × 1 mL) and then dried to obtain the target compound as a red crystalline solid (82.1 mg, 35% yield). Crystals suitable for x-ray analysis were grown by vapor diffusion of *n*-hexane into a solution of the material in THF. **IR (ATR):** ν = 2951.2 (w), 2865.4 (w), 1593.5 (w), 1552.7 (s), 1469.9 (m), 1441.3 (m), 1421.3 (s), 1382.3 (s), 1352.2 (m), 1286.2 (m), 1256.1 (w), 1200.7 (m), 1131.8 (w), 1093.4 (w), 1068.9 (w), 1043.9 (w), 1023.5 (w), 955 (m), 902.8 (w), 836.1 (m), 769.3 (m), 663.1 (w), 626.4 (w) cm^{-1}; **^{1}H-NMR (400 MHz, $CDCl_3$):** δ[ppm] = 8.32 (d, J = 1.9 Hz, 2H), 7.88 (dd, J = 4.4, 1.7 Hz, 2H), 7.81 (dd, J = 8.2, 1.7 Hz, 2H), 6.88 – 6.80 (m, 4H), 1.50 (s, 18H); **^{13}{^{1}H}-NMR (100 MHz, $CDCl_3$):** δ[ppm] = 151.60, 146.28, 143.83, 139.86, 136.80, 129.48, 120.97, 108.18, 107.23, 35.46, 31.63; **MS [ESI]:** m/z = 829.3933 $[M+H]^+$ (calc. m/z = 829.3931);

Zinc complex 1i (nitrile substituents)
8-((6-Cyanoquinoline-8-yl)amino)quinoline-6-carbonitrile **5i** (106.2 mg, 0.332 mmol, 2.0 equiv.) was dissolved in THF (2.5 mL) and potassium *tert*-butoxide (38.6 mg, 0.344 mmol, 2.1 equiv.) was added. The mixture was stirred for 30 min, then $ZnCl_2$ (22.4 mg, 0.164 mmol, 1.0 equiv.) was added. The mixture was stirred for 2 d. The reaction mixture was given into an extractor and the reaction vessel was washed with THF (3 × 1 mL) and the washes were added to the extractor as well. Additional THF (6 mL) was added to the extractor and the material was extracted for 3 d. The extracted was filtered and the residue was washed with THF (2 × 1 mL) and the dried to obtain the target material as a red solid (46.9 mg, 40% yield). Crystals suitable for x-ray analysis were grown by vapor diffusion of *n*-hexane into a solution of the material in THF. **IR (ATR):** ν = 1725 (w), 1560 (w), 1467 (s), 1451 (s), 1418 (s), 1383 (s), 1329 (s), 1230 (s), 1196 (m), 1136 (m),

974 (m), 902 (m), 845 (m), 822 (m), 811 (m), 787 (m), 683 (w), 626 (s) cm^{-1}; **^{1}H-NMR (400 MHz, $CDCl_3$):** δ[ppm] = 8.13 (d, J = 1.6 Hz, 4H), 8.04 – 7.97 (m, 4H), 7.99 (s, 4H), 7.38 (d, J = 1.5 Hz, 4H), 7.12 ppm (dd, J = 7.6, 5.1 Hz, 4H);

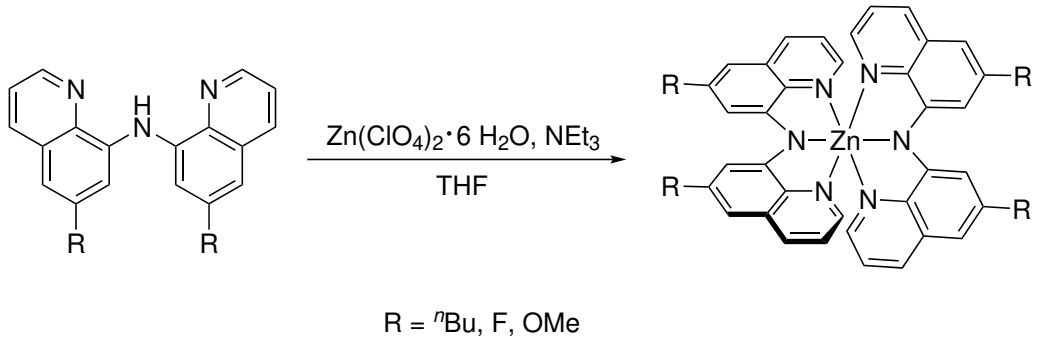

Scheme 4.10: Synthesis to obtain the Zinc complexes **1f** – **h**

Zinc complex 1f (butyl substituents)
6-butyl-N-(6-butyl-8-quinolinyl)-8-quinolinamine **5f** (150.0 mg, 0.391 mmol, 2.0 equiv.) was dissolved in THF (5 mL) and trimethylamine (220 µl, 1.56 mmol, 8.0 equiv.) was added. The mixture was stirred and $Zn(ClO4)_2 \cdot 6H_2O$ (72.8 mg, 0.196 mmol, 1.0 equiv.) dissolved in THF (1.5 mL) was added. The mixture was stirred overnight. The solvent was evaporated and the obtained solid was washed with MeOH (2 × 4 mL) and *n*-hexane (2 × 4 mL). The solid was then recrystallized from toluene/MeOH and then dried to obtain the target material as red crystals (93.0 mg, 57% yield). Crystals suitable for x-ray analysis were grown by layering a solution of the material in CDCl3 with MeOH. **IR (ATR):** ν = 3036.4 (w), 2949.2 (w), 2925.0 (w), 2854.0 (w), 1597.2 (w), 1582.7 (w), 1558.5 (m), 1472.1 (m), 1444.4 (s), 1422.1 (s), 1388.7 (s), 1357.8 (s), 1280.0 (m), 1225.0 (m), 1196.8 (m), 1149.2 (m), 1119.9 (m), 1084.0 (m), 970.9 (w), 928.8 (w), 908.8 (w), 829.6 (s), 781.6 (s), 728.9 (w), 702.4 (w), 644.4 (w), 617.3 (m) cm^{-1}; **^{1}H-NMR (400 MHz, $CDCl_3$):** δ[ppm] = 8.09 (d, J = 1.7 Hz, 2H), 7.92 (dd, J = 4.4, 1.7 Hz, 2H), 7.83 (dd, J = 8.2, 1.7 Hz, 2H), 6.89 (dd, J = 8.2, 4.4 Hz, 2H), 6.76 (s, 2H), 2.85 (t, J = 7.7 Hz, 4H), 1.89 (q, J = 7.7 Hz, 2H), 1.57 (h, J = 7.3 Hz, 3H), 1.06 (t, J = 7.3 Hz, 3H); **^{13}{^{1}H}-NMR (100 MHz, $CDCl_3$):** δ[ppm] = 146.39, 143.57, 143.28, 140.04, 136.22, 129.89, 120.96, 110.60, 110.46, 36.96, 33.71, 22.72, 14.19; **MS [ESI]:** m/z = 828.3860 $[M]^+$ (calc. m/z = 828.3858);

Zinc complex 1g (fluoro substituents)
6-fluoro-N-(6-fluoro-8-quinolinyl)-8-quinolinamine **5g** (150.0 mg, 0.488 mmol, 2.0 equiv.) was dissolved in THF (5 mL) and trimethylamine (270 µl, 1.92 mmol, 8.0 equiv.) was added. The mixture was stirred and $Zn(ClO4)_2 \cdot 6H_2O$ (90.9 mg, 0.244 mmol, 1.0 equiv.) dissolved in THF (2.0 mL) was added. The mixture was stirred for 2 d. The mixture was filtered and the residue was washed with toluene (2 × 1 mL) and *n*-hexane (2 × 1 mL). The solid was then dried to obtain the target material as an orange powder (62.6 mg, 38% yield). Crystals suitable for x-ray analysis were grown by vapor diffusion of n-pentane into a solution of the material in DCM. **IR (ATR):** ν = 1600.3 (w), 1556.7 (m), 1489.9 (s), 1444.9 (s), 1426.5 (s), 1390.5 (s), 1276.7 (m), 1227.2 (w), 1205.5 (w), 1185.8 (m), 1133.4 (m),

1039.9 (w), 1007.0 (m), 911.5 (m), 822.2 (m), 806.5 (m), 785.4 (s), 680.2 (w), 640.5 (w), 626.3 (m) cm^{-1}; **^{1}H-NMR (400 MHz, $CDCl_3$):** δ[ppm] = 7.95 – 7.88 (m, 8H), 7.83 (dd, J = 13.1, 2.5 Hz, 4H), 7.06 – 7.00 (m, 4H), 6.67 (dd, J = 9.0, 2.5 Hz, 4H); **MS [ESI]:** m/z = 668.1037 M^+ (calc. m/z = 668.1035);

Zinc complex 1h (methoxy substituents)
6-methoxy-N-(6-methoxy-8-quinolinyl)-8-quinolinamine **5h** (150.0 mg, 0.453 mmol, 2.0 equiv.) was dissolved in THF (5 mL) and trimethylamine (250 µl, 1.81 mmol, 8.0 equiv.) was added. The mixture was stirred and $Zn(ClO4)_2 \cdot 6H_2O$ (84.3 mg, 0.226 mmol, 1.0 equiv.) dissolved in THF (1.5 mL) was added. The mixture was stirred for 3 d. The mixture was filtered and the residue was washed with DCM (3 × 1 mL). The solid was then dried to obtain the target material as an orange powder (102.9 mg, 63% yield). Crystals suitable for x-ray analysis were grown by vapor diffusion of n-pentane into a solution of the material in DCM. **IR (ATR):** ν = 2932.5 (w), 1559.2 (m), 1484.0 (m), 1445.2 (s), 1417.8 (m), 1387.0 (s), 1285.8 (w), 1228.5 (m), 1199.8 (s), 1157.8 (m), 1143.4 (m), 1074.6 (w), 1032.9 (w), 956.6 (w), 912.6 (w), 815.6 (m), 748.9 (m), 707.4 (w), 675.5 (w), 633.4 (w) cm^{-1}; **^{1}H-NMR (400 MHz, $CDCl_3$):** δ[ppm] = 7.81 – 7.66 (m, 3H), 6.84 (dd, J = 8.2, 4.4 Hz, 1H), 6.29 (d, J = 2.4 Hz, 1H), 3.91 (s, 3H); **^{13}{^{1}H}-NMR (100 MHz, $CDCl_3$):** δ[ppm] = 159.56, 146.18, 140.64, 137.42, 134.59, 129.60, 120.47, 100.58, 90.32, 54.23.; **MS [ESI]:** m/z = 725.1850 $[M+H]^+$ (calc. m/z = 725.1847);

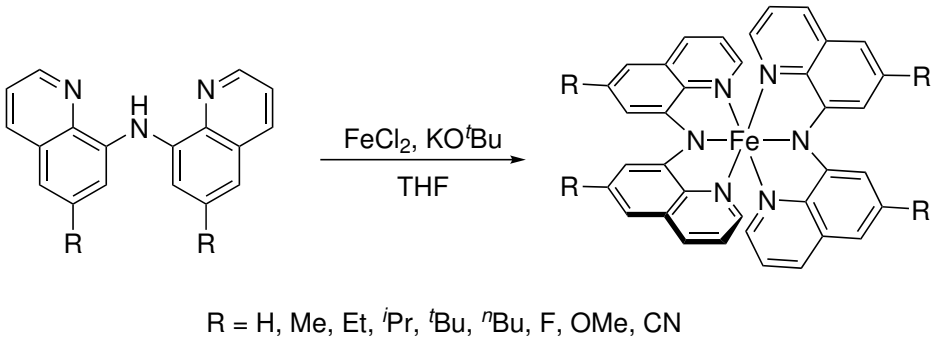

Scheme 4.11: Synthesis to obtain the Iron complexes **2a** – **h**

Iron complex 2a
BQAH **5a** (105.3 mg, 0.388 mmol) was dissolved in THF (3 mL) and KOtBu (43.6 mg, 0.388 mmol) was added. The mixture was stirred for 30 min, then $FeCl_2$ (24.6 mg, 0.194 mmol) was added. After stirring over night, the mixture was filtered and the residue was washed with THF (2 × 1 mL) and DCM (2 × 1 mL). The residue was then continuously extracted with DCM. The extract was filtered and the residue was dried to yield the target compound (69.0 mg, 60% yield) as a dark purple solid. Crystals suitable for X-ray structural analysis were grown by vapor diffusion of Methanol into a solution of **5a** in DCM. **IR (BaF_2):** ν = 2954 (w), 2917 (w), 2852 (w), 1594 (m), 1545 (s), 1488 (s), 1444 (s), 1434 (m), 1392 (s), 1379 (m), 1329 (w), 1278 (w), 1260 (w), 1193 (m), 1108 (w), 1011 (w), 983 (w) cm^{-1}; **IR (ATR):** ν = 3049 (w), 1589 (w), 1544 (s), 1488 (m), 1445 (s), 1392 (s), 1350 (m), 1173 (m), 1123 (m), 1094 (m), 1034 (m), 932 (m), 839 (w), 811 (m), 798 (m), 771 (m), 730 (m), 643 (w) cm^{-1}; **MS [ESI]:** m/z = 596.1413 (calc. m/z = 596.1412)

Iron complex 2b (methyl substituents)
6-Methyl-N-(6-methyl-8-quinolinyl)-8-quinolinamine **5b** (124.7 mg, 0.417 mmol, 2.0 equiv.) was dissolved in THF (3 mL) and potassium *tert*-butoxide (46.7 mg, 0.417 mmol, 2.0 equiv) was added. The mixture was stirred for 30 min, then $FeCl_2$ (26.4 mg, 0.208 mmol, 1.0 equiv.) was added. The mixture was stirred for 3 d. The reaction mixture was given into an extractor and the reaction vessel was washed with THF (3 × 1 mL) and the washes were added to the extractor as well. Additional THF (6 mL) was added to the extractor and the material was extracted for 2 d. The extract was filtered and the residue was washed with THF (2 × 1 mL). The residue was dried to obtain the target compound as a black solid (38.7 mg, 29% yield). Crystals suitable for x-ray analysis were grown by layering a solution of the material in THF with *n*-hexane. **IR (ATR):** ν = 2906 (w), 1599(w), 1553 (s), 1476 (m), 1446 (m), 1424 (s), 1384 (s), 1352 (m), 1284 (m), 1206 (m), 1148 (m), 1049 (w), 976 (w), 831 (w), 806 (m), 783 (m), 763 (m), 688 (w), 601 (w) cm^{-1}; **MS [ESI]:** m/z = 652.2038 $[M]^+$ (calc. m/z = 652.2038);

Iron complex 2c (ethyl substituents)
6-Methyl-N-(6-methyl-8-quinolinyl)-8-quinolinamine **5c** (144.7 mg, 0.442 mmol, 2.0 equiv.) was dissolved in THF (3 mL) and potassium *tert*-butoxide (49.6 mg, 0.442 mmol, 2.0 equiv) was added. The mixture was stirred for 30 min, then $FeCl_2$ (28.0 mg, 0.221 mmol, 1.0 equiv.) was added. The mixture was stirred for 2 d. The reaction mixture was given into an extractor and the reaction vessel was washed with THF (3 × 1 mL) and the washes were added to the extractor as well. Additional THF (6 mL) was added to the extractor and the material was extracted overnight. The extract was reduced to 4 mL in volume and *n*-hexane was added. The precipitate was filtered off, washed with *n*-hexane (3 × 2 mL) and then dried. The target compound was obtained as a black solid (95.0 mg, 61% yield). Crystals suitable for x-ray analysis were grown by layering a solution of the material in THF with *n*-hexane. **IR (ATR):** ν = 2960.7 (w), 1597.3 (w), 1555.7 (m), 1474.8 (m), 1443.9 (m), 1422.0 (s), 1387.1 (s), 1281.9 (m), 1200.3 (m), 1143.3 (m), 1062.9 (m), 1005.5 (m), 949.9 (w), 899.3 (w), 837.4 (m), 812.9 (w), 769.4 (m), 683.4 (m), 630.3 (w) cm^{-1}; **MS [ESI]:** m/z = 708.2662 $[M]^+$ (calc. m/z = 708.2664);

Iron complex 2d (1-methylethyl substituents)
From a stock solution of 6-(1-methylethyl)-N-(6-(1-methylethyl)-8-quinolinyl)-8-quinolinamine **5d** (373.0 mg, 1.05 mmol) a volume of 1.91 mL (0.344 mmol, 2.0 equiv.) was taken and potassium *tert*-butoxide (38.6 mg, 0.344 mmol, 2.0 equiv.) was added. The mixture was stirred for 30 min, then $FeCl_2$ (21.8 mg, 0.172 mmol, 1.0 equiv.) was added. The mixture was stirred for x d. The reaction mixture was given into an extractor and the reaction vessel was washed with THF (3 × 1 mL) and the washes were added to the extractor as well. Additional THF (6 mL) was added to the extractor and the material was extracted overnight. The extract was reduced to 4 mL in volume and *n*-hexane was added. The precipitate was filtered off, washed with *n*-hexane (2 mL) and then dried. The target compound was obtained as a black solid (84.2 mg, 64% yield). Crystals suitable for x-ray analysis were grown by layering a solution of the material in THF with *n*-hexane. **IR (ATR):** ν = 2954.6 (w), 1592.1 (w), 1551.7 (s), 1473.2 (m), 1426.0 (s), 1391.6 (s),

1353.9 (m), 1283.5 (m), 1216.3 (w), 1201.5 (m), 1134.1 (w), 1076.1 (w), 1042.3 (w), 963.7 (w), 854.3 (w), 836.0 (m), 817.1 (w), 766.4 (s), 658.9 (w), 625.7 (w) cm^{-1}; **MS [ESI]:** m/z = 764.3292 $[M]^+$ (calc. m/z = 764.3290);

Iron complex 2e (1,1-dimethylethyl substituents)
6-(1,1-dimethylethyl)-N-(6-(1,1-dimethylethyl)-8-quinolinyl)-8-quinolinamine **5e** was dissolved in THF (3 mL) and potassium *tert*-butoxide was added. The mixture was stirred for 30 min, then $ZnCl_2$ was added. The mixture was stirred for 2 d and then filtered. The residue was washed with THF (2 × 1 mL). The filtrate was layered with *n*-hexane and cooled to -30°C overnight. The precipitate was filtered off and washed with *n*-hexane (2 × 1 mL) and then dried. The target material was obtained as a dark violet solid (28.8 mg, 13% yield). Crystals suitable for x-ray analysis were grown by layering a solution of the material in THF with *n*-hexane. **IR (ATR):** ν = 2951.2(w), 2865.4 (w), 1593.5 (w), 1552.7 (s), 1469.9 (m), 1441.3 (m), 1421.3 (s), 1382.2 (s), 1352.2 (s), 1329.5 (m), 1286.2 (m), 1256.1 (w), 1200.7 (m), 1131.8 (w), 1093.4 (w), 1068.9 (w), 1043.9 (w), 1023.5 (w), 955.0 (w), 920.8 (w), 836-1 (w), 817.8 (w), 806.4 (w), 769.3 (m), 690.9 (w), 663.1 (w), 625.4 (w) cm^{-1}; **MS [ESI]:** m/z = 820.3913 $[M]^+$ (calc. m/z = 820.3916);

Iron complex 2f (butyl substituents)
6-Butyl-N-(6-butyl-8-quinolinyl)-8-quinolinamine **5f** (153.1 mg, 0.399 mmol, 2.0 equiv.) was dissolved in THF (3 mL) and potassium *tert*-butoxide (44.8 mg, 0.399 mmol, 2.0 equiv.) was added. The mixture was stirred for 30 min, then $FeCl_2$ (25.3 mg, 0.200 mmol, 1.0 equiv) was added. The mixture was stirred for 2 d. The reaction mixture was given into an extractor and the reaction vessel was washed with THF (3 × 1 mL) and the washes were added to the extractor as well. Additional THF (6 mL) was added to the extractor and the material was extracted overnight. The extract was evaporated to dryness. After that THF (1.5 mL) and *n*-hexane (4 mL) were added and the mixture was filtered. The residue was washed with *n*-hexane (3 × 2 mL) and then dried. The target material was obtained as a dark violet powder (102.5 mg, 62% yield). Crystals suitable for x-ray analysis were grown by layering a solution of the material in THF with *n*-hexane. **IR (ATR):** ν = 2954.3 (w), 2920.5 (w), 2852.1 (w), 1596.1 (w), 1552.6 (s), 1473.6 (m), 1443.7 (m), 1426.5 (s), 1389.7 (s), 1355.0 (m), 1280.7 (m), 1196.5 (m), 1146.8 (m), 1100.6 (w), 1048.0 (w), 967.9 (w). 831.3 (m), 814.0 (w), 771.3 (m), 622.3 (w) cm^{-1}; **MS [ESI]:** m/z = 820.3916 $[M]^+$ (calc. m/z = 820.3916);

Iron complex 2g (fluoro substituents)
6-Fluro-N-(6-fluoro-8-quinolinyl)-8-quinolinamine **5g** (165.8 mg, 0.540 mmol, 2.0 equiv.) was dissolved in THF (3 mL) and potassium *tert*-butoxide (60.6 mg, 0.540 mmol, 2.0 equiv.) was added. The mixture was stirred for 30 min, then $FeCl_2$ (34.2 mg, 0.270 mmol, 1.0 equiv) was added. The mixture was stirred for 3 d. The reaction mixture was given into an extractor and the reaction vessel was washed with THF (3 × 1 mL) and the washes were added to the extractor as well. Additional THF (6 mL) was added to the extractor and the material was extracted overnight. The extract was reduced to half in volume and *n*-hexane (6 mL) was added. After standing overnight the mixture was filtered. The residue was washed with *n*-hexane (3 × 2 mL) and then dried. The target material was obtained as a dark violet powder (102.4 mg, 57% yield).Crystals suitable for x-ray analysis were grown

by layering a solution of the material in THF with *n*-hexane. **IR (ATR):** ν = 1595.2 (w), 1544.2 (s), 1487.1 (m), 1443.2 (s), 1390.4 (s), 1327.8 (m), 1278.0 (m), 1209.5 (w), 1191.3 (m), 1164.8 (w), 1126.3 (m), 1107.9 (m), 1009.5 (m), 982.1 (m), 820.1 (m), 780.4 (m), 761.4 (m), 715.1 (w), 652.6 (w), 630.7 (w), 608.9 (m) cm^{-1}; **MS [ESI]:** m/z = 668.1035 $[M]^+$ (calc. m/z = 668.1037);

Iron complex 2h (methoxy substituents)
6-Methoxy-N-(6-methoxy-8-quinolinyl)-8-quinolinamine **5h** (164.2 mg, 0.495 mmol, 2.0 equiv.) was dissolved in THF (3 mL) and potassium *tert*-butoxide (55.6 mg, 0.495 mmol, 2.0 equiv.) was added. The mixture was stirred for 30 min, then $FeCl_2$ (31.4 mg, 0.248 mmol, 1.0 equiv.) was added. The mixture was stirred for 3 d and then poured into an extractor, the reaction vessel was washed with THF (3 × 1 mL) and the washes were added into the extractor as well. The material was then continuously extracted with additional THF (6 mL) for 2 d. The extract was then filtered and the residue was washed with THF (2 × 1 mL) and dried. The target material was obtain as a violet solid (61.5 mg, 34% yield). Crystals suitable for x-ray analysis were grown by layering a solution of the material in THF with *n*-hexane. **IR (ATR):** ν = 3001.5 (w), 2934.4 (w), 1586.1 (m), 1549.4 (s), 1479.2 (m), 1460.3 (m), 1443.6 (s), 1421.6 (m), 1383.9 (s), 1329.0 (m), 1285.5 (m), 1228.2 (m), 1201.4 (s), 1158.6 (m), 1137.8(s), 1066.8 (m), 1051.5 (m), 1029.1 (m), 959.9 (w), 841.9 (w), 813.4 (s), 796.5 (m), 778.7 (m), 761.7 (m), 728.8 (m), 700.7 (w), 682.4 (w), 655.3 (m), 629.8 (w) cm^{-1}; **MS [ESI]:** m/z = 716.1832 $[M]^+$ (calc. m/z = 716.1834);

Iron complex 2i (nitrile substituents)
8-((6-Cyanoquinoline-8-yl)amino)quinoline-6-carbonitrile **5i** (112.2 mg, 0.349 mmol, 2.0 equiv.) was dissolved in THF (3 mL) and potassium *tert*-butoxide (40.9 mg, 0.365 mmol, 2.1 equiv.) was added. The mixture was stirred for 30 min, then $FeCl_2$ (22.0 mg, 0.174 mmol, 1.0 equiv) was added. The mixture was stirred for 3 d. The reaction mixture was given into an extractor and the reaction vessel was washed with THF (3 × 1 mL) and the washes were added to the extractor as well. Additional THF (6 mL) was added to the extractor and the material was extracted overnight. The extract was reduced to half in volume and *n*-hexane (6 mL) was added. After standing overnight the mixture was filtered. The residue was washed with *n*-hexane (3 × 2 mL) and then dried. The target material was obtained as a dark violet powder (14.8 mg, 12% yield). Crystals suitable for x-ray analysis were grown by layering a solution of the material in THF with *n*-hexane. **IR (ATR):** ν = 2226 (w), 1552 (s), 1469 (m), 1444 (s), 1424 (s), 1383 (s), 1356 (m), 1285 (m), 1199 (m), 1138 (m), 972 (w), 840 (m), 812 (w), 777 (m), 758 (m), 701 (w), 669 (w), 626 (w) cm^{-1}; **MS [ESI]:** m/z = 696.1221 $[M]^+$ (calc. m/z = 696.1222);

Chromium complex 3
BQAH (120.5 mg, 0.444 mmol, 2.0 equiv.) was dissolved in THF (3 mL) and potassium *tert*-butoxide (49.9 mg, 0.444 mmol, 2.0 equiv.) was added. The mixture was stirred for 30 min, followed by the addition of $CrCl_2$ (27.3 mg, 0.222 mmol, 1.0 equiv.). After stirring overnight, the mixture was filtered and the residue was washed with THF (2 × 1 mL) and DCM (2 × 1 mL). The residue was then continuously extracted with DCM. The extract was evaporated to dryness to obtain the target material as a dark red solid (38.7 mg, 29% yield). Crystals suitable for x-ray analysis were grown by slow evaporation

of a concentrated solution of Cr(BQA)2 in DCM. **IR (BaF_2):** ν = 2916 (w), 1574 (m), 1561 (m), 1534 (m), 1494 (s), 1456 (s), 1434 (w), 1389 (s), 1376 (m), 1331 (w), 1315 (w), 1130 (w) cm^{-1}; **MS [ESI]:** m/z = 592.1467 $[M]^+$ (calc. m/z = 592.1468);

Chromium complex $[Cr(BQA)_2]Cl$
BQAH (100.7 mg mg, 0.371 mmol) was dissolved in THF (3 mL) and potassium *tert*-butoxide (41.7 mg, 0.371 mmol) was added. The mixture was stirred for 30 min, followed by the addition of $CrCl_3$ (29.4 mg, 0.186 mmol). After stirring overnight, the mixture was filtered and the residue was washed with THF (2 × 1 1 mL). The residue was taken up in DCM (2 mL) and filtered again. This procedure was repeated twice. The combined filtrates were evaporated to dryness to obtain a sample of $[Cr(BQA)_2]Cl$ as a dark red solid. **IR (BaF_2):** ν = 2922 (w), 1563 (m), 1494 (m), 1460 (s), 1454 (s), 1427 (w), 1386 (s), 1371 (m), 1327 (w), 1129 (w) cm^{-1}; **MS [ESI]:** m/z = 592.1467 (calc. m/z = 592.1468);

Manganese complex 4
BQAH (123.3 mg, 0.454 mmol, 2.0 equiv.) was dissolved in THF (3 mL) and potassium *tert*-butoxide (51.0 mg, 0.454 mmol, 2.0 equiv.) was added. The mixture was stirred for 30 min, followed by addition of $MnCl_2$ (28.6 mg, 0.22 mmol, 1.0 equiv.). After stirring overnight, the mixture was filtered and the residue was washed with THF (2 × 1 mL). The filtrate was layered with *n*-hexane and cooled to –30 °C. After three days the formed crystals were filtered off, washed with *n*-hexane (3 × 1 mL) and dried. The target compound was obtained as a dark orange solid (55.8 mg, 41% yield). Crystals suitable for x-ray analysis were grown by vapor diffusion of *n*-hexane into a concentrated solution of Mn(BQA)2 in THF. **IR (BaF_2):** ν = 2921 (w), 2850 (w), 1552 (m), 1499 (m), 1490 (m), 1448 (s), 1423 (w), 1387 (s), 1331 (m), 1229 (w), 1179 (m), 1119 (m) cm^{-1}; **MS [ESI]:** m/z = 595.1448 $[M]^+$ (calc. m/z = 595.1443);

Bibliography

[1] E. A. Alsema and E. Nieuwlaar. Energy viability of photovoltaic systems. *Energy Policy*, 28(14):999 – 1010, 2000.

[2] L. B. Kish. End of moore's law: thermal (noise) death of integration in micro and nano electronics. *Physics Letters A*, 305(3):144 – 149, 2002.

[3] L. Clavelier, C. Le Royer, Y. Morand, C. Deguet, B. Vincent, J.-François Damlencourt, J.-Michel Hartmann, O. Kermarrec, T. Signamarcheix, B. Depuydt, A. Theuwis, C. Quaeyhaegens, N. Cherkashin, P. Rivallin, C. Tabone, S. Lagrasta, Y. Campidelli, S. Descombes, L. Sanchez, T. Akastu, A. Rigny, D. Bensahel, T. Billon, N. Kernevez, and S. Deleonibus. Review of some critical aspects of ge and geoi substrates. *ECS Transactions*, 3(7):789–805, 2006.

[4] J. S. Blakemore. Semiconducting and other major properties of gallium arsenide. *Journal of Applied Physics*, 53(10):R123–R181, 1982.

[5] D. E. Carter, H. Vasken Aposhian, and A. Jay Gandolfi. The metabolism of inorganic arsenic oxides, gallium arsenide, and arsine: a toxicochemical review. *Toxicology and Applied Pharmacology*, 193(3):309 – 334, 2003.

[6] A. Tanaka. Toxicity of indium arsenide, gallium arsenide, and aluminium gallium arsenide. *Toxicology and Applied Pharmacology*, 198(3):405 – 411, 2004.

[7] H. Minemawari, T. Yamada, H. Matsui, J.'ya Tsutsumi, S. Haas, R. Chiba, R. Kumai, and T. Hasegawa. Inkjet printing of single-crystal films. *Nature*, 475(7356):364–367, 2011.

[8] D. A. Pardo, G. E. Jabbour, and N. Peyghambarian. Application of screen printing in the fabrication of organic light-emitting devices. *Advanced Materials*, 12(17):1249–1252, 2000.

[9] F. C. Krebs. Fabrication and processing of polymer solar cells: A review of printing and coating techniques. *Solar Energy Materials and Solar Cells*, 93(4):394 – 412, 2009.

[10] G. Lligadas, J. C. Ronda, M. Galià, and V. Cádiz. Renewable polymeric materials from vegetable oils: a perspective. *Materials Today*, 16(9):337 – 343, 2013.

[11] Y. Qian, X. Zhang, L. Xie, D. Qi, B. K. Chandran, X. Chen, and W. Huang. Stretchable organic semiconductor devices. *Advanced Materials*, 28(42):9243–9265, 2016.

[12] Y. Qian, X. Zhang, D. Qi, L. Xie, B. K. Chandran, X. Chen, and W. Huang. Thin-film organic semiconductor devices: from flexibility to ultraflexibility. *Science China Materials*, 59(7):589–608, Jul 2016.

[13] B. Lüssem, M. Riede, and K. Leo. Doping of organic semiconductors. *Physica Status Solidi A*, 210(1):9–43, 2013.

[14] I. Salzmann, G. Heimel, M. Oehzelt, S. Winkler, and N. Koch. Molecular electrical doping of organic semiconductors: Fundamental mechanisms and emerging dopant design rules. *Accounts of Chemical Research*, 49(3):370–378, 2016.

[15] J. T. E. Quinn, J. Zhu, X. Li, J. Wang, and Y. Li. Recent progress in the development of n-type organic semiconductors for organic field effect transistors. *J. Mater. Chem. C*, 5:8654–8681, 2017.

[16] L. Chan, P. nad Kwok. The motivation for and challenges to scaling down organic field-effect transistors. *Advanced Electronic Materials*, 5(7):1900029, 2019.

[17] G. Horowitz. Organic thin film transistors: From theory to real devices. *Journal of Materials Research*, 19(7):1946–1962, 2004.

[18] D. Ebeling, M. Šekutor, M. Stiefermann, J. Tschakert, J. E. P. Dahl, R. M. K. Carlson, A. Schirmeisen, and P. R. Schreiner. London dispersion directs on-surface self-assembly of [121]tetramantane molecules. *ACS Nano*, 11(9):9459–9466, 2017. PMID: 28846392.

[19] S. Rösel, C. Balestrieri, and P. R. Schreiner. Sizing the role of london dispersion in the dissociation of all-meta tert-butyl hexaphenylethane. *Chem. Sci.*, 8:405–410, 2017.

[20] J. P. Wagner and P. R. Schreiner. London dispersion in molecular chemistry—reconsidering steric effects. *Angewandte Chemie International Edition*, 54(42):12274–12296, 2015.

[21] V. Coropceanu, J. Cornil, D. A. da Silva Filho, Y. Olivier, R. Silbey, and J.-L. Brédas. Charge transport in organic semiconductors. *Chemical Reviews*, 107(4):926–952, 2007. PMID: 17378615.

[22] C. Reese, M. E. Roberts, S. R. Parkin, and Z. Bao. Tuning crystalline solid-state order and charge transport via building-block modification of oligothiophenes. *Advanced Materials*, 21(36):3678–3681, 2009.

[23] J.-Hu Dou, Y.-Qing Zheng, Z.-Fan Yao, Z.-Ao Yu, T. Lei, X. Shen, X.-Yi Luo, J. Sun, S.-Ding Zhang, Y.-Fan Ding, G. Han, Y. Yi, J.-Yu Wang, and J. Pei. Fine-tuning of crystal packing and charge transport properties of bdopv derivatives through fluorine substitution. *Journal of the American Chemical Society*, 137(50):15947–15956, 2015. PMID: 26619351.

[24] Z.-Fan Yao, J.-Yu Wang, and J. Pei. Control of π–π stacking via crystal engineering in organic conjugated small molecule crystals. *Crystal Growth & Design*, 18(1):7–15, 2018.

[25] A. Köhler and H. Bässler. *Electronic and Optical Processes of Organic Semiconductors*, chapter 3, pages 193–305. John Wiley & Sons, Ltd, 2015.

[26] A. Tsumura, H. Koezuka, and T. Ando. Macromolecular electronic device: Field-effect transistor with a polythiophene thin film. *Applied Physics Letters*, 49(18):1210–1212, 1986.

[27] B. S. Ong, Y. Wu, P. Liu, and S. Gardner. High-performance semiconducting polythiophenes for organic thin-film transistors. *Journal of the American Chemical Society*, 126(11):3378–3379, 2004. PMID: 15025437.

[28] I. McCulloch, C. Bailey, M. Giles, M. Heeney, I. Love, M. Shkunov, D. Sparrowe, and S. Tierney. Influence of molecular design on the field-effect transistor characteristics of terthiophene polymers. *Chemistry of Materials*, 17(6):1381–1385, 2005.

[29] Y. D. Park, D. H. Kim, Y. Jang, J. H. Cho, M. Hwang, H. S. Lee, J. A. Lim, and K. Cho. Effect of side chain length on molecular ordering and field-effect mobility in poly(3-alkylthiophene) transistors. *Organic Electronics*, 7(6):514 – 520, 2006.

[30] A. Assadi, C. Svensson, M. Willander, and O. Inganäs. Field-effect mobility of poly(3-hexylthiophene). *Applied Physics Letters*, 53(3):195–197, 1988.

[31] R. J. Kline, M. D. McGehee, E. N. Kadnikova, J. Liu, J. M. J. Fréchet, and M. F. Toney. Dependence of regioregular poly(3-hexylthiophene) film morphology and field-effect mobility on molecular weight. *Macromolecules*, 38(8):3312–3319, 2005.

[32] A. Zen, M. Saphiannikova, D. Neher, J. Grenzer, S. Grigorian, U. Pietsch, U. Asawapirom, S. Janietz, U. Scherf, I. Lieberwirth, and G. Wegner. Effect of molecular weight on the structure and crystallinity of poly(3-hexylthiophene). *Macromolecules*, 39(6):2162–2171, 2006.

[33] R. Zhang, B. Li, M. C. Iovu, M. Jeffries-EL, G. Sauvé, J. Cooper, S. Jia, S. Tristram-Nagle, D. M. Smilgies, D. N. Lambeth, R. D. McCullough, and T. Kowalewski. Nanostructure dependence of field-effect mobility in regioregular poly(3-hexylthiophene) thin film field effect transistors. *Journal of the American Chemical Society*, 128(11):3480–3481, 2006. PMID: 16536496.

[34] M. Surin, P. Leclère, R. Lazzaroni, J. D. Yuen, G. Wang, D. Moses, A. J. Heeger, S. Cho, and K. Lee. Relationship between the microscopic morphology and the charge transport properties in poly(3-hexylthiophene) field-effect transistors. *Journal of Applied Physics*, 100(3):033712, 2006.

[35] J.-F. Chang, B. Sun, D. W. Breiby, M. M. Nielsen, T. I. Sölling, M. Giles, I. McCulloch, and H. Sirringhaus. Enhanced mobility of poly(3-hexylthiophene) transistors by spin-coating from high-boiling-point solvents. *Chemistry of Materials*, 16(23):4772–4776, 2004.

[36] L. A. Majewski, J. W. Kingsley, C. Balocco, and A. M. Song. Influence of processing conditions on the stability of poly(3-hexylthiophene)-based field-effect transistors. *Applied Physics Letters*, 88(22):222108, 2006.

[37] H. Jia, S. Gowrisanker, G. K. Pant, R. M. Wallace, and B. E. Gnade. Effect of poly (3-hexylthiophene) film thickness on organic thin film transistor properties. *Journal of Vacuum Science & Technology A*, 24(4):1228–1232, 2006.

[38] G. Horowitz, D. Fichou, X. Peng, and F. Garnier. Thin-film transistors based on alpha-conjugated oligomers. *Synthetic Metals*, 41(3):1127 – 1130, 1991. Proceedings of the International Conference on Science and Technology of Synthetic Metals (ICSM '90).

[39] Y. Lin, D. J. Gundlach, S. F. Nelson, and T. N. Jackson. Stacked pentacene layer organic thin-film transistors with improved characteristics. *IEEE Electron Device Letters*, 18(12):606–608, Dec 1997.

[40] M. Shtein, J. Mapel, J. B. Benziger, and S. R. Forrest. Effects of film morphology and gate dielectric surface preparation on the electrical characteristics of organic-vapor-phase-deposited pentacene thin-film transistors. *Applied Physics Letters*, 81(2):268–270, 2002.

[41] A. Di Carlo, F. Piacenza, A. Bolognesi, B. Stadlober, and H. Maresch. Influence of grain sizes on the mobility of organic thin-film transistors. *Applied Physics Letters*, 86(26):263501, 2005.

[42] J. Y. Lee, S. Roth, and Y. W. Park. Anisotropic field effect mobility in single crystal pentacene. *Applied Physics Letters*, 88(25):252106, 2006.

[43] T. Minakata and Y. Natsume. Direct formation of pentacene thin films by solution process. *Synthetic Metals*, 153(1):1 – 4, 2005. Proceedings of the International Conference on Science and Technology of Synthetic Metals.

[44] A. Afzali, C. D. Dimitrakopoulos, and T. L. Breen. High-performance, solution-processed organic thin film transistors from a novel pentacene precursor. *Journal of the American Chemical Society*, 124(30):8812–8813, 2002. PMID: 12137531.

[45] K. P. Weidkamp, A. Afzali, R. M. Tromp, and R. J. Hamers. A photopatternable pentacene precursor for use in organic thin-film transistors. *Journal of the American Chemical Society*, 126(40):12740–12741, 2004. PMID: 15469245.

[46] X. Zhan, A. Facchetti, S. Barlow, T. J. Marks, M. A. Ratner, M. R. Wasielewski, and S. R. Marder. Rylene and related diimides for organic electronics. *Advanced Materials*, 23(2):268–284, 2011.

[47] D. Shukla, S. F. Nelson, D. C. Freeman, M. Rajeswaran, W. G. Ahearn, D. M. Meyer, and J. T. Carey. Thin-film morphology control in naphthalene-diimide-based semiconductors: High mobility n-type semiconductor for organic thin-film transistors. *Chemistry of Materials*, 20(24):7486–7491, 2008.

[48] B. A. Jones, A. Facchetti, M. R. Wasielewski, and T. J. Marks. Tuning orbital energetics in arylene diimide semiconductors. materials design for ambient stability of n-type charge transport. *Journal of the American Chemical Society*, 129(49):15259–15278, 2007. PMID: 17999505.

[49] G. H. Gelinck, T. C. T. Geuns, and D. M. de Leeuw. High-performance all-polymer integrated circuits. *Applied Physics Letters*, 77(10):1487–1489, 2000.

[50] D. Voss. Cheap and cheerful circuits. *Nature*, 407:442–444, 2000.

[51] S. E. Burns, C. Kuhn, K. Jacobs, J. D. MacKenzie, C. Ramsdale, A. C. Arias, J. Watts, M. Etchells, K. Chalmers, P. Devine, N. Murton, S. Norval, J. King, J. Mills, H. Sirringhaus, and R. H. Friend. Printing of polymer thin-film transistors for active-matrix-display applications. *Journal of the Society for Information Display*, 11(4):599–604, 2003.

[52] J. A. Rogers, Z. Bao, K. Baldwin, A. Dodabalapur, B. Crone, V. R. Raju, V. Kuck, H. Katz, K. Amundson, J. Ewing, and P. Drzaic. Paper-like electronic displays: Large-area rubber-stamped plastic sheets of electronics and microencapsulated electrophoretic inks. *Proceedings of the National Academy of Sciences*, 98(9):4835–4840, 2001.

[53] G. H. Gelinck, H. E. A. Huitema, E. van Veenendaal, E. Cantatore, L. Schrijnemakers, J. B. P. H. van der Putten, T. C. T. Geuns, M. Beenhakkers, J. B. Giesbers, B.-H. Huisman, E. J. Meijer, E. M. Benito, F. J. Touwslager, A. W. Marsman, B. J. E. van Rens, and D. M. de Leeuw. Flexible active-matrix displays and shift registers based on solution-processed organic transistors. *Nature Materials*, 3:106–110, 2004.

[54] B. K. Crone, A. Dodabalapur, R. Sarpeshkar, A. Gelperin, H. E. Katz, and Z.-Mou Bao. Organic oscillator and adaptive amplifier circuits for chemical vapor sensing. *Journal of Applied Physics*, 91(12):10140–10146, 2002.

[55] P. F. Baude, D. A. Ender, M. A. Haase, T. W. Kelley, D. V. Muyres, and S. D. Theiss. Pentacene-based radio-frequency identification circuitry. *Applied Physics Letters*, 82(22):3964–3966, 2003.

[56] S. Khan, L. Lorenzelli, and R. S. Dahiya. Technologies for printing sensors and electronics over large flexible substrates: A review. *IEEE Sensors Journal*, 15(6):3164–3185, June 2015.

[57] A. Naibi Lakshminarayana, A. Ong, and C. Chi. Modification of acenes for n-channel ofet materials. *J. Mater. Chem. C*, 6:3551–3563, 2018.

[58] J. Feng, W. Jiang, and Z. Wang. Synthesis and application of rylene imide dyes as organic semiconducting materials. *Chemistry – An Asian Journal*, 13(1):20–30, 2018.

[59] Q. Liu, S. E. Bottle, and P. Sonar. Developments of diketopyrrolopyrrole-dye-based organic semiconductors for a wide range of applications in electronics. *Advanced Materials*, 32(4):1903882, 2020.

[60] Y. Zhang, I. Murtaza, and H. Meng. Development of fullerenes and their derivatives as semiconductors in field-effect transistors: exploring the molecular design. *J. Mater. Chem. C*, 6:3514–3537, 2018.

[61] B. I. Kharisov, U. Ortiz Mendez, and J. Rivera de la Rosa. Low-temperature synthesis of phthalocyanine and its metal complexes. *Russian Journal of Coordination Chemistry*, 32(9):617–631, Sep 2006.

[62] A. K. Asatkar, A. Bedi, and S. S. Zade. Metallo-organic conjugated systems for organic electronics. *Israel Journal of Chemistry*, 54(5-6):467–495, 2014.

[63] L. Li, Q. Tang, H. Li, Hu W., X. Yang, Z. Shuai, Y. Liu, and D. Zhu. Organic thin-film transistors of phthalocyanines. *Pure and Applied Chemistry*, 80(11):2231–2240, 2008.

[64] Z. Bao, A. J. Lovinger, and J. Brown. New air-stable n-channel organic thin film transistors. *Journal of the American Chemical Society*, 120(1):207–208, 1998.

[65] J. Šebera, S. Nešpůrek, I. Kratochvílová, S. Záliš, G. Chaidogiannos, and N. Glezos. Charge carrier mobility in sulphonated and non-sulphonatedni phthalocyanines: experiment and quantum chemical calculations. *The European Physical Journal B*, 72(3):385, Oct 2009.

[66] G. Chaidogiannos, F. Petraki, N. Glezos, S. Kennou, and S. Nešpůrek. Low voltage operating ofets based on solution-processed metal phthalocyanines. *Applied Physics A*, 96(3):763–767, Aug 2009.

[67] L. Li, Q. Tang, H. Li, X. Yang, W. Hu, Y. Song, Z. Shuai, W. Xu, Y. Liu, and D. Zhu. An ultra closely π-stacked organic semiconductor for high performance field-effect transistors. *Advanced Materials*, 19(18):2613–2617, 2007.

[68] P. Turek, P. Petit, J. J. Andre, J. Simon, R. Even, B. Boudjema, G. Guillaud, and M. Maitrot. A new series of molecular semiconductors: phthalocyanine radicals. *Journal of the American Chemical Society*, 109(17):5119–5122, 1987.

[69] Y. Chen, W. Su, M. Bai, J. Jiang, X. Li, Y. Liu, L. Wang, and S. Wang. High performance organic field-effect transistors based on amphiphilic tris(phthalocyaninato) rare earth triple-decker complexes. *Journal of the American Chemical Society*, 127(45):15700–15701, 2005. PMID: 16277501.

[70] E. C. P. Smits, T. D. Anthopoulos, S. Setayesh, E. van Veenendaal, R. Coehoorn, P. W. M. Blom, B. de Boer, and D. M. de Leeuw. Ambipolar charge transport in organic field-effect transistors. *Phys. Rev. B*, 73:205316, May 2006.

[71] George C. Papavassiliou, George C. Anyfantis, and George A. Mousdis. Neutral metal 1,2-dithiolenes: Preparations, properties and possible applications of unsymmetrical in comparison to the symmetrical. *Crystals*, 2(3):762–811, 2012.

[72] C. Pearson, A.J. Moore, J.E. Gibson, M.R. Bryce, and M.C. Petty. A field effect transistor based on langmuir-blodgett films of an ni(dmit)2 charge transfer complex. *Thin Solid Films*, 244(1):932 – 935, 1994.

[73] Tomohiro Taguchi, Hiroshi Wada, Takuya Kambayashi, Bunpei Noda, Masanao Goto, Takehiko Mori, Ken Ishikawa, and Hideo Takezoe. Comparison of p-type and n-type organic field-effect transistors using nickel coordination compounds. *Chemical Physics Letters*, 421(4):395 – 398, 2006.

[74] Hiroshi Wada, Tomohiro Taguchi, Bunpei Noda, Takuya Kambayashi, Takehiko Mori, Ken Ishikawa, and Hideo Takezoe. Air stability of n-channel organic transistors based on nickel coordination compounds. *Organic Electronics*, 8(6):759 – 766, 2007.

[75] J.-Yang Cho, B. Domercq, S. C. Jones, J. Yu, X. Zhang, Z. An, M. Bishop, S. Barlow, S. R. Marder, and B. Kippelen. High electron mobility in nickel bis(dithiolene) complexes. *J. Mater. Chem.*, 17:2642–2647, 2007.

[76] L. Qu, Y. Guo, H. Luo, C. Zhong, G. Yu, Y. Liu, and J. Qin. A simple nickel bis(dithiolene) complex as an excellent n-type molecular semiconductor for field-effect transistors. *Chem. Commun.*, 48:9965–9967, 2012.

[77] S.-I. Noro, H.-C. Chang, T. Takenobu, Y. Murayama, T. Kanbara, T. Aoyama, T. Sassa, T. Wada, D. Tanaka, S. Kitagawa, Y. Iwasa, T. Akutagawa, and T. Nakamura. Metal-organic thin-film transistor (motft) based on a bis(o-diiminobenzosemiquinonate) nickel(ii) complex. *Journal of the American Chemical Society*, 127(28):10012–10013, 2005. PMID: 16011360.

[78] D. Sheberla, L. Sun, M. A. Blood-Forsythe, S. Er, C. R. Wade, C. K. Brozek, A. Aspuru-Guzik, and M. Dincă. High electrical conductivity in ni3(2,3,6,7,10,11-hexaiminotriphenylene)2, a semiconducting metal–organic graphene analogue. *Journal of the American Chemical Society*, 136(25):8859–8862, 2014. PMID: 24750124.

[79] G. Magadur, J.-Sébastien Lauret, G. Charron, F. Bouanis, E. Norman, V. Huc, C.-Sorin Cojocaru, S. Gómez-Coca, E. Ruiz, and T. Mallah. Charge transfer and tunable ambipolar effect induced by assembly of cu(ii) binuclear complexes on carbon nanotube field effect transistor devices. *Journal of the American Chemical Society*, 134(18):7896–7901, 2012. PMID: 22524256.

[80] H.-H. Liao, C.-M. Yang, C.-C. Liu, S.-F. Horng, H.-F. Meng, and J.-T. Shy. Dynamics and reversibility of oxygen doping and de-doping for conjugated polymer. *Journal of Applied Physics*, 103(10):104506, 2008.

[81] M. Honda, K. Kanai, K. Komatsu, Y. Ouchi, H. Ishii, and K. Seki. Atmospheric effect of air, n2, o2, and water vapor on the ionization energy of titanyl phthalocyanine thin film studied by photoemission yield spectroscopy. *Journal of Applied Physics*, 102(10):103704, 2007.

[82] H. Shirakawa, E. J. Louis, A. G. MacDiarmid, C. K. Chiang, and A. J. Heeger. Synthesis of electrically conducting organic polymers: halogen derivatives of polyacetylene, (ch). *J. Chem. Soc., Chem. Commun.*, pages 578–580, 1977.

[83] H. Tada, H. Touda, M. Takada, and K. Matsushige. Quasi-intrinsic semiconducting state of titanyl-phthalocyanine films obtained under ultrahigh vacuum conditions. *Applied Physics Letters*, 76(7):873–875, 2000.

[84] N. Ljungqvist and T. Hjertberg. Oxidative degradation of poly(3-octylthiophene). *Macromolecules*, 28(18):5993–5999, 1995.

[85] C. Krellner, S. Haas, C. Goldmann, K. P. Pernstich, D. J. Gundlach, and B. Batlogg. Density of bulk trap states in organic semiconductor crystals: Discrete levels induced by oxygen in rubrene. *Phys. Rev. B*, 75:245115, Jun 2007.

[86] W. L. Kalb, K. Mattenberger, and B. Batlogg. Oxygen-related traps in pentacene thin films: Energetic position and implications for transistor performance. *Phys. Rev. B*, 78:035334, Jul 2008.

[87] R. C. Haddon, A. F. Hebard, M. J. Rosseinsky, D. W. Murphy, S. J. Duclos, K. B. Lyons, B. Miller, J. M. Rosamilia, R. M. Fleming, A. R. Kortan, S. H. Glarum, A. V. Makhija, A. J. Muller, R. H. Eick, S. M. Zahurak, R. Tycko, G. Dabbagh, and F. A. Thiel. Conducting films of c_{60} and c_{70} by alkali-metal doping. *Nature*, 350:320–322, 1991.

[88] C. Y. H. Chan, C. M. Chow, and S. K. So. Using transistor technique to study the effects of transition metal oxide dopants on organic charge transporters. *Organic Electronics*, 12(8):1454 – 1458, 2011.

[89] M. Kröger, S. Hamwi, J. Meyer, T. Riedl, W. Kowalsky, and A. Kahn. P-type doping of organic wide band gap materials by transition metal oxides: A case-study on molybdenum trioxide. *Organic Electronics*, 10(5):932 – 938, 2009.

[90] J.-H. Lee, D.-S. Leem, and J.-J. Kim. Effect of host organic semiconductors on electrical doping. *Organic Electronics*, 11(3):486 – 489, 2010.

[91] J. Meyer, S. Hamwi, S. Schmale, T. Winkler, H.-Hermann Johannes, T. Riedl, and W. Kowalsky. A strategy towards p-type doping of organic materials with HOMO levels beyond 6 eV using tungsten oxide. *J. Mater. Chem.*, 19:702–705, 2009.

[92] D. Zhang, J. Feng, L. Chen, H. Wang, Y. Liu, Y. Jin, Y. Bai, Y. Zhong, and H. Sun. Role of Fe_3O_4 as a *p*-dopant in improving the hole injection and transport of organic light-emitting devices. *IEEE Journal of Quantum Electronics*, 47(5):591–596, May 2011.

[93] J.-H. Lee, H.-M. Kim, K.-B. Kim, and J.-J. Kim. Origin of charge generation efficiency of metal oxide p-dopants in organic semiconductors. *Organic Electronics*, 12(6):950 – 954, 2011.

[94] P.-C. Kao, J.-H. Lin, J.-Y. Wang, C.-H. Yang, and S.-H. Chen. Li_2CO_3 as an n-type dopant on Alq_3 organic light emitting devices. *Journal of Applied Physics*, 109(9):094505, 2011.

[95] P.-C. Kao, J.-Y. Wang, J.-H. Lin, and C.-H. Yang. Effects of the Na_2CO_3 dopant on electron injection and transport in organic light emitting devices. *Thin Solid Films*, 527:338 – 343, 2013.

[96] P.-C. Kao, C.-C. Chang, and S.-Y. Lin. Role of k2co3 as an n-type dopant in enhancing the electron injection and transport of organic light-emitting devices. *Surface and Coatings Technology*, 231:135 – 139, 2013. Taiwan Association for Coating and Thin Film Technology (TACT 2011).

[97] D.-S. Leem, S.-Y. Kim, J.-J. Kim, M.-H. Chen, and C.-I. Wu. Rubidium-carbonate-doped 4,7-diphenyl-1,10-phenanthroline electron transporting layer for high-efficiency p-i-n organic light emitting diodes. *Electrochemical and Solid-State Letters*, 12(1):J8–J10, 2009.

[98] J. Lee, H. Lee, P. Jeon, K. Jeong, T. Gun Kim, J. Won Kim, and Y. Yi. Direct evidence of n-type doping in organic light-emitting devices: N free cs doping from csn3. *Applied Physics Letters*, 100(20):203301, 2012.

[99] K. S. Yook, S. O. Jeon, C. W. Joo, J. Y. Lee, T.-W. Lee, T. Noh, H.-J. Yang, and S.-K. Kang. Air stable and low temperature evaporable Li_3N as a n type dopant in organic light-emitting diodes. *Synthetic Metals*, 159(15):1664 – 1666, 2009.

[100] C. Yueh Kao, B. Lee, L. S. Wielunski, M. Heeney, I. McCulloch, E. Garfunkel, L. C. Feldman, and V. Podzorov. Doping of conjugated polythiophenes with alkyl silanes. *Advanced Functional Materials*, 19(12):1906–1911, 2009.

[101] C. Ganzorig and M. Fujihira. Improved drive voltages of organic electroluminescent devices with an efficient p-type aromatic diamine hole-injection layer. *Applied Physics Letters*, 77(25):4211–4213, 2000.

[102] B. Maennig, M. Pfeiffer, A. Nollau, X. Zhou, K. Leo, and P. Simon. Controlled p-type doping of polycrystalline and amorphous organic layers: Self-consistent description of conductivity and field-effect mobility by a microscopic percolation model. *Phys. Rev. B*, 64:195208, Oct 2001.

[103] D. T. Duong, C. Wang, E. Antono, M. F. Toney, and A. Salleo. The chemical and structural origin of efficient p-type doping in P3HT. *Organic Electronics*, 14(5):1330 – 1336, 2013.

[104] J. E. Cochran, M. J. N. Junk, A. M. Glaudell, P. Levi Miller, J. S. Cowart, M. F. Toney, C. J. Hawker, B. F. Chmelka, and M. L. Chabinyc. Molecular interactions and ordering in electrically doped polymers: Blends of PBTTT and F4TCNQ. *Macromolecules*, 47(19):6836–6846, 2014.

[105] Y. Zhang, B. de Boer, and P. W. M. Blom. Controllable molecular doping and charge transport in solution-processed polymer semiconducting layers. *Advanced Functional Materials*, 19(12):1901–1905, 2009.

[106] J. E. Rainbolt, P. K. Koech, E. Polikarpov, J. S. Swensen, L. Cosimbescu, A. Von Ruden, L. Wang, L. S. Sapochak, A. B. Padmaperuma, and D. J. Gaspar. Synthesis and characterization of p-type conductivity dopant 2-(3-(adamantan-1-yl)propyl)-3,5,6-trifluoro-7,7,8,8-tetracyanoquinodimethane. *J. Mater. Chem. C*, 1:1876–1884, 2013.

[107] G. M. Rangger, O. T. Hofmann, B. Bröker, and E. Zojer. A particularly strong organic acceptor for tuning the hole-injection barriers in modern organic devices. *Synthetic Metals*, 160(13):1456 – 1462, 2010.

[108] Y. Qi, T. Sajoto, S. Barlow, E.-Gun Kim, J.-Luc Brédas, S. R. Marder, and A. Kahn. Use of a high electron-affinity molybdenum dithiolene complex to p-dope hole-transport layers. *Journal of the American Chemical Society*, 131(35):12530–12531, 2009. PMID: 19678703.

[109] A. Nollau, M. Pfeiffer, T. Fritz, and K. Leo. Controlled n-type doping of a molecular organic semiconductor: Naphthalenetetracarboxylic dianhydride (ntcda) doped with bis(ethylenedithio)-tetrathiafulvalene (bedt-ttf). *Journal of Applied Physics*, 87(9):4340–4343, 2000.

[110] S. Tanaka, K. Kanai, E. Kawabe, T. Iwahashi, T. Nishi, Y. Ouchi, and K. Seki. Doping effect of tetrathianaphthacene molecule in organic semiconductors on their interfacial electronic structures studied by UV photoemission spectroscopy. *Japanese Journal of Applied Physics*, 44(6A):3760–3763, jun 2005.

[111] W. W. Porter and T. P. Vaid. Doping of an organic molecular semiconductor by substitutional cocrystallization with a molecular n-dopant. *J. Mater. Chem.*, 17:469–475, 2007.

[112] C. K. Chan, F. Amy, Q. Zhang, S. Barlow, S. Marder, and A. Kahn. N-type doping of an electron-transport material by controlled gas-phase incorporation of cobaltocene. *Chemical Physics Letters*, 431(1):67 – 71, 2006.

[113] C. K. Chan, A. Kahn, Q. Zhang, S. Barlow, and S. R. Marder. Incorporation of cobaltocene as an n-dopant in organic molecular films. *Journal of Applied Physics*, 102(1):014906, 2007.

[114] M. L. Tietze, B. D. Rose, M. Schwarze, A. Fischer, S. Runge, J. Blochwitz-Nimoth, B. Lüssem, K. Leo, and J.-L. Brédas. Passivation of molecular n-doping: Exploring the limits of air stability. *Advanced Functional Materials*, 26(21):3730–3737, 2016.

[115] M. L. Tietze, F. Wölzl, T. Menke, A. Fischer, M. Riede, K. Leo, and B. Lüssem. Self-passivation of molecular n-type doping during air exposure using a highly efficient air-instable dopant. *Physica Status Solidi A*, 210(10):2188–2198, 2013.

[116] B. A. Gregg and R. A. Cormier. Doping molecular semiconductors: n-type doping of a liquid crystal perylene diimide. *Journal of the American Chemical Society*, 123(32):7959–7960, 2001. PMID: 11493091.

[117] J. Zhang, H. Wang, X. Yan, J. Wang, J. Shi, and D. Yan. Phthalocyanine composites as high-mobility semiconductors for organic thin-film transistors. *Advanced Materials*, 17(9):1191–1193, 2005.

[118] R. Ruiz, D. Choudhary, B. Nickel, T. Toccoli, K.-C. Chang, A. C. Mayer, P. Clancy, J. M. Blakely, R. L. Headrick, S. Iannotta, and G. G. Malliaras. Pentacene thin film growth. *Chemistry of Materials*, 16(23):4497–4508, 2004.

[119] S. Steudel, S. De Vusser, S. De Jonge, D. Janssen, S. Verlaak, J. Genoe, and P. Heremans. Influence of the dielectric roughness on the performance of pentacene transistors. *Applied Physics Letters*, 85(19):4400–4402, 2004.

[120] D. Knipp, R. A. Street, and A. R. Völkel. Morphology and electronic transport of polycrystalline pentacene thin-film transistors. *Applied Physics Letters*, 82(22):3907–3909, 2003.

[121] S. E. Fritz, T. W. Kelley, and C. D. Frisbie. Effect of dielectric roughness on performance of pentacene tfts and restoration of performance with a polymeric smoothing layer. *The Journal of Physical Chemistry B*, 109(21):10574–10577, 2005. PMID: 16852282.

[122] K. Shankar and T. N. Jackson. Morphology and electrical transport in pentacene films on silylated oxide surfaces. *Journal of Materials Research*, 19(7):2003–2007, 2004.

[123] D. Knipp, R. A. Street, A. Völkel, and J. Ho. Pentacene thin film transistors on inorganic dielectrics: Morphology, structural properties, and electronic transport. *Journal of Applied Physics*, 93(1):347–355, 2003.

[124] D. H. Kim, Y. D. Park, Y. Jang, H. Yang, Y. H. Kim, J. I. Han, D. G. Moon, S. Park, T. Chang, C. Chang, M. Joo, C. Y. Ryu, and K. Cho. Enhancement of field-effect mobility due to surface-mediated molecular ordering in regioregular polythiophene thin film transistors. *Advanced Functional Materials*, 15(1):77–82, 2005.

[125] S. Kobayashi, T. Nishikawa, T. Takenobu, S. Mori, T. Shimoda, T. Mitani, H. Shimotani, N. Yoshimoto, S. Ogawa, and Y. Iwasa. Control of carrier density by self-assembled monolayers in organic field-effect transistors. *Nature Materials*, 3:317–322, 2004.

[126] K. P. Pernstich, S. Haas, D. Oberhoff, C. Goldmann, D. J. Gundlach, B. Batlogg, A. N. Rashid, and G. Schitter. Threshold voltage shift in organic field effect transistors by dipole monolayers on the gate insulator. *Journal of Applied Physics*, 96(11):6431–6438, 2004.

[127] C. Boulas, J. V. Davidovits, F. Rondelez, and D. Vuillaume. Suppression of charge carrier tunneling through organic self-assembled monolayers. *Phys. Rev. Lett.*, 76:4797–4800, Jun 1996.

[128] M. Halik, H. Klauk, U. Zschieschang, G. Schmid, C. Dehm, M. Schütz, S. Maisch, F. Effenberger, M. Brunnbauer, and F. Stellacci. Low-voltage organic transistors with an amorphous molecular gate dielectric. *Nature*, 431:963–966, Oct 2004.

[129] Y. D. Park, D. H. Kim, Y. Jang, M. Hwang, J. A. Lim, and K. Cho. Low-voltage polymer thin-film transistors with a self-assembled monolayer as the gate dielectric. *Applied Physics Letters*, 87(24):243509, 2005.

[130] H. Klauk, M. Halik, U. Zschieschang, G. Schmid, W. Radlik, and W. Weber. High-mobility polymer gate dielectric pentacene thin film transistors. *Journal of Applied Physics*, 92(9):5259–5263, 2002.

[131] W. Koenigs. Synthesen des chinolins. *Berichte der deutschen chemischen Gesellschaft*, 13(1):911–913, 1880.

[132] R. H. Manske. The chemistry of quinolines. *Chemical Reviews*, 30(1):113–144, 1942.

[133] S. A. Yamashkin and E. A. Oreshkina. Traditional and modern approaches to the synthesis of quinoline systems by the skraup and doebner-miller methods. (review). *Chemistry of Heterocyclic Compounds*, 42(6):701–718, Jun 2006.

[134] M. Grazia Ferlin, G. Chiarelotto, and I. Castagliuolo. Synthesis and characterization of some n-mannich bases of [1,2,3]triazoloquinolines. *Journal of Heterocyclic Chemistry*, 39(4):631–638, 2002.

[135] F. Paul, J. Patt, and J. F. Hartwig. Palladium-catalyzed formation of carbon-nitrogen bonds. reaction intermediates and catalyst improvements in the hetero cross-coupling of aryl halides and tin amides. *Journal of the American Chemical Society*, 116(13):5969–5970, 1994.

[136] A. S. Guram and S. L. Buchwald. Palladium-catalyzed aromatic aminations with in situ generated aminostannanes. *Journal of the American Chemical Society*, 116(17):7901–7902, 1994.

[137] P. Ruiz-Castillo and S. L. Buchwald. Applications of palladium-catalyzed c–n cross-coupling reactions. *Chemical Reviews*, 116(19):12564–12649, 2016. PMID: 27689804.

[138] M. R. Biscoe, T. E. Barder, and S. L. Buchwald. Electronic effects on the selectivity of pd-catalyzed c–n bond-forming reactions using biarylphosphine ligands: The competitive roles of amine binding and acidity. *Angewandte Chemie International Edition*, 46(38):7232–7235, 2007.

[139] L. Canovese, F. Visentin, G. Chessa, C. Levi, and P. Nikolov. Luminescent complexes of the zinc triad with n-substituted 8-amino-quinoline ligands: Synthesis and comparative study on the stability constants and related photophysical properties. *Inorganica Chimica Acta*, 362(11):3925 – 3933, 2009.

[140] D. Maiti, H. Paul, N. Chanda, S. Chakraborty, B. Mondal, V. G. Puranik, and G. K. Lahiri. Synthesis, structure, spectral and electron-transfer properties of octahedral-[coiii(l)2]+/[znii(l)2] and square planar-[cuii(l){OC(O)CH3}] complexes incorporating anionic form of tridentate bis(8-quinolinyl)amine [n1c9h6-n2-c9h6n3, l-] ligand. *Polyhedron*, 23(5):831 – 840, 2004.

[141] O. A. Melville, B. H. Lessard, and T. P. Bender. Phthalocyanine-based organic thin-film transistors: A review of recent advances. *ACS Applied Materials & Interfaces*, 7(24):13105–13118, 2015.

[142] L. Canovese, F. Visentin, G. Chessa, C. Levi, and P. Nikolov. Luminescent complexes of the zinc triad with n-substituted 8-amino-quinoline ligands: Synthesis and comparative study on the stability constants and related photophysical properties. *Inorganica Chimica Acta*, 362(11):3925 – 3933, 2009.

[143] T. A. Betley, B. A. Qian, and J. C. Peters. Group viii coordination chemistry of a pincer-type bis(8-quinolinyl)amido ligand. *Inorganic Chemistry*, 47(24):11570–11582, 2008.

[144] J. C. Peters, S. B. Harkins, S. D. Brown, and M. W. Day. Pincer-like amido complexes of platinum, palladium, and nickel. *Inorganic Chemistry*, 40(20):5083–5091, 2001.

[145] J. P. Puzas, R. Nakon, and J. L. Petersen. Direct evidence for an sn1cb mechanism. 4. crystal and molecular structure of chloro(bis(8-quinolinyl)amido-n1,n2,n3)copper(ii), a metal chelate containing an sp2-hybridized deprotonated amine. *Inorganic Chemistry*, 25(21):3837–3840, 1986.

[146] R. Miyaji, K. Asano, and S. Matsubara. Induction of axial chirality in 8-arylquinolines through halogenation reactions using bifunctional organocatalysts. *Chemistry – A European Journal*, 23(42):9996–10000, 2017.

[147] D. A. Conlon, A. Drahus-Paone, G.-Jie Ho, B. Pipik, R. Helmy, J. M. McNamara, Y.-Jun Shi, J. Michael Williams, D. Macdonald, D. Deschênes, M. Gallant, A. Mastracchio, B. Roy, and J. Scheigetz. Process development and large-scale synthesis of a pde4 inhibitor. *Organic Process Research & Development*, 10(1):36–45, 2006.

[148] H. Gershon, D. D. Clarke, and M. Gershon. Preparation of 6-fluoro-8-quinolinol and related 6-fluoroquinolines. *Monatshefte für Chemie / Chemical Monthly*, 133(11):1437–1442, Oct 2002.

[149] Z. Wu, Y. He, C. Ma, X. Zhou, X. Liu, Y. Li, T. Hu, P. Wen, and G. Huang. Oxidative remote c–h trifluoromethylation of quinolineamides on the c5 position with iodobenzene diacetate as the oxidizing agent. *Asian Journal of Organic Chemistry*, 5(6):724–728, 2016.

[150] T. Rösener, A. Hoffmann, and S. Herres-Pawlis. Next generation of guanidine quinoline copper complexes for highly controlled atrp: Influence of backbone substitution on redox chemistry and solubility. *European Journal of Inorganic Chemistry*, 2018(27):3164–3175, 2018.

[151] I. Trenkmann, C. von Borczyskowski, and H. Graaf. Shift of absorption energy during thin dye film growth: interpretation by geometric models of the growth morphology. *Thin Solid Films*, 573:41 – 47, 2014.

[152] U. Heinemeyer, K. Broch, A. Hinderhofer, M. Kytka, R. Scholz, A. Gerlach, and F. Schreiber. Real-time changes in the optical spectrum of organic semiconducting films and their thickness regimes during growth. *Phys. Rev. Lett.*, 104:257401, Jun 2010.

[153] F. Stephen A. The path to ubiquitous and low-cost organic electronic appliances on plastic. *Nature*, 428:911–918, Apr 2004.

[154] Z. Bao, A. J. Lovinger, and A. Dodabalapur. Highly ordered vacuum-deposited thin films of metallophthalocyanines and their applications in field-effect transistors. *Advanced Materials*, 9(1):42–44, 1997.

[155] T. Steiner. C–h · · · o hydrogen bonding in crystals. *Crystallography Reviews*, 9(2-3):177–228, 2003.

[156] J. P. Perdew, K. Burke, and M. Ernzerhof. Generalized gradient approximation made simple. *Phys. Rev. Lett.*, 77:3865–3868, Oct 1996.

[157] F. Weigend. Accurate coulomb-fitting basis sets for h to rn. *Phys. Chem. Chem. Phys.*, 8:1057–1065, 2006.

[158] F. Weigend and R. Ahlrichs. Balanced basis sets of split valence, triple zeta valence and quadruple zeta valence quality for h to rn: Design and assessment of accuracy. *Phys. Chem. Chem. Phys.*, 7:3297–3305, 2005.

[159] I. M. Dixon, S. Khan, F. Alary, M. Boggio-Pasqua, and J.-L. Heully. Probing the photophysical capability of mono and bis(cyclometallated) fe(ii) polypyridine complexes using inexpensive ground state dft. *Dalton Trans.*, 43:15898–15905, 2014.

[160] L. Krause, R. Herbst-Irmer, G. M. Sheldrick, and D. Stalke. Comparison of silver and molybdenum microfocus X-ray sources for single-crystal structure determination. *Journal of Applied Crystallography*, 48(1):3–10, Feb 2015.

[161] G. M. Sheldrick. *SHELXT* – Integrated space-group and crystal-structure determination. *Acta Crystallographica Section A*, 71(1):3–8, Jan 2015.

[162] G. M. Sheldrick. Crystal structure refinement with *SHELXL*. *Acta Crystallographica Section C*, 71(1):3–8, Jan 2015.

[163] Cambridge Crystallographic Data Centre. Cambridge structural database, 2019.

Abbreviations & acronyms

BINAP	2,2'-Bis(diphenylphosphino)-1,1'-binaphthyl
BQA	*N*-8-Quinolinyl-8-quinolinamide
BQAH	*N*-8-Quinolinyl-8-quinolinamine
DCM	Dichloromethane
EtOAc	Ethyl acetate
F_4-TCNQ	2,3,5,6-Tetrafluoro-7,7,8,8-tetracyanoquinodimethane
FET	Field effect transistor
HMDS	Hexamethyldisilazane
MeOH	Methanol
OFET	Organic field effect transistor
P3HT	Poly(3-hexylthiophene)
Pc	Phthalocyanine dianion
PEDOT:PSS	poly(3,4-ethylenedioxythiophene):poly(4-styrenesulfonate)
$Pd_2(dba)_3$	Tris(dibenzylideneacetone)dipalladium(0)
SAM	Self-assembled monolayer
SPhos	2-Dicyclohexylphosphino-2',6'-dimethoxybiphenyl
THF	Tetrahydrofuran
TLC	Thin-layer chromatography
Xantphos	4,5-Bis(diphenylphosphino)-9,9-dimethylxanthene